Small molecule-mediated insulin hypersecretion induces transient unfolded protein response and loss of beta cell function

Short title: Transient ER stress response in beta cells

Karina Rodrigues-dos-Santos[1†], Gitanjali Roy[1†], Derk D. Binns[2†], Magdalena G. Grzemska[2], Luiz F. Barella[1], Fiona Armoo[1], Melissa K. McCoy[3], Andrew V. Huynh[2], Jonathan Z. Yang[2], Bruce A. Posner[3], Melanie H. Cobb[2], and Michael A. Kalwat[1,4, *]

[1]Lilly Diabetes Center of Excellence, Indiana Biosciences Research Institute, Indianapolis, IN, USA;

Departments of [2]Pharmacology and [3]Biochemistry, UT Southwestern Medical Center, Dallas, TX, USA;

[4]Center for Diabetes and Metabolic Diseases, Indiana University School of Medicine, Indianapolis, IN, USA.

[†]Authors contributed equally

ORCID identifier: MAK, 0000-0002-8349-9470

*Correspondence: mkalwat@indianabiosciences.org or mkalwat@iu.edu

DISCLOSURE SUMMARY: The authors have nothing to disclose.

ABSTRACT:

Pancreatic islet beta cells require a fine-tuned ER stress response for normal function; abnormal ER stress contributes to diabetes pathogenesis. Here, we identified a small molecule, SW016789, with time-dependent effects on beta cell ER stress and function. Acute treatment with SW016789 potentiated nutrient-induced calcium influx and insulin secretion, while chronic exposure to SW016789 transiently induced ER stress and shut down secretory function in a reversible manner. Distinct from the effects of thapsigargin, SW016789 did not affect beta cell viability or apoptosis, potentially due to a rapid induction of adaptive genes, weak signaling through the eIF2α kinase PERK, and lack of oxidative stress gene *Txnip* induction. We determined that SW016789 acted upstream of voltage-dependent calcium channels (VDCCs) and potentiated nutrient- but not KCl-stimulated calcium influx. Measurements of metabolomics, oxygen consumption rate, and G protein-coupled receptor signaling did not explain the potentiating effects of SW016789. In

chemical co-treatment experiments we discovered synergy between SW016789 and activators of protein kinase C (PKC) and VDCCs, suggesting involvement of these pathways in the mechanism of action. Finally, chronically elevated calcium influx was required for the inhibitory impact of SW016789, as blockade of VDCCs protected human islets and MIN6 beta cells from hypersecretion-induced dysfunction. We conclude that beta cells undergoing this type of pharmacological hypersecretion have the capacity to suppress their function to mitigate ER stress and avoid apoptosis. These results have the potential to uncover beta cell ER stress mitigation factors and add support to beta cell rest strategies to preserve function.

INTRODUCTION

Pancreatic islet beta cells sense and control circulating glucose concentrations by secreting insulin. In type 1 diabetes (T1D), autoimmune attack on beta cells results in their death and thus a lack of insulin. In type 2 diabetes (T2D), beta cells initially compensate for insulin resistance but eventually fail to secrete sufficient insulin to maintain euglycemia [1]. Interventions are aimed at restoring beta cell functionality, lowering insulin resistance, and reducing hyperglycemia. However, existing therapeutics have limitations, necessitating identification of new targets and pathways.

Beta cells sense elevated circulating blood glucose concentrations via the glucose transporters GLUT1/3 [2]. Upon cellular entry, glucose metabolism via glycolysis and the tricarboxylic acid cycle yields a relative increase in [ATP/ADP], causing ATP-sensitive potassium (K_{ATP}) channel closure. This closure reduces the plasma membrane permeability to potassium, causing membrane depolarization, opening of voltage-dependent Ca^{2+} channels (VDCCs) and Ca^{2+} influx [3]. Ca^{2+} influx also stimulates oxidative phosphorylation in the mitochondria, driving a metabolic cycle that sustains ATP production and insulin secretion [4, 5]. Ca^{2+} influx triggers the fusion of insulin secretory vesicles with the plasma membrane resulting in insulin exocytosis [6]. Nutrient metabolism further enhances secretion without further Ca^{2+} influx via the amplifying pathway [7-9]. To handle their specialized secretory function, beta cells engage the unfolded protein response of the endoplasmic reticulum (UPR^{ER}) [10]. The UPR^{ER} is crucial in beta cells, as its disruption (e.g., PERK loss-of-function) leads to beta cell failure and diabetes [11]. Conversely, unmitigated UPR^{ER} is also detrimental to beta cell function and survival, eventually leading to induction of pro-apoptotic transcription factors including *Ddit3* (CHOP) and *Txnip* [12, 13].

Many studies have elucidated aspects of beta cell biology that may be targeted to improve overall beta cell health and function, including the UPR^{ER}, beta cell dedifferentiation, and the role of immature beta cells in whole islet function [14-18]. However, the high-throughput identification of novel small molecules that alter pancreatic beta cell function has lagged in comparison. Here, we used a secreted insulin-luciferase-based high-throughput screening tool to identify a small molecule, SW016789, which acutely and chronically alters beta cell secretory responses [19, 20]. We hypothesized the chronic effects on function were a result of acute hypersecretion which induced stress pathways (e.g., ER stress) that led to a shutdown of beta cell function, but not beta cell death. We investigated the mechanisms of action of SW016789 using a multipronged approach including measuring Ca^{2+} influx and insulin secretion; metabolomics and mitochondrial function; gene expression; and co-treatment with compounds that may interfere with the effects of SW016789. Our results with SW016789 agree with a model of beta cell plasticity wherein the effects of persistent secretory stress are mitigated to avoid cell death at the expense of function. Chemical tools like SW016789 present an opportunity to discover previously unrecognized or poorly characterized genes and pathways involved in these processes in the beta cell.

METHODS:

Antibodies and Reagents – Source information for all small molecules and antibodies used in this work are listed in electronic supplementary material (ESM) **Table S4**.

Small molecule screening –High-throughput screening of small molecules in Ins-GLuc MIN6 cells was as described [21]. Briefly, cells were seeded at ~15e6 cells per T175 flask and grown 7 days until confluence, then trypsinized, resuspended in medium, passed through a 40 µm cell strainer and diluted to 1.5e6 cells/ml. Cells were dispensed at 50 µl per well in 384-well opaque white cell culture dishes using a BioTek Multiflo FX liquid handler to yield 7.5e4 cells/well. Plates were placed in a tissue culture incubator for 72 h. Next, 0.5 µl each of DMSO (negative control, 1%), thapsigargin (positive control, 1 mM), and small molecules (5 µM) were added robotically to the plates and the cells were incubated 24 h. On the day of the assay, using a BioTek Multiflo FX liquid handler, cells were washed twice with KRBH (75 µL then 50 µL). To remove medium and buffer between washes, plates were centrifuged upside-down in collection trays at 30 x g for 1 min. Cells were then incubated in 25 µl of KRBH containing 200 mM diazoxide for 60 min. Next, 25 µl of 2X stimulation buffer in KBRH was added to yield a final concentration of 20 mM glucose, 35 mM KCl and 250 mM diazoxide in a total volume of 50 µl. The plates were incubated for 60 min

93 at 37°C in a tissue culture incubator. Afterward, 20 µl of GLuc assay working solution (5 mM KCl,
94 15 mM Hepes pH 7.4, 24 mM NaHCO3, 1 mM MgCl2, 2 mM CaCl2, 300 mM sodium ascorbate,
95 and 3.54 µM coelenterazine) was added to each well. Within 10-20 min, the luminescence from
96 each well of the plates was measured using a Perkin Elmer EnVision multi-mode plate reader with
97 0.1 sec integration time. The raw data were corrected for plate effects using a GeneData
98 proprietary algorithm and then each value on a per plate basis was subjected to either single-point
99 or two-point normalization, followed by calculation of the robust Z (RZ) score for each well. Hit
100 compounds with an |RZ|>3 were selected for structural clustering analysis. Representative
101 compounds were then cherry picked and confirmed in triplicate in the same InsGLuc-MIN6
102 secretion assay and tested for toxicity in MIN6 cells by Cell Titer Glo assay after 72 h exposure.
103
104 **Cell culture and treatments** – Culture of MIN6 beta cells has been described [20]. MIN6 cells
105 were cultured in high glucose DMEM containing 10% FBS, 50 µM beta-mercaptoethanol, 1 mM
106 pyruvate, 100 U/ml penicillin, and 100 µg/ml streptomycin. Prior to glucose stimulation
107 experiments (as in **Fig. 3a-d**), cells were washed twice with and incubated for 2 h in freshly
108 prepared glucose-free modified Krebs-Ringer bicarbonate (KRBH) buffer (5 mM KCl, 120 mM
109 NaCl, 15 mM HEPES, pH 7.4, 24 mM $NaHCO_3$, 1 mM $MgCl_2$, 2 mM $CaCl_2$, and 1 mg/ml
110 radioimmunoassay-grade BSA). MIN6 cells were stimulated with glucose as indicated and
111 secreted insulin and insulin content were measured using HTRF assays (Cisbio). To generate
112 lysates for immunoblotting, cells were lysed in 1% NP40 lysis buffer (25 mM HEPES, pH 7.4, 1%
113 Nonidet P-40, 10% glycerol, 137 mM NaCl, 1 mM EDTA, 1 mM EGTA, 50 mM sodium fluoride, 10
114 mM sodium pyrophosphate, 1 mM sodium orthovanadate, 1 mM phenylmethylsulfonyl fluoride, 10
115 µg/ml aprotinin, 1 µg/ml pepstatin, 5 µg/ml leupeptin), rotated (10 min, 4°C), centrifuged (10,000 x
116 g; 10 min; 4°C), and stored at -80°C. InsGLuc-MIN6 cells were generated and characterized as
117 previously described [20] and were determined to be negative for mycoplasma. Mouse intestinal L
118 cell line GLUTag was originally generated by Daniel Drucker (Mount Sinai Hospital) and were
119 obtained from the lab of George G. Holz (Upstate Medical University). GLUTag cells were cultured
120 in low glucose DMEM with 10% FBS and 100 U/ml penicillin, 100 µg/ml streptomycin. The human
121 somatostatinoma line QGP-1 was provided by Dawn E. Quelle (University of Iowa). QGP-1 cells
122 were cultured in RPMI-1640 with 10% FBS, 1 mM pyruvate, 100 U/ml penicillin, and 100 µg/ml
123 streptomycin. GLUTag and QGP-1 cells were plated in 12 well dishes and treated in medium as
124 indicated in the figure legend before harvesting for RNA purification and downstream gene
125 expression analysis.

126

127 **Secreted Gaussia luciferase assays** – InsGLuc-MIN6 cells were plated in 96-well dishes at 1e5
128 cells/well and cultured for 3-4 days before compound treatment either overnight (24 h) in medium
129 or acutely (1 h) in KRBH. Treatments in 96-well assays were performed with at least three
130 replicate wells and in at least three independent passages of cells. For assays, cells were washed
131 twice with KRBH and preincubated in 100 µl of KRBH (250 µM diazoxide where indicated) for 1 h.
132 The solution was then removed, and cells were washed once with 100 µl of KRBH and then
133 incubated in KRBH with or without the indicated stimulation and compound treatments for 1 h. 50
134 µl of KRBH was collected from each well and pipetted into a white opaque 96-well plate Optiplate-
135 96 (Perkin-Elmer). Fresh GLuc assay working solution was then prepared by adding
136 coelenterazine stock solution into assay buffer to a final concentration of 10 µM. 50 µl of working
137 solution was then rapidly added to the wells using an Integra Voyager 1250 µl electric multi-
138 channel pipette for a final concentration of 5 µM coelenterazine. After adding reagent to the plate,
139 plates were spun briefly, and luminescence was measured on a Synergy H1M2 plate reader
140 (BioTek). The Gen5 software protocol was set to shake the plate orbitally for 3 seconds and then
141 read the luminescence of each well (integration, 100 ms; gain,150).

142

143 **Human islet culture, drug treatments and static culture secretion assays** – Cadaveric human
144 islets were obtained through the Integrated Islet Distribution Program (IIDP). Islets were isolated
145 by the affiliated islet isolation center and cultured in PIM medium (PIM-R001GMP, Prodo Labs)
146 supplemented with glutamine/glutathione (PIM-G001GMP, Prodo Labs), 5% Human AB serum
147 (100512, Gemini Bio Products), and ciprofloxacin (61-277RG, Cellgro, Inc) at 37°C and 5% CO2
148 until shipping at 4°C overnight. Human islets were cultured upon receipt in complete CMRL-1066
149 (10% FBS, 100 U/ml penicillin, 100 µg/ml streptomycin). For drug treatments and static culture,
150 human islets (50-75) were hand-picked under a dissection microscope and transferred to low-
151 binding 1.5 ml tubes (50 islets/tube). Islets were cultured 24 h in 500 µL of complete CMRL-1066
152 medium containing indicated drug treatments. For static culture insulin secretion experiments, the
153 islets were washed twice with 500 µL of KRBH (134 mM NaCl, 4.8 mM KCl, 1 mM $CaCl_2$, 1.2 mM
154 $MgSO_4$, 1.2 mM KH_2PO_4, 5 mM $NaHCO_3$, 10 mM HEPES pH 7.4, 0.1% radioimmunoassay-grade
155 BSA) and preincubated in KRBH (500 µL, 1 mM glucose; 1 h) before switching to 500µL KRBH
156 containing either 1 or 16 mM glucose for 1 h. Supernatants were collected, centrifuged (10,000 x
157 g; 5 min) and transferred to fresh tubes for storage at -80°C. Total insulin content was extracted
158 by acid-ethanol (1.5% HCl in 70% ethanol) overnight at -80°C and the solution was neutralized

159 with an equal volume of 1 M Tris pH 7.4 prior to insulin assays. Secreted insulin and insulin
160 content were measured using HTRF assays. Human islet characteristics and donor information
161 are listed in **ESM Human Islet Checklist**.
162
163 **Cell death and viability assays** – To measure live and dead cells as well as the live/dead cell
164 ratio, MultiTox-Fluor (Promega) was used according to the manufacturer's instructions. Briefly,
165 MIN6 cells were seeded into 96 well black-walled clear bottom tissue culture dishes at 5e4-1e5
166 cells/well and culture for 3-5 d before treatment with compounds as indicated in the figure legend.
167 On the day of the assay, cell-permeant GF-AFC substrate (live cell readout) and cell-impermeant
168 bis-AAF-R110 substrate (dead cell readout) reagents were diluted into kit assay buffer as a 2X
169 working solution. 100 µL of 2X working solution was added to each well of cells in 100 µL of
170 medium and incubated 30 min at 37°C. Plates were read on a BioTek Synergy H1M2 plate reader
171 ($400_{Ex}/505_{Em}$ for live cells; $485_{Ex}/520_{Em}$ for dead cells). Digitonin was a positive control for cell
172 death which lysed cells immediately prior to addition of 2X working solution. Viability and death
173 were normalized to DMSO control.
174
175 **Ca^{2+} influx assays** – Ca^{2+} influx measurements were completed in MIN6 cells plated in triplicate
176 in black-walled clear-bottom 96-well tissue culture imaging plates. Cells were preincubated for 1 h
177 in glucose-free KRBH, followed by loading with Fura-2-LR-AM (5 µM) for 25 min and a 5 min
178 washout. Using a BioTek Synergy H1 plate reader equipped with dual monochromators, relative
179 Ca^{2+} levels were measured ($Ex_{340/380}/Em_{510}$ gain=150). Recordings included 5 min baseline
180 followed by 5-30 min post-addition of stimulation as indicated. Data were normalized by
181 subtracting the mean of the respective baseline reads. Area under the curves (AUCs) were
182 calculated from peaks detected in GraphPad Prism using a baseline of 0 ΔRFU, restricted to
183 peaks that go above baseline by more than 0.05 ΔRFU and defined by at least 10 adjacent points.
184
185 **Immunoblotting** – 40-50 µg of cleared cell lysates were separated on 10% gels by SDS-PAGE
186 and transferred to nitrocellulose for immunoblotting. All membranes were blocked in Odyssey
187 blocking buffer (Licor) for 1 h before overnight incubation with primary antibodies diluted in
188 blocking buffer (**ESM Table 4**). After three 10 min washes in TBS-T (20 mM Tris-HCl pH 7.6, 150
189 mM NaCl, 0.1% Tween-20), membranes were incubated with fluorescent secondary antibodies for
190 1 h at room temperature. After three 10 min washes in TBS-T, membranes were imaged on a
191 Licor Odyssey scanner.

192

193 **Relative gene expression** – RNA was isolated from MIN6 cells using the PureLink RNA Mini Kit
194 (Life Technologies) or the Aurum Total RNA Mini kit (Bio-Rad). Briefly, after indicated treatments,
195 medium was removed from cells and lysis buffer (with β-mercaptoethanol) was added to cells.
196 Cells were scraped, lysates transferred to 1.5 mL tubes on ice and then transferred to -80°C for
197 storage. Samples were processed according to the kit manufacturer's instructions, including on-
198 column digestion with RNase-free DNase. RNA concentration was measured using an Implen
199 Nanophotometer or Nanodrop spectrophotometer and verified to have $A_{260/280}$ ratios >2.0. 1000 ng
200 of RNA was converted into cDNA using the iScript cDNA synthesis kit (Bio-Rad) following
201 manufacturer instructions and the resulting cDNA was diluted 20-fold with water. One µl of diluted
202 cDNA was used in 10 µl qPCR reactions using 2X SYBR Bio-Rad master mix and 250 nM of each
203 primer. Reactions were run in 384-well format on a CFX384 (Bio-Rad) or QuantStudio 5 (Thermo).
204 qPCR data was analyzed using CFX Manager (Bio-Rad) with 18S RNA as the reference gene.
205 Relative expression was calculated by the $2^{-\Delta\Delta Ct}$ method. All primer details are listed in ESM **Table**
206 **4.**
207

208 **Bioenergetics** – Oxygen consumption rates were measured using a Seahorse XFe96 (Agilent).
209 MIN6 cells were seeded at a density of 5e4 cells/well in XF96 cell culture microplates and cultured
210 for 48 h. On the day before the assay a Seahorse cartridge was hydrated with calibrant solution
211 and incubated overnight. On the day of the assay, the XFe96 PrepStation was set to 37°C and
212 hydrated cartridge was placed inside. MIN6 cells were washed twice with Seahorse-modified
213 Krebs-Ringer HEPES buffer (S-KRH: 5 mM KCl, 114 mM NaCl, 20 mM Hepes pH 7.4, 1.2 mM
214 $MgSO_4$, 2.5 mM $CaCl_2$, 1.2 mM KH_2PO_4 and pH carefully adjusted to 7.4, BSA and $NaHCO_3$ are
215 not present) and placed in the PrepStation to equilibrate for 1 h. The hydrated Seahorse cartridge
216 was placed on an empty utility plate to be loaded with compounds diluted in S-KRH. The drug
217 cartridge was returned to the utility plate with calibrant solution and inserted into the XFe96 for
218 calibration. After calibration, the cell culture plate was inserted into the XFe96 and MIN6 cells
219 were monitored for three 3 min cycles to measure baseline oxygen consumption (OCR) and
220 extracellular acidification rates (ECAR). Stimulations were injected as indicated and after each
221 stimulation cells were monitored for three 3 min cycles. Data were analyzed in the Seahorse
222 WAVE software (version 2.61.53).
223

224 **Metabolomics** – Metabolomic analysis was performed as described [22, 23]. MIN6 cells grown to
225 confluence in 6 well dishes were preincubated in glucose-free KRBH for 2 h at 37°C. DMSO
226 (0.1%), SW016789 (5 μM), and/or glucose (20 mM) were added as indicated and cells were
227 incubated a further 30 min at 37°C. After indicated treatments, cells were washed with 1 ml ice
228 cold saline and harvested in 1 ml of 80% methanol at 80°C. Cells were scraped and transferred to
229 1.5 ml tubes for three freeze-thaw cycles in liquid nitrogen. Lysates were clarified at 14,000 rpm
230 for 15 min at 4°C. Metabolite containing supernatants were transferred to a new 1.5 ml tube and
231 lyophilized using a SpeedVac. Breathable membranes were placed on top of the open tubes to
232 prevent cross contamination and the SpeedVac was operated without heat for 4 h. Pellets were
233 stored at 80°C prior to analysis by the Metabolomics Facility at Children's Medical Center
234 Research Institute at UT Southwestern (Dallas, TX). Metabolites were reconstituted in 100 ml of
235 0.03% formic acid in analytical grade water, vortex mixed, and centrifuged to remove debris.
236 Thereafter, the supernatant was transferred to a high-performance liquid chromatography (HPLC)
237 vial for the metabolomics study. Targeted metabolite profiling was performed using a liquid
238 chromatography mass spectrometry/mass spectrometry (LC/MS/MS) approach. Separation was
239 achieved on a Phenomenex Synergi Polar RP HPLC column (150 x 2 mm, 4 μm, 80 Å) using a
240 Nexera Ultra High Performance Liquid Chromatograph (UHPLC) system (Shimadzu Corporation).
241 The mobile phases employed were 0.03% formic acid in water (A) and 0.03% formic acid in
242 acetonitrile (B). The gradient program was as follows: 0-3 min, 100% A; 3-15 min, 100% - 0% A;
243 15-21 min, 0% A; 21-21.1 min, 0% - 100% A; 21.1-30 min, 100% A. The column was maintained
244 at 35°C and the samples kept in the autosampler at 4°C. The flow rate was 0.5 ml/min, and
245 injection volume 10 μl. The mass spectrometer was an AB QTRAP 5500 (Applied Biosystems
246 SCIEX) with electrospray ionization (ESI) source in multiple reaction monitoring (MRM) mode.
247 Sample analysis was performed in positive/negative switching mode. Declustering potential (DP)
248 and collision energy (CE) were optimized for each metabolite by direct infusion of reference
249 standards using a syringe pump prior to sample analysis. The MRM MS/MS detector conditions
250 were set as follows: curtain gas 30 psi; ion spray voltages 5000 V (positive) and 1500 V
251 (negative); temperature 650°C; ion source gas 150 psi; ion source gas 250 psi; interface heater
252 on; entrance potential 10 V. Dwell time for each transition was set at 3 msec. Samples were
253 analyzed in a randomized order, and MRM data was acquired using Analyst 1.6.1 software
254 (Applied Biosystems SCIEX). Chromatogram review and peak area integration were performed
255 using MultiQuant software version 2.1 (Applied Biosystems SCIEX). Although the numbers of cells
256 were similar and each sample was processed identically and randomly, the peak area for each

257 detected metabolite was normalized against the protein content of that sample to correct any
258 variations introduced from sample handling through instrument analysis. The normalized area
259 values were used as variables for the multivariate and univariate statistical data analysis. The
260 chromatographically co eluted metabolites with shared MRM transitions were shown in a grouped
261 format, i.e., leucine/isoleucine. Principle component analysis (PCA) was completed using SIMCA-
262 P software (version 13.0.1, Umetrics). To generate heat maps, metabolite TIC values were
263 normalized to the average of 'DMSO Basal' and expressed in $\log_2$. Heatmap was generated using
264 MetaboAnalyst 5.0 [24] using Euclidean distance with the Ward clustering algorithm, without
265 autoscaling of the features. Statistical differences were assessed by one-way ANOVA with
266 Fisher's LSD post-hoc test with an FDR <0.05 in MetaboAnalyst 5.0. Raw TIC values and table of
267 significantly altered metabolites are provided in **ESM Table 3**.
268
269 **Statistical Analysis** – Quantitated data are expressed as mean ± SD. Data were evaluated using
270 one- or two-way ANOVA as indicated and considered significant if $P < 0.05$. Graphs were made in
271 GraphPad Prism 9 and figures assembled in Affinity Designer (Serif).
272
273 **RESULTS**

274 **High-throughput screen identifies small molecule modulator of insulin secretion.**

275 In order to discover small molecules that alter beta cell function, we utilized the insulin-
276 Gaussia luciferase (GLuc) fusion reporter expressed in MIN6 beta cells (InsGLuc-MIN6) [20].
277 InsGLuc is processed and leads to co-secretion of Gaussia luciferase (GLuc) with insulin.
278 Secreted GLuc activity in this manner has been well-established as a proxy for insulin release [19,
279 25-29]. Our approach involved treating InsGLuc-MIN6 beta cells for 24 h with compounds followed
280 by a brief wash-out prior to testing their sustained impact on insulin secretion. This strategy
281 probes a distinct phenotypic space and is complementary to results from studies utilizing acute
282 treatments during stimulation [19]. We screened an 8,320 compound diversity subset
283 approximately representing the chemical space of the >300,000 compound library at the UT
284 Southwestern Medical Center High-Throughput Screening Core. InsGLuc-MIN6 beta cells were
285 treated with control and test compounds for 24 h in normal medium followed by a washout and
286 stimulation with glucose and KCl in the presence of diazoxide (**Fig. 1a**). Among the hits, chronic
287 exposure to SW016789 caused inhibition of secretion in InsGLuc-MIN6 cells with an IC_{50} <1 μM
288 (**Fig. 1b**) and was chosen for further study. Glucose-stimulated InsGLuc secretion was blunted in

289 MIN6 cells chronically exposed to resupplied stocks of SW016789, validating screening results
290 (**Fig. 1c**). Chronic pretreatment (24 h) of isolated human islets with SW016789 also impaired
291 glucose-stimulated insulin secretion (GSIS) (**Fig. 1d,e**), without a significant impact on insulin
292 content (**Fig. 1f**). SW016789 did not impact cell viability (**Fig. 1g**), cell death (**Fig. 1h**), or the
293 live/dead cell ratio (**Fig. 1i**) in MIN6 cells treated for up to 72 h. During this time course,
294 SW016789-treated cells remained unresponsive to stimulation with glucose or KCl (**Fig. 1j**), but
295 were able to mount significant, although blunted, responses to glucose if combined with
296 stimulators of cAMP generation or protein kinase C (PKC) activation (**Fig. 1j**). Beta cells exposed
297 to SW016789 for 24 h recovered function after a 48 h washout (**Fig. 1k**), indicating the effects are
298 reversible.

299 **SW016789 acutely potentiates nutrient-stimulated insulin secretion**

300 We determined that exposure of InsGLuc-MIN6 cells to SW016789 for 4-8 h resulted in
301 significant inhibition of GSIS while acute (≤2 h) exposure caused a marked potentiation of GSIS
302 (EC_{50} = 2.7 μM) (**Fig. 2a, ESM Fig. 1a,b**). Structure-activity relationship studies revealed that
303 while SW016789 is chiral, both enantiomers retain activity (**ESM Fig. 1c-f**) and the alcohol at the
304 chiral center is important for activity (**ESM Fig. 1g**). SW016789 potentiated amino acid-induced
305 secretion (**Fig. 2b**) but had no effect in cells treated with diazoxide and depolarizing KCl (**Fig. 2c**).
306 However, SW016789 elicited a response from cells treated with diazoxide and glucose without
307 elevated KCl. These data suggested the pathway activated by SW016789 requires nutrient
308 metabolism and may impact Ca^{2+} influx. Accordingly, chronic SW016789 treatment suppressed
309 glucose-stimulated Ca^{2+} influx (GSCa) (**Fig. 3a,b**), and acute SW016789 treatment potentiated
310 nutrient- but not KCl-stimulated Ca^{2+} influx (**Fig. 3c-f**). Considering these results, we determined
311 the effects of SW016789 on Ca^{2+} influx in the diazoxide paradigm. Beta cells were either pre-
312 treated for 24 h or treated with compound simultaneously with stimulation. With chronic
313 SW016789, stimulation with depolarizing KCl or KCl/glucose caused a rapid and sustained rise in
314 Ca^{2+} influx which was significantly lower than control by ~40% (**ESM Fig. 2a**), while acute
315 SW016789 had no impact (**ESM Fig. 2b**). We also observed a slight increase in GSCa even in the
316 presence of diazoxide and low KCl (**ESM Fig. 2c**), which was consistent with secretion data (**Fig.
317 2c**).

318 A potential source of the SW016789-enhanced Ca^{2+} influx is the endoplasmic reticulum
319 (ER). We tested whether SW016789 impacted ER Ca^{2+} stores or store-operated Ca^{2+} entry
320 (SOCE). MIN6 beta cells were pre-treated with SW016789 for 2, 6, and 24 h and subjected to

321 Ca^{2+} assays including thapsigargin stimulation to block SERCA2, leading to an observable Ca^{2+}
322 leak into the cytosol (**ESM Fig. 2d**). Treatment with SW016789 did not alter this indirect measure
323 of ER Ca^{2+}. Subsequently, Ca^{2+} was reintroduced to measure SOCE. Pre-exposure to SW016789
324 for 2-6 h caused a small, but significant, decrease in SOCE, but this effect was absent in cells
325 treated for 24 h, suggesting that in beta cells exposed to SW016789, ER Ca^{2+} and SOCE
326 responses were unmodified and may not underlie the acute potentiating or chronic inhibitory
327 effects of SW016789. Additionally, acute SW016789 exposure did not impact muscarinic receptor-
328 linked Gαq-stimulated Ca^{2+} influx (**ESM Fig. 2e**).

329 **SW016789 is unlikely to exert its beta cell effects via G protein-coupled receptors**

330 Because of its acute potentiating activity, we considered SW016789 may act through a G
331 protein-coupled receptors (GPCRs). Acute potentiation of insulin secretion can occur via activation
332 of Gαs-linked GPCRs and resultant cAMP generation [30]. To monitor relative cAMP production,
333 we used the BRET reporter CAMYEL stably expressed in MIN6 cells [31]. The positive control
334 (forskolin+IBMX) caused a marked increase in cAMP, while acute stimulation with SW016789,
335 with or without glucose, yielded no consistent alterations in signal (**ESM Fig. 3a,b**). To test a wider
336 range of GPCRs we also submitted SW016789 for screening against the GPCR library at the
337 NIMH Psychoactive Drug Screening Program at University of North Carolina [32] (**ESM Fig. 3c**).
338 Overall, SW016789 exhibited little to no activity against the GPCRs in the panel, including well-
339 known beta cell GPCRs (**ESM Table 1**). Only CXCR7 (ACKR3) out of 320 GPCRs was a
340 substantial primary hit, however confirmation studies determined the EC_{50} of SW016789 on
341 CXCR7 was ~26 μM (**ESM Fig. 3d**), well above the EC_{50} for beta cell activity (**Fig. 1b, ESM Fig.
342 1a**). In line with this result, the CXCR7 agonist VUF11207 [33] had a negligible impact on InsGLuc
343 secretion during chronic or acute treatments (**ESM Table 2**). These data suggested CXCR7 is
344 unlikely to mediate the effects of SW016789 in beta cells where its activity is observed in the 1-5
345 μM range. Together, these data suggested SW016789 does not exhibit substantial off-target
346 activity on GPCRs and that other mechanisms may be involved in its effects in beta cells.

347 **Beta cell metabolomic and mitochondrial responses are normal following acute SW016789
348 exposure**

349 Because SW016789 required nutrient co-stimulation to elicit effects on Ca^{2+} influx, we
350 hypothesized altered metabolism may contribute to the mechanism of action. To test this, we
351 performed targeted metabolomics on normal MIN6 beta cells stimulated with or without glucose in

352 the presence of DMSO or SW016789 for 30 min (**Fig. 4a**). The amplifying effect of SW016789 on
353 GSIS was confirmed by insulin measurements and the cellular extracts were submitted for
354 metabolomic analysis (**Fig. 4b, ESM Table 3**). Expectedly, glucose induced glycolysis and TCA
355 intermediates and the reduced/oxidized glutathione ratio (**Fig. 4c,d**). In each of these cases,
356 SW016789 had no impact. These results suggested SW016789 is unlikely to exert effects by
357 acutely altering well-known metabolic pathways. Beta cell oxygen consumption rates and
358 extracellular acidification rates were also unaffected by acute exposure to SW016789 as
359 measured by Seahorse assays (**Fig. 4e-g**).

360 **Chronic amplification of secretion leads to transient UPR^{ER} and shutdown of beta cell**
361 **function**

362 Acute SW016789-induced insulin hypersecretion eventually caused beta cells to lose
363 normal GSCa and GSIS responses which we hypothesized was due to the UPR^{ER}. To test this,
364 we treated MIN6 cells in a time-course with SW016789 or thapsigargin and collected RNA and
365 protein for analysis (**Fig. 5a**). Acute SW016789 increased immediate early gene (IEG) expression
366 within 1 h which decreased to near baseline by 2-6 h (**Fig. 5b**), in agreement with observed GSCa
367 effects. Thapsigargin did not affect expression these IEGs. SW016789 also induced expression of
368 UPR^{ER} genes by ~1 h with a peak from 2-6 h depending on the specific gene (**Fig. 5c**), followed
369 by a return to near baseline by 24 h. This was in stark contrast to thapsigargin which caused a
370 similar fold induction, but delayed peak of UPR^{ER} gene expression which persisted at 24 h.
371 Notably, the oxidative stress transcription factor *Txnip* was induced only by thapsigargin. Over the
372 time-course, SW016789 did not significantly alter insulin gene expression, but thapsigargin
373 caused a decrease after 24 h (**Fig. 5d**). SW016789 decreased insulin protein content at 6 h but
374 caused no further decrease by 24 h (**Fig. 5e**), suggesting the effect may be due to the induced
375 hypersecretion and implied that after shutdown of beta cell function the drop in insulin content
376 halted. We observed a similar pattern of induction and return to baseline of UPR^{ER} genes with
377 higher doses of SW016789 (**ESM Fig. 4a**), indicating SW016789 did not induce terminal UPR^{ER}
378 as occurs with thapsigargin. We also tested other endocrine cells that express stimulus-secretion
379 coupling machinery similar to beta cells, including a human delta cell line and a mouse intestinal L
380 cell line. SW016789 had minimal effects on IEGs or UPR^{ER} genes in these lines, while
381 thapsigargin robustly induced the UPR^{ER} (**ESM Fig. 4b-c**).

382 We also observed differences at the protein level between SW016789 and thapsigargin for
383 UPR^{ER} and apoptotic components (**Fig. 6a**). Thapsigargin, but not SW016789, significantly

384 induced the apoptosis markers CHOP and cleaved PARP by 24 h. Phosphorylated PERK was
385 significantly induced by thapsigargin at both 6 and 24 h, while the effects of SW01789 were
386 minimal. Alterations in phosphorylated eIF2α were variable and not significantly different with any
387 treatment at 6 and 24 h; however, thapsigargin induced BiP by 24 h. ATF3 and ATF4 protein
388 expression was induced only at 6 h by SW016789 and to a lesser extent than with thapsigargin
389 (**Fig. 6b**). Amounts of beta cell transcription factors Pdx1 and MafA were unaltered by 6 or 24 h of
390 SW016789 or thapsigargin (**Fig. 6c**). Together, these results partially explain why even though
391 SW016789 amplified secretion and caused ER stress, beta cells only ceased their secretory
392 function and did not undergo terminal UPR^{ER}.

393 **Acute effects of SW016789 are mediated via Ca^{2+} influx and PKCs**

394 The UPR^{ER} effects of SW016789 in beta cells appeared to stem from the enhancement of
395 nutrient-stimulated Ca^{2+} influx and insulin secretion. To elucidate the mechanisms underlying
396 SW016789-induced hypersecretion of insulin and subsequent UPR^{ER} induction, we took two
397 chemical approaches. In the first approach, we co-treated beta cells acutely with SW016789 and
398 candidate compounds to identify any synergy or disruption in SW016789 actions. Among the
399 stimuli tested, we discovered SW061789 exhibited synergy between and phorbol esters as well as
400 Ca^{2+} channel openers. PKC activation by the phorbol ester phorbol 12-myristate 13-acetate (PMA)
401 has well known effects on beta cells [34, 35]. Phorbol esters, including PMA, activate a subset of
402 PKCs, as well as other targets [36], to potentiate nutrient-stimulated insulin secretion. While
403 SW016789 and PMA each independently amplified GSIS, the combination of PMA and
404 SW016789 elicited a marked synergistic insulin secretion response in the absence of nutrients
405 (**Fig. 7a, DMSO pretreated**). To further explore the role of PMA-activated PKCs in the response
406 to SW016789, we exploited the property of chronic (>16 h) treatment with PMA which causes the
407 degradation of the PMA-responsive PKCs [35]. According to this paradigm, we pre-treated beta
408 cells overnight with PMA and repeated the acute stimulation experiment. Under these conditions,
409 SW016789 and PMA no longer stimulated secretion in the absence of nutrients and the effect of
410 SW016789 on GSIS was no longer significant (**Fig. 7a, PMA pretreated**). These results indicated
411 SW016789 may act in part though PKCs to elicit its acute effects. We also tested the effects of
412 directly opening VDCCs in the presence or absence of SW016789. The potent VDCC activator
413 FPL64176 phenocopied SW016789 in chronic (**Fig. 7b**) and acute (**Fig. 7c**) assays in beta cells.
414 FPL64176 had distinct characteristics, including acutely synergizing with SW016789 in the
415 absence of nutrients to induce Ca^{2+} influx and insulin secretion (**Fig. 7c,d**) and impacting GSCa

416 almost immediately compared to the more delayed effect of SW016789 (**Fig. 7d**). These data
417 suggested that FPL64176 and SW016789 act by different mechanisms.

418 In a second approach we used a chemical suppressor screen to disrupt potentially involved
419 pathways by co-treating cells with SW016789 and with compounds having known mechanisms.
420 Compounds were tested for their ability to protect against chronic inhibitory effects of SW016789
421 (**Fig. 8a, ESM Table 2**). The VDCC blocker nifedipine was identified as a hit and was selected for
422 further studies. Co-treatment of InsGLuc-MIN6 beta cells with SW016789 and nifedipine
423 significantly blocked the chronic inhibitory effects of SW016789 on GSIS (**Fig. 8b**) and partially
424 mitigated the induction of *Ddit3* (CHOP) expression at 6 h (**Fig. 8c**). We confirmed the acute
425 potentiating effects of SW016789 on GSIS were indeed dependent on VDCC-mediated Ca^{2+}
426 influx, as co-treatment with nifedipine completely blocked all stimulated secretion in the presence
427 or absence of SW016789 (**Fig. 8d**). Furthermore, the protective effects of nifedipine against
428 chronic SW016789 exposure were confirmed in human islet static culture GSIS experiments (**Fig.
429 8e**).

430 **DISCUSSION**

431 **Deconvolving the mechanism of action of SW016789**

432 A few conclusions can be made about the mechanism of SW016789 based on the acute
433 phenotype in beta cells. GSCa and GSIS were enhanced by SW016789, but KCl-induced
434 responses were unaffected, suggesting the involvement of metabolism. Metabolic measurements
435 suggested that SW016789 affects nutrient-induced insulin secretion downstream of ATP
436 generation to enhance Ca^{2+} influx. We discovered intersections of SW016789-mediated actions
437 with the PKC activator PMA and VDCC activator FPL64176. This raised concerns about the
438 requirement for nutrient-stimulated ATP production given that SW016789, PMA, and FPL64176
439 are not nutrients and individually do not stimulate substantial Ca^{2+} influx or insulin secretion (**ESM
440 Fig. 5**). In beta cells, phorbol esters potentiate GSIS through PKC activation [37, 38], but PKCs
441 are not required for normal GSIS [35, 39]. Synergy between phorbol esters and SW016789 may
442 occur through PKC-mediated phosphorylation of substrates involved in insulin exocytosis that
443 lower the threshold for SW016789 to cause enhanced Ca^{2+} influx [40]. We also observed a small,
444 but clear impact of SW016789 on Ca^{2+} influx and InsGLuc secretion in the presence of diazoxide
445 and low KCl which was glucose-dependent (**Fig. 2c, ESM 2c)**. This suggests SW016789 can
446 bypass K_{ATP} to cause membrane depolarization or VDCC opening. SW016789 could potentially

447 outcompete the effect of diazoxide on K_{ATP}, although we think this is unlikely because of
448 estimations that >90% of K_{ATP} channels must close before beta cells depolarize [3, 41, 42].

449 Given the prominent role of cAMP in the potentiation of insulin secretion, we had initially
450 suspected SW016789 might act through a Gαs-coupled GPCR. However, we did not observe a
451 major impact of SW016789 in cAMP reporter assays (**ESM Fig. 3a-b**). We also did not observe
452 protection from chronic SW016789 effects by co-treatment with inhibitors of cAMP pathways (e.g.
453 PKA inhibitor H89, adenylyl cyclase inhibitor ddAd) (**Fig. 8A**). While previous work has shown that
454 the cAMP-PKA pathway can protect against thapsigargin-mediated beta cell death [43],
455 SW016789 did not cause cell death (**Fig. 1g-i**) and the UPR^{ER} dynamics induced by SW016789
456 appear to be quite different compared to thapsigargin.

457 Among compounds tested for protection against SW016789, the most consistent hits were
458 from the dihydropyridine VDCC inhibitor family. We surmise that preventing increased Ca^{2+} influx
459 abrogates SW016789-enhanced insulin secretion, thereby preventing downstream UPR^{ER} and
460 preserving beta cell function. As blocking VDCCs prevents both Ca^{2+} influx and subsequent
461 insulin secretion, it is unclear whether downstream stress and functional loss is induced
462 specifically because of chronically increased Ca^{2+}, enhanced insulin release, or both. Indeed,
463 genetically reducing insulin production by 50% mitigated stress in mouse beta cells [44],
464 suggesting the possibility that in our system, blocking insulin secretion itself using VDCC inhibitors
465 may be responsible for mitigating hypersecretion-induced stress.

466 **Beta cell adaptation and dysfunction in response to chronic secretory demand**

467 Chronic metabolic stress leads to beta cell dysfunction and two recent studies provide
468 prime examples [45, 46]. Sustained physiological hyperglycemia (72 h) increases absolute insulin
469 secretion but impairs beta cell function as gauged by the disposition index [45]. Accordingly,
470 human islets exposed to glucolipotoxic stress for 48 h were unable to recover GSIS, while islets
471 exposed to milder stress (high glucose or palmitate alone) were able to recover function [46].
472 Under our culture conditions SW016789 initially potentiated beta cell function, but the secretory
473 response shut down by 4 h. Although UPR^{ER} induction was transient, returning to baseline after
474 24 h, beta cell function in terms of insulin secretion remained impaired. Beta cells recovered from
475 this inhibited state after a 48 h washout, indicating the changes were reversible. A potential
476 explanation is that a protein(s) affected by SW016789 signaling are degraded/reduced and require
477 the washout period to recover. Recently, multiple groups have shown that transient UPR^{ER}, either

478 downstream of partial pancreatectomy [47] or via inhibition of salt-inducible kinase (SIK) [48], is
479 associated with enhanced beta cell proliferation. While we did not observe significant alterations in
480 cell viability or death over a 72 h exposure to SW016789, it is possible the mechanism of UPR^{ER}
481 induction due to hypersecretion in this case is different from that of pancreatectomy or SIK
482 inhibition.

483 SW016789 selectively and transiently induced canonical UPR^{ER} stress response genes,
484 but with a distinct temporal pattern from that of thapsigargin. A lesser induction of ATF3/4, p-
485 PERK, and p-eIF2α may indicate an overall weaker induction of the PERK arm of the UPR^{ER} by
486 SW016789. Our findings also suggest a lack of oxidative stress induction by SW016789
487 ascertained by no observed changes in glutathione redox state or *Txnip* expression. SW016789-
488 treated beta cells were therefore able to downregulate their response to transiently enhanced Ca^{2+}
489 influx. Relative induction of pro-survival versus pro-apoptotic genes may underlie the effects of
490 SW016789-mediated UPR^{ER}. For example, the Ca^{2+}-activated gene *Npas4* was shown to have a
491 protective role in beta cells and was highly induced by SW016789, but not by thapsigargin [49,
492 50]. A gene program that mitigates stress within the first 6 h of drug treatment may allow
493 SW016789-treated beta cells to downregulate UPR^{ER} pathway before the point of no return.
494 SW016789 will be a useful tool compound for discovering genes involved in adaptive versus
495 maladaptive responses to chronic Ca^{2+} influx or secretory pressure.

496 **Role of pharmacological modulation of VDCC activity for beta cell protective effects**

497 Ca^{2+} channel blockers have been in the spotlight for their therapeutic value in both type 1
498 [51] and type 2 diabetes [52]. For example, verapamil improved beta cell function in a clinical trial
499 of recent-onset type 1 diabetes [51]. The proposed mechanism of action is that suppressing beta
500 cell Ca^{2+} influx reduces expression of the cellular redox regulator *Txnip*, leading to protection from
501 apoptosis [53]. In our studies SW016789 did not induce *Txnip*, suggesting an alternate
502 mechanism. In addition, the VDCC blockers of the dihydropyridine class (nifedipine, nimodipine,
503 amlodipine), as well as the phenylalkylamine class (verapamil) protected beta cells from
504 SW016789-induced dysfunction. Our results showing the protective effects of nifedipine agree
505 with previous findings in beta cells using other stressors including hyperglycemia and palmitate
506 [54-56]. Distinct VDCC inhibitor mechanisms of action may underlie the differences between
507 dihydropyridine and phenylalkylamine-mediated beta cell protection [57] and may imply that
508 SW016789 acts through a mechanism or pathway which is more dependent on VDCCs in the
509 inactivated state. Because amplified GSCa was confirmed as a major mechanism underlying the

510 effects of SW016789, we hypothesized that directly activating VDCCs using FPL64176 could
511 phenocopy SW016789 [58]. While SW016789 activity on Ca^{2+} influx was inhibited by nifedipine, it
512 also synergized with FPL64176 to enhance Ca^{2+} influx and secretion. The kinetics of Ca^{2+} influx
513 induced by FPL64176 or SW016789 in the presence of glucose differed greatly. In agreement with
514 our findings with FPL64176 and SW016789, prior work showed that chronic treatment with VDCC
515 activator BayK8644 caused insulin secretion defects attributed to decreased abundance of K_{ATP}
516 channel and VDCC subunits [59]. Although not assessed in those studies, beta cells likely
517 underwent transient UPR^{ER} concomitant with or prior to losing function.

518 Nifedipine or newer generation dihydropyridines like amlodipine, may also be useful
519 therapeutics for conditions that cause hyperinsulinemia or where beta cell VDCCs are
520 dysfunctional. A recent example is an individual with congenital hyperinsulinism with a gain-of-
521 function mutation at a conserved residue in the α1 pore-forming subunit of Cav1.3 (L271H),
522 encoded by *CACNA1D* [60]. Hyperinsulinism in this individual was successfully treated with
523 nifedipine and diazoxide. However, chronic blockade of beta cell VDCCs should be carefully
524 considered, as preliminary findings with genetic deletion of Cav1.3 in mice suggest a positive role
525 in beta cell mass [61]. Auxiliary channel subunits can also impact beta cell function in diabetes.
526 For example, the VDCC β_3 subunit (*Cacnb3*) is upregulated in islets from diabetic animals and
527 was associated with decreased channel function. Deletion of *Cacnb3* improved beta cell function
528 in a mouse model of diabetes [62, 63]. Future research into precision targeting of VDCCs or their
529 regulatory partners may be a promising avenue for diseases of beta cell dysfunction.

530 In conclusion, we discovered a new compound and potentially novel pathway that
531 modulates beta cell function and may expand the cohort of targets for disease mitigation.
532 Simultaneously, these discoveries also generate new knowledge about the mechanics of nutrient-
533 and hormone-regulated exocytosis from specialized secretory cell types, including insights into the
534 metabolic amplifying pathway.

535 **FIGURE LEGENDS**

536 **Fig. 1. Discovery of SW016789 as a small molecule chronic suppressor of insulin secretion.**
537 **(a)** High-throughput screening workflow leading to the discovery of SW016789. Screening was
538 performed on an 8,320-compound diversity subset representing the chemical space of the full
539 compound library at the UT Southwestern Medical Center High-Throughput Screening Core. Cells
540 were treated with control and test compounds for 24 h in normal medium followed by a washout

541 and stimulation with glucose and KCl in the presence of diazoxide and finally subjected to
542 InsGLuc assays. These maximal stimulatory conditions afforded the assay a large dynamic range
543 (average Z-score >0.5) and resulted in 168 primary hits which after structural clustering were
544 narrowed down to 82, of which 32 confirmed in triplicate. **(b)** Concentration response curve testing
545 to determine EC_{50} of SW016789 InsGLuc-MIN6 after a 24 h exposure. Data are the mean ± SD of
546 three independent assays. **(c,d)** In mouse InsGLuc-MIN6 beta cells (**c**) and human islets (**d**), 24 h
547 exposure to SW016789 (5 μM) resulted in suppression of GSIS during assays in the absence of
548 compound. Data are the mean ± SD of 3-4 independent experiments. **(g-i)** Exposure of MIN6 beta
549 cells to DMSO (0.1%) or SW016789 (5 μM) for up to 72 h did not alter relative amounts of (**g**) live
550 cells, (**h**) dead cells, or (**i**) the live/dead cell ratio. Digitonin (Dgt) treatment was a positive control
551 for cell death added just prior to the assay. **(j)** InsGLuc-MIN6 cells were exposed to SW016789 (5
552 μM) for 24-72 h followed by a 1 h washout in glucose-free KRBH. Cells were then stimulated for 1
553 h with the indicated treatments (0G, glucose-free; 20G, glucose 20 mM; Fsk, forskolin 10 μM;
554 IBMX 100 μM; PMA, phorbol myristate acetate 100 nM). *, P<0.05 vs respective Basal; †, P<0.05
555 vs respective DMSO. **(k)** InsGLuc-MIN6 cells were exposed to SW016789 (5 μM) for 24 h
556 followed by a 48 h washout in complete medium. Cells were then assayed for glucose-stimulated
557 InsGLuc secretion. All data are the mean ± SD of at least three independent experiments. *,
558 P<0.05 by two-way ANOVA.

559 **Figure 2. Time-course studies and phenotypic assays reveal SW016789 as an acute**
560 **potentiator of nutrient-stimulated insulin secretion. (a)** InsGLuc-MIN6 cells were treated with
561 SW016789 (5 μM) in a time-course as indicated in the diagram. At the end of the time-course,
562 glucose-stimulated InsGLuc secretion was assayed. Data are the mean ± SD of N=4. **(b)** InsGLuc-
563 MIN6 cells were exposed to SW016789 (5 μM) for 1 h during stimulation with glucose (20 mM),
564 leucine (5 mM), or leucine/glutamine (Leu/Gln; 5mM each) or **(c)** in the presence of diazoxide (250
565 μM) with or without KCl (35 mM) or glucose (20 mM). Data are the mean ± SD of N=3. *, P<0.05
566 by two-way ANOVA.

567 **Figure 3. SW016789 treatment modulates nutrient-stimulated Ca^{2+} influx. (a)** MIN6 beta cells
568 pre-treated 24 h with SW016789 (5 μM) or DMSO (0.1%) followed by washout prior to glucose-
569 stimulated Ca^{2+} influx assays and **(b)** area-under-the-curve (AUC) calculation. *, P<0.05 by
570 unpaired Student's t-test. **(c-f)** MIN6 beta cells acutely treated with SW016789 (5 μM) or DMSO
571 (0.1%) followed by **(c)** glucose-, **(d)** leucine/glutamine-, or **(e)** KCl-stimulated Ca^{2+} influx assays

572 and **(f)** associated AUCs. Data are the mean ± SD of three independent experiments. *, P<0.05 by
573 two-way ANOVA.

574 **Figure 4. SW016789 does not impact oxygen consumption rate or canonical glycolysis and**
575 **TCA cycle metabolites in MIN6 beta cells. (a)** Experimental design for targeted metabolomics in
576 MIN6 cells preincubated in glucose-free KRBH for 2 h and then treated with or without glucose (0
577 vs 20 mM) in the presence of DMSO (0.1%) (DMSO_0G and DMSO_20G) or SW016789 (5 μM)
578 (SW_0G and SW_20G). **(b)** KRBH supernatants were collected for insulin ELISA to verify that
579 SW016789 potentiated insulin secretion under these conditions. **(c)** Metabolomic data are
580 represented as the $\log_2$ fold-change with respect to DMSO_0G of three independent experiments.
581 **(d)** Representative metabolites showing glucose induced changes in glycolysis (glucose 6-
582 phosphate, fructose-1,6-bisphosphate), TCA cycle (citrate, α-ketoglutarate, and malate), amino
583 acids (cysteine, lysine), adenosine monophosphate, and redox potential (reduced glutathione
584 (GSH) / oxidized glutathione (GSSG)) in MIN6 cells. **(e-g)** MIN6 beta cells were subjected to
585 Seahorse analysis. Cells were preincubated in glucose-free KRBH and **(e)** oxygen consumption
586 rate (OCR), **(f)** extracellular acidification rate (ECAR), and **(g)** calculated Seahorse parameters
587 were measured during stimulation with glucose (20 mM) in the presence or absence of SW016789
588 (5 μM) or DMSO (0.1%). Subsequently all cells were sequentially stimulated with oligomycin,
589 FCCP, and Antimycin A. Data represent the mean ± SD of three independent experiments.

590 **Figure 5. SW016789 transiently induces the unfolded protein response (UPR^{ER}). (a)** MIN6
591 beta cells were treated with DMSO (0.1%), SW016789 (5 μM), or thapsigargin (Tg, 100 nM) in
592 complete medium for 0-24 has indicated. **(b-d)** Compound additions were staggered to allow
593 simultaneous sample harvesting. Expression of **(b)** immediate early genes and **(c)** adaptive and
594 maladaptive UPR^{ER} genes are shown. **(d)** Expression of *Ins1/2* in the time course and **(e)** insulin
595 content. All data are the mean ± SD of three independent experiments. *, P<0.05 vs DMSO.

596 **Figure 6. SW016789 and thapsigargin have distinct effects on UPR^{ER}-related proteins. (a)**
597 MIN6 beta cells were treated with SW016789 (5 μM) or thapsigargin (Tg, 500 nM) for either 6 or
598 24 h in complete medium and lysates were immunoblotted. Thapsigargin, but not SW016789,
599 induced pro-apoptotic markers CHOP and cleaved-PARP (cl-PARP). Alterations in UPR^{ER}
600 markers pS51-eIF2α, pT980-PERK, and BiP are shown. **(b)** SW016789 and Tg increased the
601 stress-induced transcription factors ATF4 and ATF3. Data are the mean ± SD of 3 independent
602 experiments. **(c)** Beta cell transcription factors Pdx1 and MafA were not significantly affected by

603 either drug. Data are the mean ± SD of 2-3 independent experiments. In all immunoblots either
604 actin or GAPDH were used as loading controls. *, P<0.05 by two-way ANOVA.

605 **Figure 7. SW016789 acutely synergizes with activators of PKC and VDCCs to induce**
606 **secretion. (a)** InsGLuc-MIN6 cells were treated 24 h with either DMSO (0.1%) or PMA (100 nM)
607 in complete medium. Cells were then washed and preincubated in glucose-free KBRH for 1 h prior
608 to stimulation with SW016789 (5 μM), PMA (100 nM), or both in the presence or absence of
609 glucose (20 mM) for 1 h. Afterward, buffer was collected for InsGLuc assays. Data are the mean ±
610 SD of eight independent experiments. *,P<0.05 by two-way ANOVA. **(b)** InsGLuc-MIN6 cells were
611 treated for 24 h with DMSO or the VDCC activator FPL64176 followed by glucose-stimulated
612 InsGLuc secretion assay in the absence of compounds. Data are the mean ± SD of four
613 independent experiments. *,P<0.05 Basal vs. Glucose. **(c)** InsGLuc-MIN6 cells were acutely
614 treated for 1h with DMSO, FPL64176, or FPL64176 + SW016789 in the presence or absence of
615 glucose. Data are the mean ± SD of four independent experiments. *,P<0.05 vs DMSO. **(d)**
616 Normal GSCa can be observed with glucose and DMSO (peach) and is enhanced by SW016789
617 (red). FPL64176 rapidly potentiates glucose-stimulated Ca^{2+} influx in MIN6 cells (green). In the
618 absence of glucose, DMSO (black), FPL64176 (grey) and SW016789 (blue) have little effect
619 individually, but together FPL64176 and SW016789 synergize to stimulate Ca^{2+} influx (pink). Data
620 are the mean ± SD of three independent experiments.

621 **Figure 8. Chemical suppressor screen uncovers VDCC inhibitors as protective agents in**
622 **chronic SW016789 treatment in MIN6 beta cells and human islets. (a)** InsGLuc-MIN6 cells
623 were co-incubated with SW016789 (5 μM), and candidate small molecules as indicated. Following
624 24 h incubation, all treatments were removed and glucose-stimulated InsGLuc secretion
625 responses were assessed. **(b)** InsGLuc-MIN6 cells pretreated in complete medium for 24 h with
626 DMSO (0.1%) or SW016789 (5 μM) in the presence or absence of nifedipine (10 μM). After
627 compound washout cells were stimulated with or without glucose (20 mM) for 1 h for InsGLuc
628 assays. Data are the mean ± SD of five independent experiments. **(c)** Cells were treated as in **(b)**
629 and *Ddit3* gene expression was measured. Data are the mean ± SD of four independent
630 experiments. **(d)** InsGLuc-MIN6 cells were acutely incubated with DMSO (0.1%), nifedipine
631 (10μM), SW016789 (5μM), or nifedipine + SW016789 for 1h in the presence or absence of
632 glucose (20mM). Data are the mean ± SD of four independent experiments. **(e)** Human islets were
633 treated 24 h in complete medium with DMSO (0.1%) and SW016789 (5 μM) in the presence or
634 absence of nifedipine (10 μM). Islets were washed and incubated in low glucose (1 mM) KRBH for

1 h, buffer discarded, then incubated 1 h in low (1 mM) or high (16 mM) glucose KRBH for 1 h. Data represent the mean ± SD of insulin measured in supernatant normalized to total insulin content from six different donor islet preparations. *, P<0.05 by two-way ANOVA.

Acknowledgements

We thank past and present members of the Cobb lab, Whitehurst lab and D. Rosenbaum at UT Southwestern; D. Eizirik and M. Cnop at Université libre de Bruxelles; and A. Templin at IBRI for helpful discussions. Thanks to C. Cheng in the Whitehurst lab and C. Llamas in the Mishra lab at UT Southwestern for training and advice on Seahorse experiments. Thanks to the L. Zacharias and the DeBerardinis lab at UT Southwestern for advice on metabolomics analyses. Agonist and antagonist functional data on GPCRs for SW016789 were generously provided by B. Roth's group through the National Institute of Mental Health's Psychoactive Drug Screening Program, Contract # HHSN-271-2018-00023-C (NIMH PDSP). MIN6 beta cells were originally generated by J Miyazaki [64] and were kindly shared with us via the late J.C. Hutton. Human QGP1 somatostatinoma cells were a gift from D. Quelle (University of Iowa Carver College of Medicine). Mouse intestinal GLUTag L cells were originally generated by D. Drucker (Mount Sinai Hospital) and were shared with us by the lab of G.G. Holz (Upstate Medical University).

Data availability: All data generated or analyzed during this study are included in this published article (and its electronic supplementary materials).

Funding: This work was supported by the Juvenile Diabetes Research Foundation (2-SRA-2019-702-Q-R to MAK), the Diabetes Research Connection (to MAK), internal funding from the Indiana Biosciences Research Institute (to MAK), and the Welch Foundation (I1243 to MHC). Human pancreatic islets were provided by the National Institute of Diabetes and Digestive and Kidney Diseases (NIDDK)-funded Integrated Islet Distribution Program (IIDP) (RRID:SCR_014387) at City of Hope (National Institutes of Health Grant # 2UC4DK098085) and the JDRF-funded IIDP Islet Award Initiative (BS438P to MAK).

Contribution statement:

Conceptualization: M.A. Kalwat.

Data curation: M.A. Kalwat.

Formal analysis: K. Rodrigues-dos-Santos, G. Roy, D.D. Binns, F. Armoo, and M.A. Kalwat.

Funding acquisition: M.A. Kalwat and M.H. Cobb.

668 Investigation: K. Rodrigues-dos-Santos, G. Roy, D.D. Binns, M.G. Grzemska, F. Armoo, M.K.
669 McCoy, A. Huynh, J.Z. Yang, and M.A. Kalwat.
670 Methodology: M.A. Kalwat.
671 Project administration: M.A. Kalwat.
672 Resources: B.A. Posner, M.H. Cobb, and M.A. Kalwat
673 Supervision: M.H. Cobb and M.A. Kalwat
674 Validation: K. Rodrigues-dos-Santos, G. Roy, D.D. Binns, M.G. Grzemska, J.Z. Yang, and M.A.
675 Kalwat.
676 Visualization: K. Rodrigues-dos-Santos, G. Roy, and M.A. Kalwat.
677 Writing - original draft: M.A. Kalwat.
678 Writing - review & editing: K. Rodrigues-dos-Santos, G. Roy, D.D. Binns, L. Barella, M.H. Cobb,
679 and M.A. Kalwat
680 M.A. Kalwat is the guarantor and accepts full responsibility for the work and/or the conduct of the
681 study, had access to the data, and controlled the decision to publish.

682 **References**

683 1. Alejandro EU, Gregg B, Blandino-Rosano M, Cras-Meneur C, Bernal-Mizrachi E. Natural
684 history of beta-cell adaptation and failure in type 2 diabetes. Mol Aspects Med. 2015;42:19-
685 41. doi: 10.1016/j.mam.2014.12.002. PMID: 25542976. PMCID: PMC4404183.
686 2. Berger C, Zdzieblo D. Glucose transporters in pancreatic islets. Pflugers Arch.
687 2020;472(9):1249-72. doi: 10.1007/s00424-020-02383-4. PMID: 32394191. PMCID:
688 PMC7462922.
689 3. Rorsman P, Ashcroft FM. Pancreatic beta-Cell Electrical Activity and Insulin Secretion: Of
690 Mice and Men. Physiol Rev. 2018;98(1):117-214. doi: 10.1152/physrev.00008.2017. PMID:
691 29212789. PMCID: PMC5866358.
692 4. Lewandowski SL, Cardone RL, Foster HR, Ho T, Potapenko E, Poudel C, et al. Pyruvate
693 Kinase Controls Signal Strength in the Insulin Secretory Pathway. Cell Metab.
694 2020;32(5):736-50 e5. doi: 10.1016/j.cmet.2020.10.007. PMID: 33147484. PMCID:
695 PMC7685238.
696 5. Nicholls DG. The Pancreatic beta-Cell: A Bioenergetic Perspective. Physiol Rev.
697 2016;96(4):1385-447. doi: 10.1152/physrev.00009.2016. PMID: 27582250.
698 6. Thurmond DC, Gaisano HY. Recent insights into beta-cell exocytosis in type 2 diabetes. J
699 Mol Biol. 2019. doi: 10.1016/j.jmb.2019.12.012. PMID: 31863749.
700 7. Henquin JC. Triggering and amplifying pathways of regulation of insulin secretion by
701 glucose. Diabetes. 2000;49(11):1751-60. doi: 10.2337/diabetes.49.11.1751. PMID:
702 11078440.
703 8. Kalwat MA, Cobb MH. Mechanisms of the amplifying pathway of insulin secretion in the
704 beta cell. Pharmacol Ther. 2017;179:17-30. doi: 10.1016/j.pharmthera.2017.05.003. PMID:
705 28527919. PMCID: PMC7269041.
706 9. Prentki M, Matschinsky FM, Madiraju SR. Metabolic signaling in fuel-induced insulin
707 secretion. Cell Metab. 2013;18(2):162-85. doi: 10.1016/j.cmet.2013.05.018. PMID:
708 23791483.

10. Kalwat MA, Scheuner D, Rodrigues Dos Santos K, Eizirik DL, Cobb MH. The pancreatic beta cell response to secretory demands and adaption to stress. Endocrinology. 2021. doi: 10.1210/endocr/bqab173. PMID: 34407177.
11. Delepine M, Nicolino M, Barrett T, Golamaully M, Lathrop GM, Julier C. EIF2AK3, encoding translation initiation factor 2-alpha kinase 3, is mutated in patients with Wolcott-Rallison syndrome. Nat Genet. 2000;25(4):406-9. doi: 10.1038/78085. PMID: 10932183.
12. Shalev A, Pise-Masison CA, Radonovich M, Hoffmann SC, Hirshberg B, Brady JN, et al. Oligonucleotide microarray analysis of intact human pancreatic islets: identification of glucose-responsive genes and a highly regulated TGFbeta signaling pathway. Endocrinology. 2002;143(9):3695-8. doi: 10.1210/en.2002-220564. PMID: 12193586.
13. Oyadomari S, Koizumi A, Takeda K, Gotoh T, Akira S, Araki E, et al. Targeted disruption of the Chop gene delays endoplasmic reticulum stress–mediated diabetes. Journal of Clinical Investigation. 2002;109(4):525-32. doi: 10.1172/jci200214550.
14. Sharma RB, O'Donnell AC, Stamateris RE, Ha B, McCloskey KM, Reynolds PR, et al. Insulin demand regulates beta cell number via the unfolded protein response. J Clin Invest. 2015;125(10):3831-46. doi: 10.1172/JCI79264. PMID: 26389675. PMCID: PMC4607122.
15. Lee H, Lee YS, Harenda Q, Pietrzak S, Oktay HZ, Schreiber S, et al. Beta Cell Dedifferentiation Induced by IRE1alpha Deletion Prevents Type 1 Diabetes. Cell Metab. 2020;31(4):822-36 e5. doi: 10.1016/j.cmet.2020.03.002. PMID: 32220307. PMCID: PMC7346095.
16. Eizirik DL, Pasquali L, Cnop M. Pancreatic beta-cells in type 1 and type 2 diabetes mellitus: different pathways to failure. Nat Rev Endocrinol. 2020;16(7):349-62. doi: 10.1038/s41574-020-0355-7. PMID: 32398822.
17. Engin F. ER stress and development of type 1 diabetes. J Investig Med. 2016;64(1):2-6. doi: 10.1097/JIM.0000000000000229. PMID: 26230493.
18. Herbert TP, Laybutt DR. A Reevaluation of the Role of the Unfolded Protein Response in Islet Dysfunction: Maladaptation or a Failure to Adapt? Diabetes. 2016;65(6):1472-80. doi: 10.2337/db15-1633. PMID: 27222391.
19. Burns SM, Vetere A, Walpita D, Dancik V, Khodier C, Perez J, et al. High-throughput luminescent reporter of insulin secretion for discovering regulators of pancreatic Beta-cell function. Cell Metab. 2015;21(1):126-37. doi: 10.1016/j.cmet.2014.12.010. PMID: 25565210.
20. Kalwat MA, Wichaidit C, Nava Garcia AY, McCoy MK, McGlynn K, Hwang IH, et al. Insulin promoter-driven Gaussia luciferase-based insulin secretion biosensor assay for discovery of beta-cell glucose-sensing pathways. ACS Sens. 2016;1(10):1208-12. doi: 10.1021/acssensors.6b00433. PMID: 27819058. PMCID: PMC5089812.
21. Kalwat MA. High-Throughput Screening for Insulin Secretion Modulators. Methods Mol Biol. 2021;2233:131-8. doi: 10.1007/978-1-0716-1044-2_9. PMID: 33222132. PMCID: PMC8812827.
22. Mullen AR, Hu Z, Shi X, Jiang L, Boroughs LK, Kovacs Z, et al. Oxidation of alpha-ketoglutarate is required for reductive carboxylation in cancer cells with mitochondrial defects. Cell Rep. 2014;7(5):1679-90. doi: 10.1016/j.celrep.2014.04.037. PMID: 24857658. PMCID: 4057960.
23. Kalwat MA, Huang Z, Wichaidit C, McGlynn K, Earnest S, Savoia C, et al. Isoxazole alters metabolites and gene expression, decreasing proliferation and promoting a neuroendocrine phenotype in beta-cells. ACS Chem Biol. 2016;11(4):1128-36. doi: 10.1021/acschembio.5b00993. PMID: 26828310. PMCID: PMC5198576.
24. Chong J, Soufan O, Li C, Caraus I, Li S, Bourque G, et al. MetaboAnalyst 4.0: towards more transparent and integrative metabolomics analysis. Nucleic Acids Res.

2018;46(W1):W486-W94. doi: 10.1093/nar/gky310. PMID: 29762782. PMCID: PMC6030889.
25. Kalwat MA, Hwang IH, Macho J, Grzemska MG, Yang JZ, McGlynn K, et al. Chromomycin A2 potently inhibits glucose-stimulated insulin secretion from pancreatic beta cells. J Gen Physiol. 2018;150(12):1747-57. doi: 10.1085/jgp.201812177. PMID: 30352794. PMCID: PMC6279362.
26. Hager R, Pitsch J, Kerbl-Knapp J, Neuhauser C, Ollinger N, Iken M, et al. A High-Content Screen for the Identification of Plant Extracts with Insulin Secretion-Modulating Activity. Pharmaceuticals (Basel). 2021;14(8). doi: 10.3390/ph14080809. PMID: 34451906. PMCID: PMC8402219.
27. Praznik A, Fink T, Franko N, Lonzaric J, Bencina M, Jerala N, et al. Regulation of protein secretion through chemical regulation of endoplasmic reticulum retention signal cleavage. Nat Commun. 2022;13(1):1323. doi: 10.1038/s41467-022-28971-9. PMID: 35260576.
28. Cardenas-Diaz FL, Leavens KF, Kishore S, Osorio-Quintero C, Chen YJ, Stanger BZ, et al. A Dual Reporter EndoC-betaH1 Human beta-Cell Line for Efficient Quantification of Calcium Flux and Insulin Secretion. Endocrinology. 2020;161(2). doi: 10.1210/endocr/bqaa005. PMID: 31960055. PMCID: PMC7028009.
29. Shariati K, Pappalardo Z, Chopra DG, Yiv N, Sheen R, Ku G. Selective monitoring of insulin secretion after CRISPR interference in intact pancreatic islets despite submaximal infection. Islets. 2020:1-11. doi: 10.1080/19382014.2020.1752072. PMID: 32579048.
30. Barella LF, Jain S, Kimura T, Pydi SP. Metabolic roles of G protein-coupled receptor signaling in obesity and type 2 diabetes. FEBS J. 2021. doi: 10.1111/febs.15800. PMID: 33682344.
31. Jiang LI, Collins J, Davis R, Lin KM, DeCamp D, Roach T, et al. Use of a cAMP BRET sensor to characterize a novel regulation of cAMP by the sphingosine 1-phosphate/G13 pathway. J Biol Chem. 2007;282(14):10576-84. doi: 10.1074/jbc.M609695200. PMID: 17283075. PMCID: PMC2526465.
32. Kroeze WK, Sassano MF, Huang XP, Lansu K, McCorvy JD, Giguere PM, et al. PRESTO-Tango as an open-source resource for interrogation of the druggable human GPCRome. Nat Struct Mol Biol. 2015;22(5):362-9. doi: 10.1038/nsmb.3014. PMID: 25895059. PMCID: PMC4424118.
33. Wijtmans M, Maussang D, Sirci F, Scholten DJ, Canals M, Mujić-Delić A, et al. Synthesis, modeling and functional activity of substituted styrene-amides as small-molecule CXCR7 agonists. European Journal of Medicinal Chemistry. 2012;51:184-92. doi: 10.1016/j.ejmech.2012.02.041.
34. Santo-Domingo J, Chareyron I, Dayon L, Nunez Galindo A, Cominetti O, Pilar Giner Gimenez M, et al. Coordinated activation of mitochondrial respiration and exocytosis mediated by PKC signaling in pancreatic beta-cells. FASEB J. 2016. doi: 10.1096/fj.201600837R. PMID: 27927723.
35. Yaney GC, Fairbanks JM, Deeney JT, Korchak HM, Tornheim K, Corkey BE. Potentiation of insulin secretion by phorbol esters is mediated by PKC-alpha and nPKC isoforms. Am J Physiol Endocrinol Metab. 2002;283(5):E880-8. doi: 10.1152/ajpendo.00474.2001. PMID: 12376314.
36. Brose N, Rosenmund C. Move over protein kinase C, you've got company: alternative cellular effectors of diacylglycerol and phorbol esters. J Cell Sci. 2002;115(Pt 23):4399-411. doi: 10.1242/jcs.00122. PMID: 12414987.
37. Newton AC. Protein kinase C: perfectly balanced. Crit Rev Biochem Mol Biol. 2018;53(2):208-30. doi: 10.1080/10409238.2018.1442408. PMID: 29513138. PMCID: PMC5901981.

807 38. Hii CS, Jones PM, Persaud SJ, Howell SL. A re-assessment of the role of protein kinase C
808 in glucose-stimulated insulin secretion. Biochem J. 1987;246(2):489-93. doi:
809 10.1042/bj2460489. PMID: 3318809. PMCID: PMC1148300.
810 39. Jones PM, Persaud SJ, Howell SL. Insulin secretion and protein phosphorylation in PKC-
811 depleted islets of langerhans. Life Sciences. 1992;50(11):761-7. doi: 10.1016/0024-
812 3205(92)90180-w.
813 40. Uchida T, Iwashita N, Ohara-Imaizumi M, Ogihara T, Nagai S, Choi JB, et al. Protein
814 kinase Cdelta plays a non-redundant role in insulin secretion in pancreatic beta cells. J Biol
815 Chem. 2007;282(4):2707-16. doi: 10.1074/jbc.M610482200. PMID: 17135234.
816 41. Thompson B, Satin LS. Beta-Cell Ion Channels and Their Role in Regulating Insulin
817 Secretion. Compr Physiol. 2021;11(4):1-21. doi: 10.1002/cphy.c210004. PMID: 34636409.
818 42. Cook DL, Satin LS, Ashford ML, Hales CN. ATP-sensitive K+ channels in pancreatic beta-
819 cells. Spare-channel hypothesis. Diabetes. 1988;37(5):495-8. doi: 10.2337/diab.37.5.495.
820 PMID: 2452107.
821 43. Yusta B, Baggio LL, Estall JL, Koehler JA, Holland DP, Li H, et al. GLP-1 receptor
822 activation improves beta cell function and survival following induction of endoplasmic
823 reticulum stress. Cell Metab. 2006;4(5):391-406. doi: 10.1016/j.cmet.2006.10.001. PMID:
824 17084712.
825 44. Szabat M, Page MM, Panzhinskiy E, Skovso S, Mojibian M, Fernandez-Tajes J, et al.
826 Reduced Insulin Production Relieves Endoplasmic Reticulum Stress and Induces beta Cell
827 Proliferation. Cell Metab. 2016;23(1):179-93. doi: 10.1016/j.cmet.2015.10.016. PMID:
828 26626461.
829 45. Merovci A, Tripathy D, Chen X, Valdez I, Abdul-Ghani M, Solis-Herrera C, et al. Effect of
830 Mild Physiologic Hyperglycemia on Insulin Secretion, Insulin Clearance, and Insulin
831 Sensitivity in Healthy Glucose-Tolerant Subjects. Diabetes. 2021;70(1):204-13. doi:
832 10.2337/db20-0039. PMID: 33033064. PMCID: PMC7881846.
833 46. Marselli L, Piron A, Suleiman M, Colli ML, Yi X, Khamis A, et al. Persistent or Transient
834 Human beta Cell Dysfunction Induced by Metabolic Stress: Specific Signatures and Shared
835 Gene Expression with Type 2 Diabetes. Cell Rep. 2020;33(9):108466. doi:
836 10.1016/j.celrep.2020.108466. PMID: 33264613.
837 47. Tatsuoka H, Sakamoto S, Yabe D, Kabai R, Kato U, Okumura T, et al. Single-Cell
838 Transcriptome Analysis Dissects the Replicating Process of Pancreatic Beta Cells in Partial
839 Pancreatectomy Model. iScience. 2020;23(12):101774. doi: 10.1016/j.isci.2020.101774.
840 PMID: 33294783. PMCID: PMC7689163.
841 48. Charbord J, Ren L, Sharma RB, Johansson A, Ågren R, Chu L, et al. In vivo screen
842 identifies a SIK inhibitor that induces β cell proliferation through a transient UPR. Nature
843 Metabolism. 2021;3(5):682-700. doi: 10.1038/s42255-021-00391-x.
844 49. Speckmann T, Sabatini PV, Nian C, Smith RG, Lynn FC. Npas4 Transcription Factor
845 Expression Is Regulated by Calcium Signaling Pathways and Prevents Tacrolimus-induced
846 Cytotoxicity in Pancreatic Beta Cells. J Biol Chem. 2016;291(6):2682-95. doi:
847 10.1074/jbc.M115.704098. PMID: 26663079. PMCID: PMC4742737.
848 50. Sabatini PV, Krentz NA, Zarrouki B, Westwell-Roper CY, Nian C, Uy RA, et al. Npas4 is a
849 novel activity-regulated cytoprotective factor in pancreatic beta-cells. Diabetes.
850 2013;62(8):2808-20. doi: 10.2337/db12-1527. PMID: 23656887. PMCID: 3717850.
851 51. Ovalle F, Grimes T, Xu G, Patel AJ, Grayson TB, Thielen LA, et al. Verapamil and beta cell
852 function in adults with recent-onset type 1 diabetes. Nat Med. 2018;24(8):1108-12. doi:
853 10.1038/s41591-018-0089-4. PMID: 29988125. PMCID: PMC6092963.
854 52. Zhao D, Cao Y, Yu CG, Yuan SS, Zhang N, Zhang YY, et al. The association of calcium
855 channel blockers with beta-cell function in type 2 diabetic patients: A cross-sectional study.
856 J Clin Hypertens (Greenwich). 2019. doi: 10.1111/jch.13517. PMID: 30900372.

857 53. Xu G, Chen J, Jing G, Shalev A. Preventing beta-cell loss and diabetes with calcium
858 channel blockers. Diabetes. 2012;61(4):848-56. doi: 10.2337/db11-0955. PMID: 22442301.
859 PMCID: PMC3314354.
860 54. Syeda K, Mohammed AM, Arora DK, Kowluru A. Glucotoxic conditions induce endoplasmic
861 reticulum stress to cause caspase 3 mediated lamin B degradation in pancreatic beta-cells:
862 protection by nifedipine. Biochem Pharmacol. 2013;86(9):1338-46. doi:
863 10.1016/j.bcp.2013.08.023. PMID: 23994168. PMCID: PMC3832847.
864 55. Jeffrey KD, Alejandro EU, Luciani DS, Kalynyak TB, Hu X, Li H, et al. Carboxypeptidase E
865 mediates palmitate-induced beta-cell ER stress and apoptosis. Proceedings of the National
866 Academy of Sciences of the United States of America. 2008;105(24):8452-7. doi:
867 10.1073/pnas.0711232105. PMID: 18550819. PMCID: PMC2448857.
868 56. Wang Y, Gao L, Li Y, Chen H, Sun Z. Nifedipine protects INS-1 beta-cell from high
869 glucose-induced ER stress and apoptosis. Int J Mol Sci. 2011;12(11):7569-80. doi:
870 10.3390/ijms12117569. PMID: 22174617. PMCID: PMC3233423.
871 57. Tang L, Gamal El-Din TM, Swanson TM, Pryde DC, Scheuer T, Zheng N, et al. Structural
872 basis for inhibition of a voltage-gated Ca(2+) channel by Ca(2+) antagonist drugs. Nature.
873 2016;537(7618):117-21. doi: 10.1038/nature19102. PMID: 27556947. PMCID:
874 PMC5161592.
875 58. Zheng W, Rampe D, Triggle D. Pharmacological, radioligand binding, and
876 electrophysiological characteristics of FPL 64176, a novel nondihydropyridine Ca2+
877 channel activator, in cardiac and vascular preparations. Mol Pharm. 1991;40(5):734-41.
878 PMCID: 1719369.
879 59. Minami K, Yokokura M, Ishizuka N, Seino S. Normalization of intracellular Ca(2+) induces a
880 glucose-responsive state in glucose-unresponsive beta-cells. J Biol Chem.
881 2002;277(28):25277-82. doi: 10.1074/jbc.M203988200. PMID: 12101221.
882 60. De Mingo Alemany MC, Mifsud Grau L, Moreno Macian F, Ferrer Lorente B, Leon Carinena
883 S. A de novo CACNA1D missense mutation in a patient with congenital hyperinsulinism,
884 primary hyperaldosteronism and hypotonia. Channels (Austin). 2020;14(1):175-80. doi:
885 10.1080/19336950.2020.1761171. PMID: 32336187.
886 61. Theiner T, Jacobo-Piqueras N, Ortner NJ, Geisler SM, Tuluc P. CaV1.3 L-type Ca2+
887 channel modulates pancreatic beta-cell electrical activity and survival. J Gen Physiol.
888 2022;154(9). doi: 10.1085/jgp.2021ecc34. PMID: 34767006.
889 62. Lee K, Kim J, Kohler M, Yu J, Shi Y, Yang SN, et al. Blocking Ca(2+) Channel beta3
890 Subunit Reverses Diabetes. Cell Rep. 2018;24(4):922-34. doi:
891 10.1016/j.celrep.2018.06.086. PMID: 30044988. PMCID: PMC6083041.
892 63. Berggren PO, Yang SN, Murakami M, Efanov AM, Uhles S, Kohler M, et al. Removal of
893 Ca2+ channel beta3 subunit enhances Ca2+ oscillation frequency and insulin exocytosis.
894 Cell. 2004;119(2):273-84. doi: 10.1016/j.cell.2004.09.033. PMID: 15479643.
895 64. Miyazaki J, Araki K, Yamato E, Ikegami H, Asano T, Shibasaki Y, et al. Establishment of a
896 pancreatic beta cell line that retains glucose-inducible insulin secretion: special reference to
897 expression of glucose transporter isoforms. Endocrinology. 1990;127(1):126-32. doi:
898 10.1210/endo-127-1-126. PMID: 2163307.

899

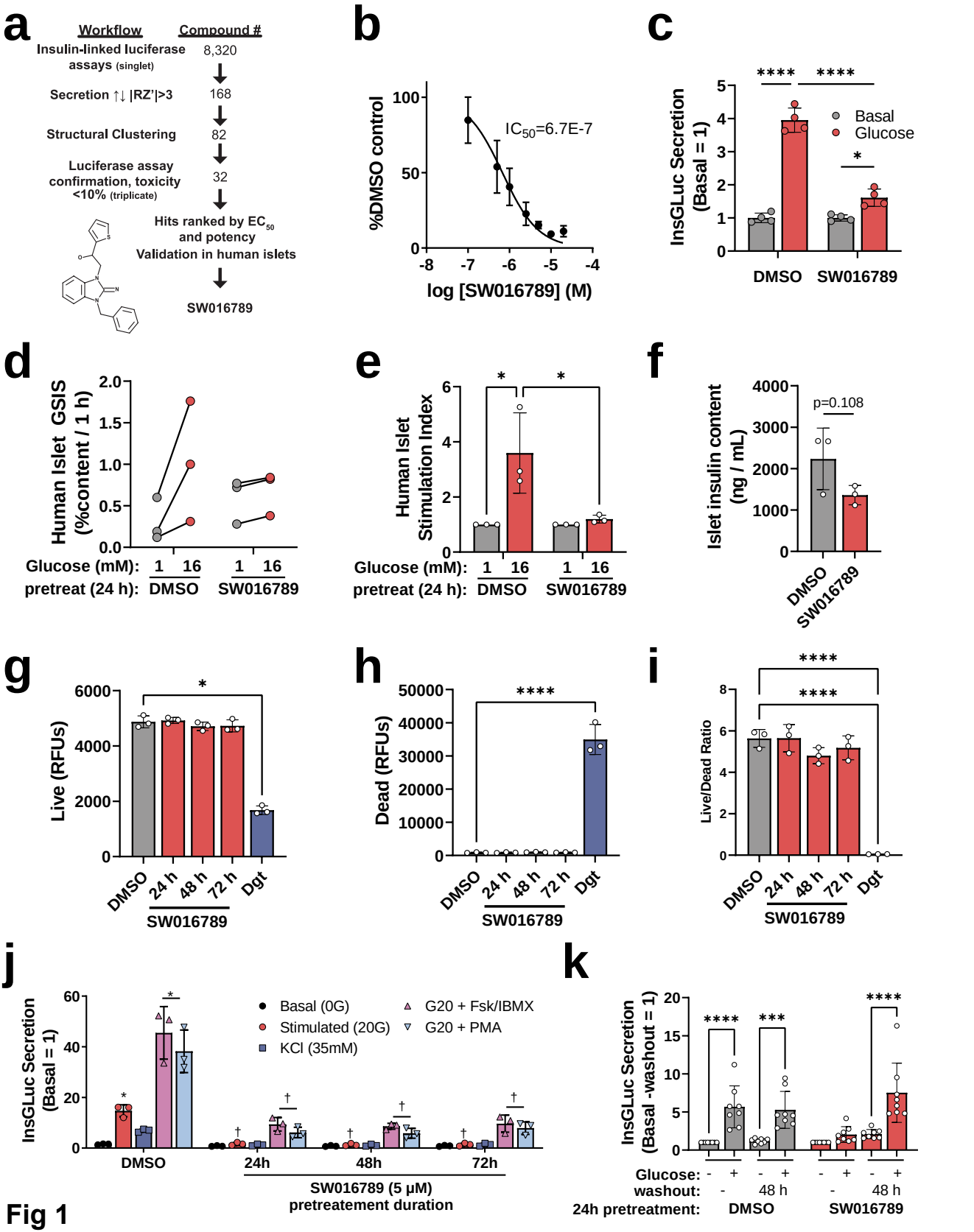
a
Workflow
Compound #
Insulin-linked luciferase assays (singlet)
8,320
Secretion ↑↓ |RZ'|>3
168
Structural Clustering
82
Luciferase assay confirmation, toxicity <10% (triplicate)
32
Hits ranked by EC50 and potency
Validation in human islets
SW016789
b
%DMSO control
IC50=6.7E-7
log [SW016789] (M)
c
InsGLuc Secretion (Basal = 1)
Basal
Glucose
DMSO
SW016789
d
Human Islet GSIS (%content / 1 h)
Glucose (mM): 1 16 1 16
pretreat (24 h): DMSO SW016789
e
Human Islet Stimulation Index
Glucose (mM): 1 16 1 16
pretreat (24 h): DMSO SW016789
f
Islet insulin content (ng / mL)
p=0.108
DMSO
SW016789
g
Live (RFUs)
DMSO
24 h
48 h
72 h
Dgt
SW016789
h
Dead (RFUs)
DMSO
24 h
48 h
72 h
Dgt
SW016789
i
Live/Dead Ratio
DMSO
24 h
48 h
72 h
Dgt
SW016789
j
InsGLuc Secretion (Basal = 1)
Basal (0G)
Stimulated (20G)
KCl (35mM)
G20 + Fsk/IBMX
G20 + PMA
DMSO
24h
48h
72h
SW016789 (5 μM) pretreatement duration
k
InsGLuc Secretion (Basal -washout = 1)
Glucose: - + - + - + - +
washout: - 48 h - 48 h
24h pretreatment: DMSO SW016789

Fig 1

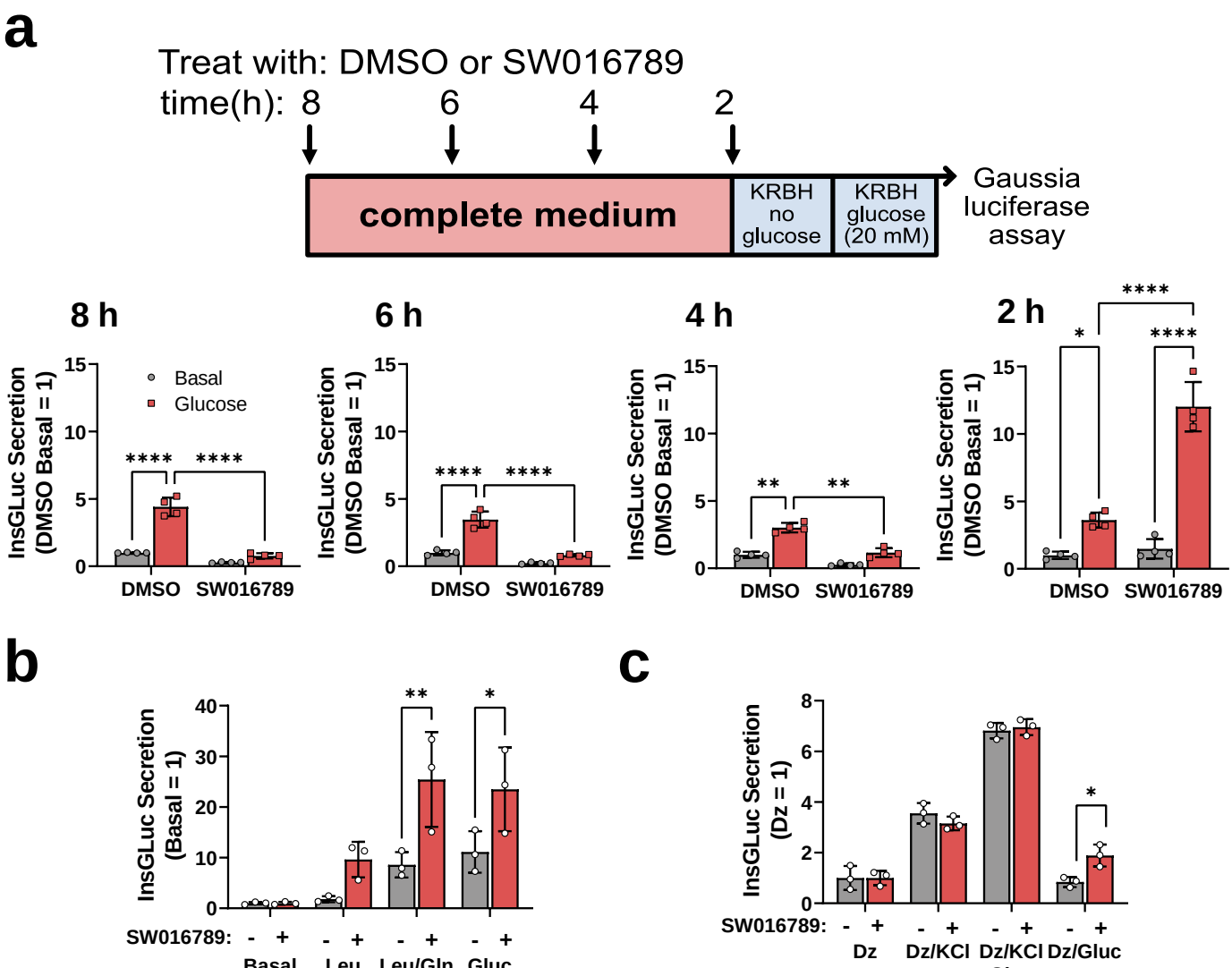
a
Treat with: DMSO or SW016789
time(h): 8 6 4 2
complete medium
KRBH no glucose
KRBH glucose (20 mM)
Gaussia luciferase assay
8 h
6 h
4 h
2 h
Basal
Glucose
InsGLuc Secretion (DMSO Basal = 1)
DMSO
SW016789
b
InsGLuc Secretion (Basal = 1)
SW016789:
Basal
Leu
Leu/Gln
Gluc
c
InsGLuc Secretion (Dz = 1)
Dz
Dz/KCl
Dz/KCl Gluc
Dz/Gluc

Fig 2

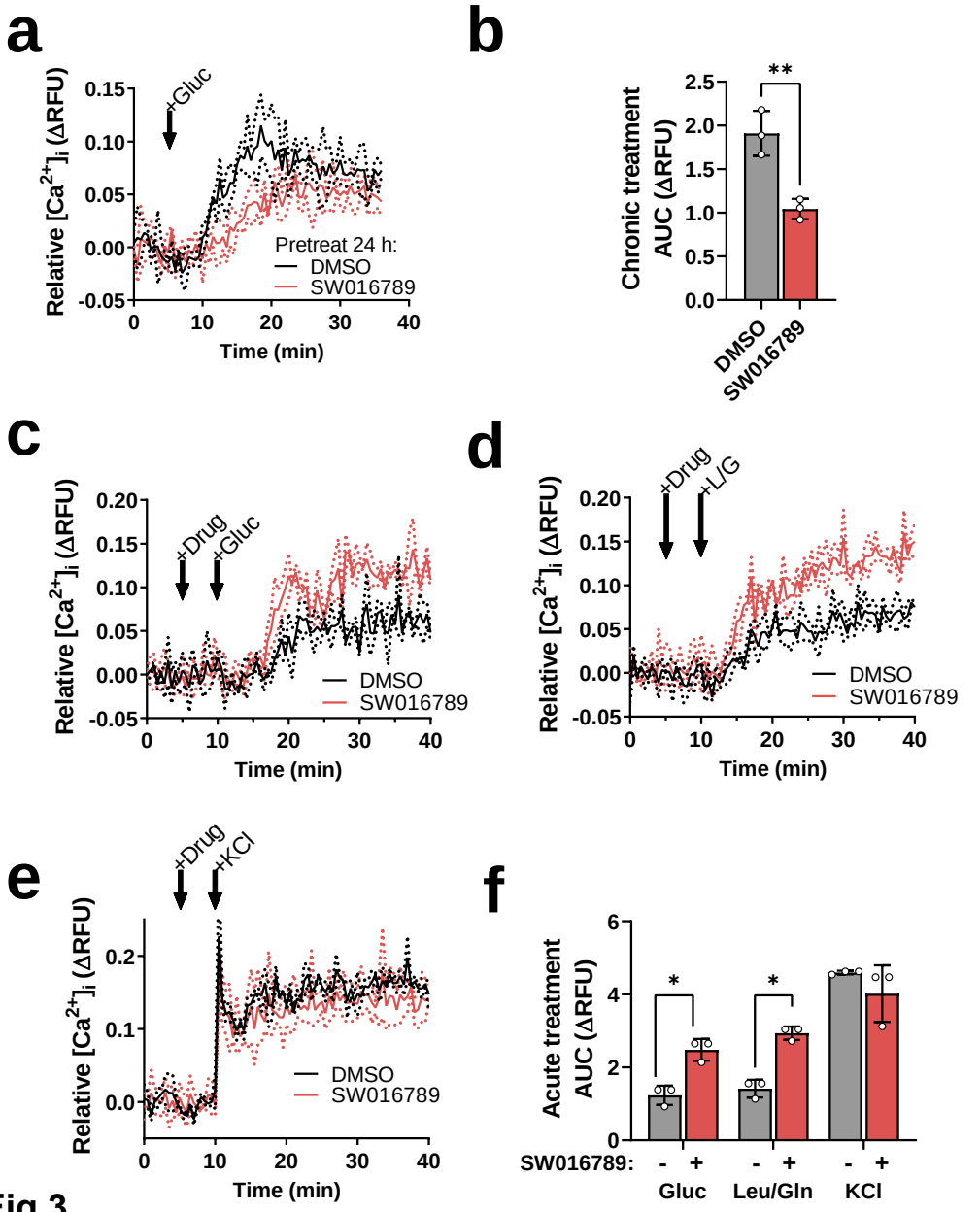
a
+Gluc
Relative [Ca2+]i (ΔRFU)
0.15
0.10
0.05
0.00
-0.05
0
10
20
30
40
Time (min)
Pretreat 24 h:
DMSO
SW016789
b
Chronic treatment AUC (ΔRFU)
2.5
2.0
1.5
1.0
0.5
0.0
**
DMSO
SW016789
c
+Drug
+Gluc
Relative [Ca2+]i (ΔRFU)
0.20
0.15
0.10
0.05
0.00
-0.05
0
10
20
30
40
Time (min)
DMSO
SW016789
d
+Drug
+L/G
Relative [Ca2+]i (ΔRFU)
0.20
0.15
0.10
0.05
0.00
-0.05
0
10
20
30
40
Time (min)
DMSO
SW016789
e
+Drug
+KCl
Relative [Ca2+]i (ΔRFU)
0.2
0.1
0.0
0
10
20
30
40
Time (min)
DMSO
SW016789
f
Acute treatment AUC (ΔRFU)
6
4
2
0
*
*
SW016789:
-
+
-
+
-
+
Gluc
Leu/Gln
KCl

Fig 3

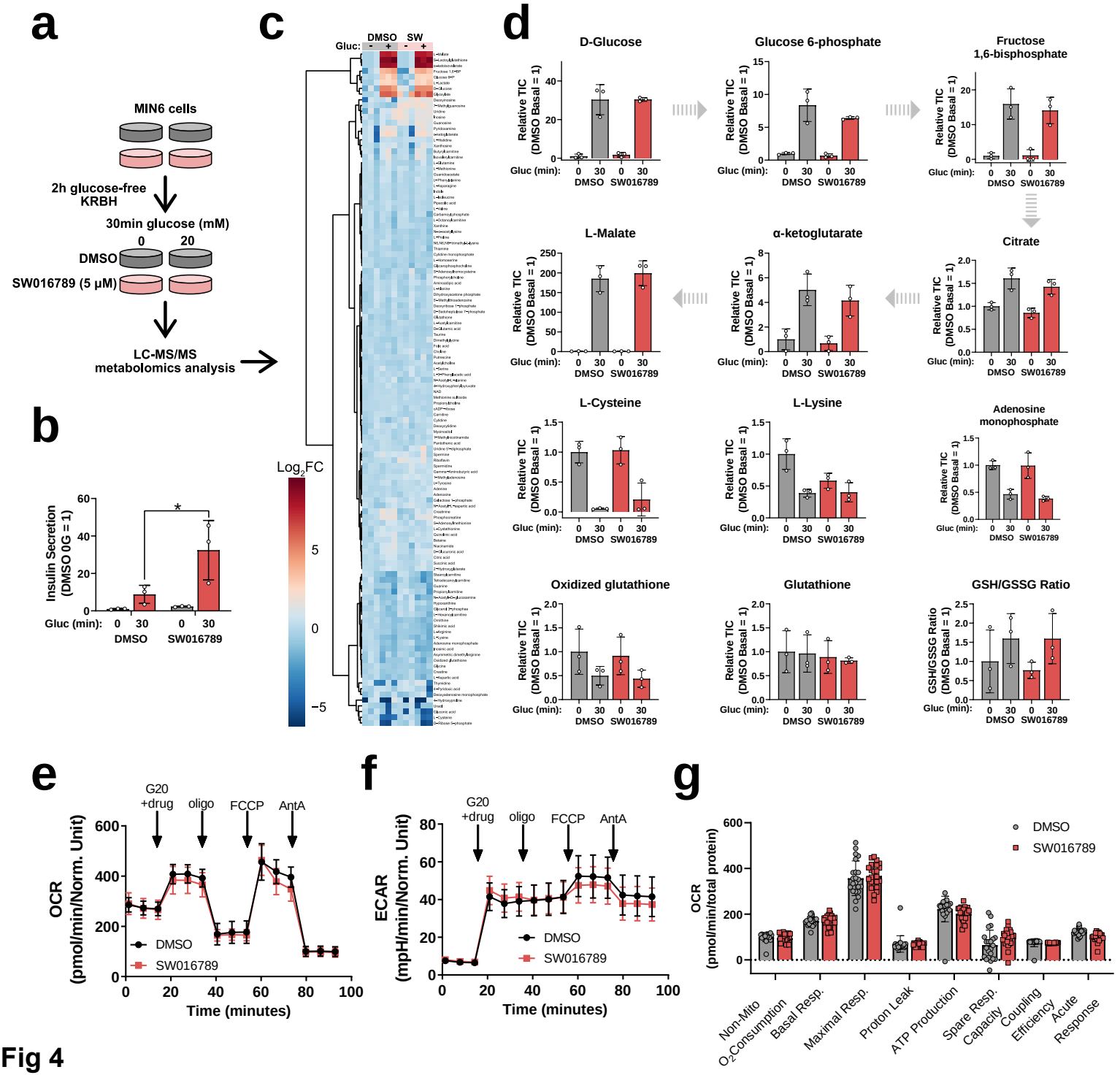
a
MIN6 cells
2h glucose-free KRBH
30min glucose (mM)
0
20
DMSO
SW016789 (5 μM)
LC-MS/MS metabolomics analysis
b
Insulin Secretion (DMSO 0G = 1)
Gluc (min):
DMSO
SW016789
c
DMSO
SW
Gluc:
Log2FC
d
D-Glucose
Glucose 6-phosphate
Fructose 1,6-bisphosphate
L-Malate
α-ketoglutarate
Citrate
L-Cysteine
L-Lysine
Adenosine monophosphate
Oxidized glutathione
Glutathione
GSH/GSSG Ratio
Relative TIC (DMSO Basal = 1)
e
G20 +drug
oligo
FCCP
AntA
OCR (pmol/min/Norm. Unit)
Time (minutes)
f
ECAR (mpH/min/Norm. Unit)
g
OCR (pmol/min/total protein)
Non-Mito O2 Consumption
Basal Resp.
Maximal Resp.
Proton Leak
ATP Production
Spare Resp. Capacity
Coupling Efficiency
Acute Response

Fig 4

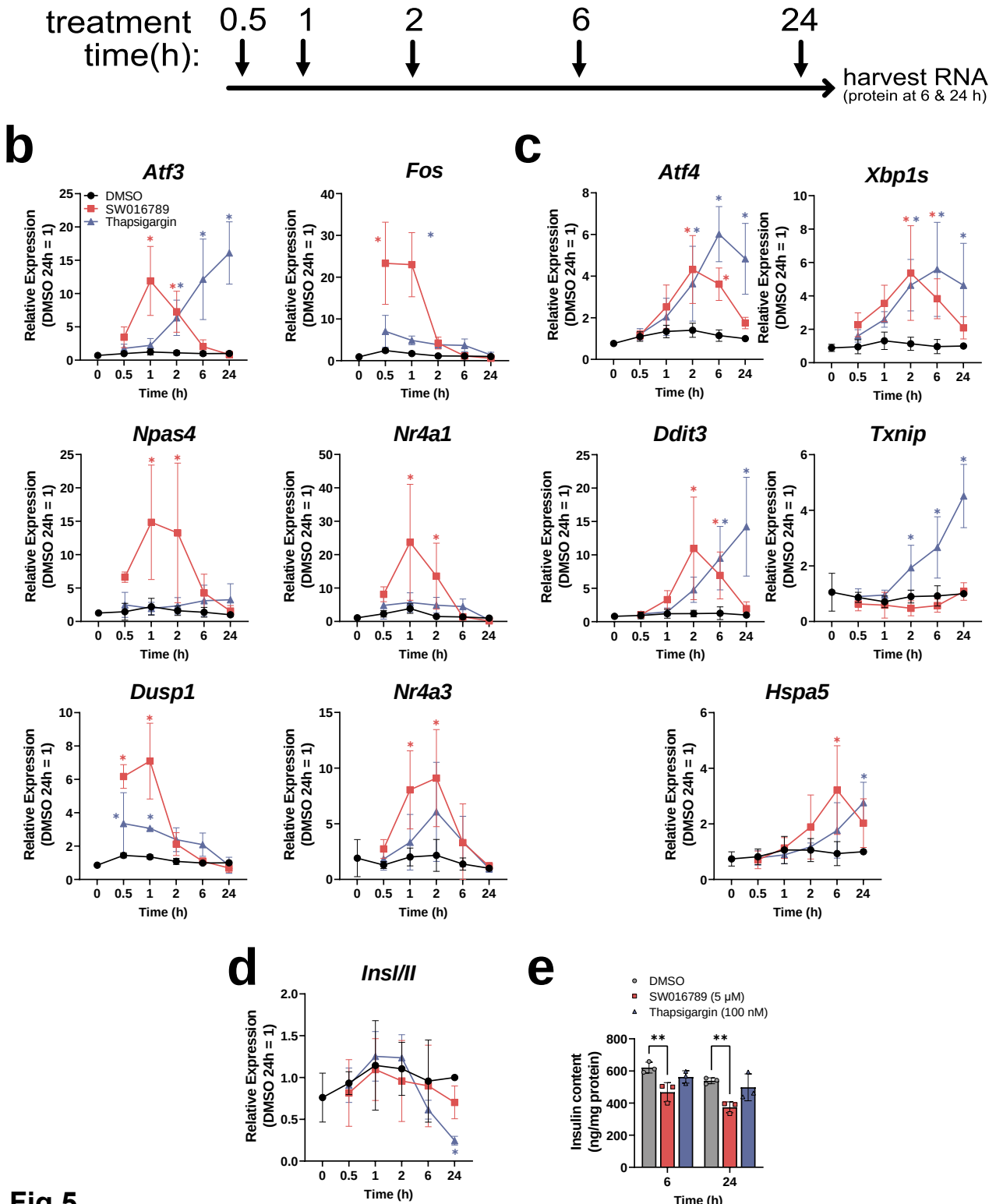
a
Treat MIN6 β cells: DMSO, SW016789, or thapsigargin
treatment time(h):
0.5
1
2
6
24
harvest RNA
(protein at 6 & 24 h)
b
c
Atf3
Fos
Atf4
Xbp1s
Npas4
Nr4a1
Ddit3
Txnip
Dusp1
Nr4a3
Hspa5
DMSO
SW016789
Thapsigargin
Relative Expression (DMSO 24h = 1)
Time (h)
d
Insl/II
e
DMSO
SW016789 (5 μM)
Thapsigargin (100 nM)
Insulin content (ng/mg protein)
Time (h)

Fig 5

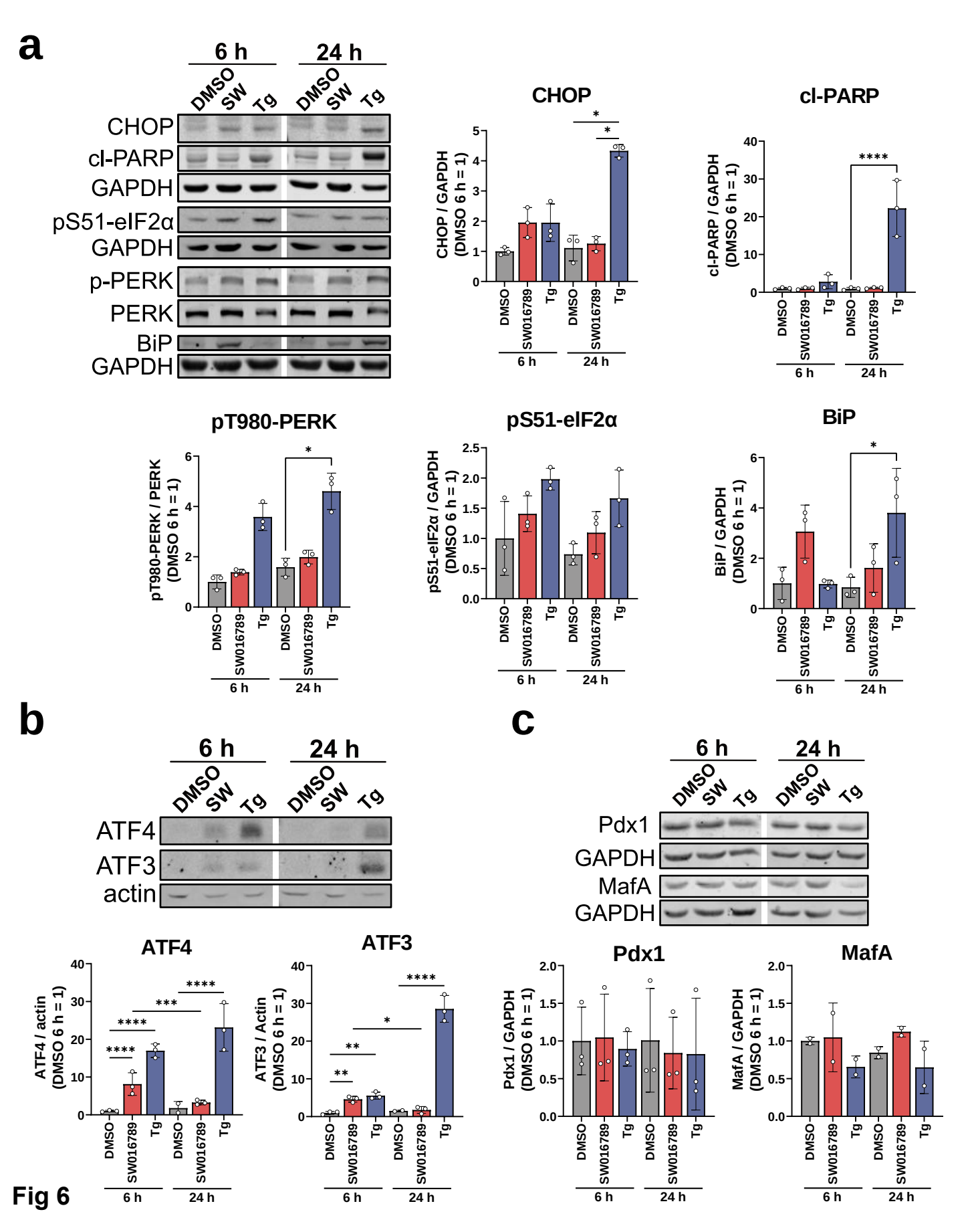
a
6 h
24 h
DMSO
SW
Tg
CHOP
cl-PARP
GAPDH
pS51-eIF2α
GAPDH
p-PERK
PERK
BiP
GAPDH
CHOP
CHOP / GAPDH (DMSO 6 h = 1)
cl-PARP
cl-PARP / GAPDH (DMSO 6 h = 1)
pT980-PERK
pT980-PERK / PERK (DMSO 6 h = 1)
pS51-eIF2α
pS51-eIF2α / GAPDH (DMSO 6 h = 1)
BiP
BiP / GAPDH (DMSO 6 h = 1)
DMSO
SW016789
Tg
6 h
24 h
b
ATF4
ATF3
actin
ATF4
ATF4 / actin (DMSO 6 h = 1)
ATF3
ATF3 / Actin (DMSO 6 h = 1)
c
Pdx1
GAPDH
MafA
GAPDH
Pdx1
Pdx1 / GAPDH (DMSO 6 h = 1)
MafA
MafA / GAPDH (DMSO 6 h = 1)

Fig 6

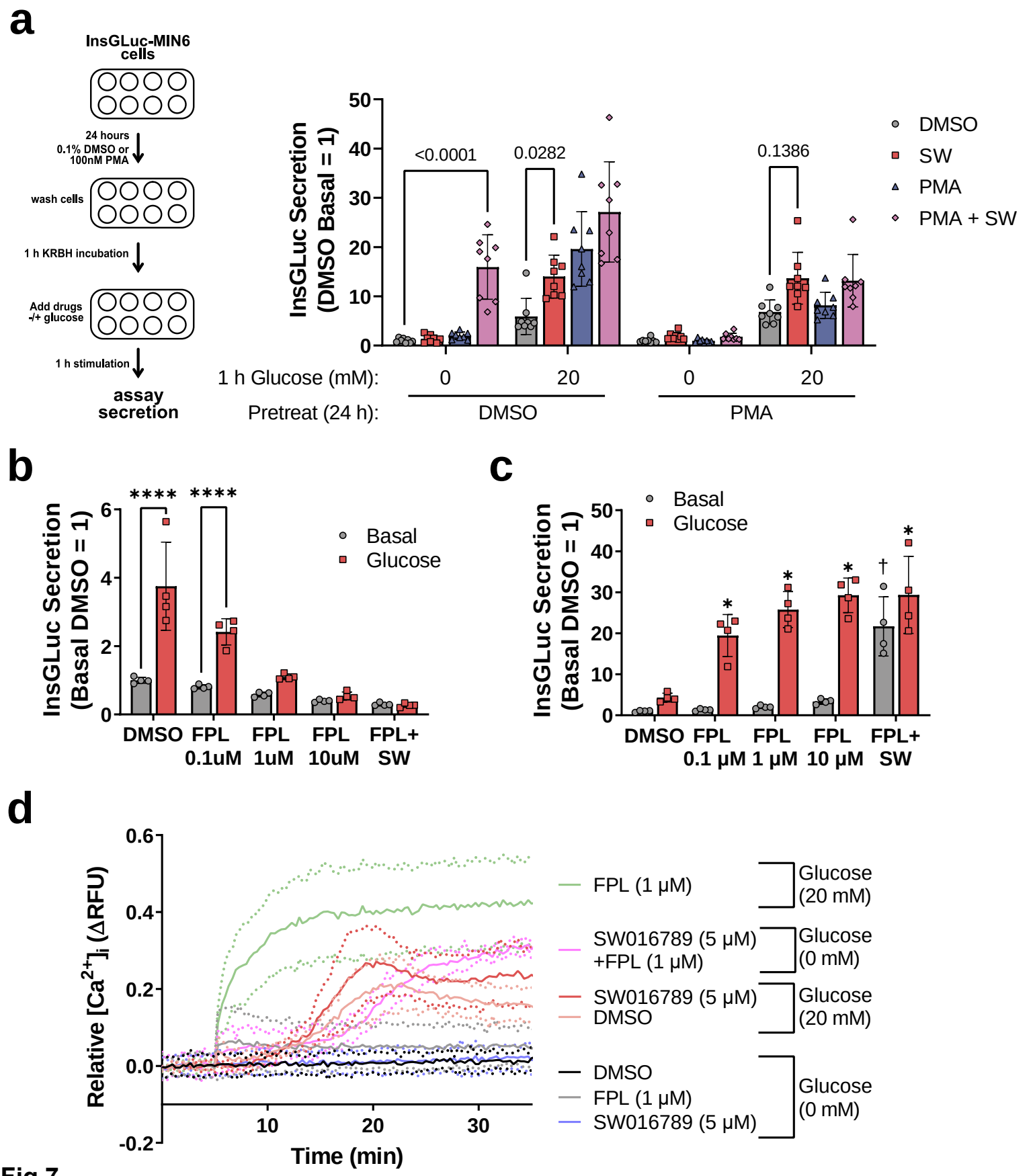
a
InsGLuc-MIN6 cells
24 hours
0.1% DMSO or 100nM PMA
wash cells
1 h KRBH incubation
Add drugs -/+ glucose
1 h stimulation
assay secretion
InsGLuc Secretion (DMSO Basal = 1)
<0.0001
0.0282
0.1386
DMSO
SW
PMA
PMA + SW
1 h Glucose (mM): 0 20 0 20
Pretreat (24 h): DMSO PMA
b
InsGLuc Secretion (Basal DMSO = 1)
****
****
Basal
Glucose
DMSO
FPL 0.1uM
FPL 1uM
FPL 10uM
FPL+ SW
c
InsGLuc Secretion (Basal DMSO = 1)
Basal
Glucose
DMSO
FPL 0.1 μM
FPL 1 μM
FPL 10 μM
FPL+ SW
d
Relative [Ca2+]i (ΔRFU)
Time (min)
FPL (1 μM)
Glucose (20 mM)
SW016789 (5 μM) +FPL (1 μM)
Glucose (0 mM)
SW016789 (5 μM)
DMSO
Glucose (20 mM)
DMSO
FPL (1 μM)
SW016789 (5 μM)
Glucose (0 mM)

Fig 7

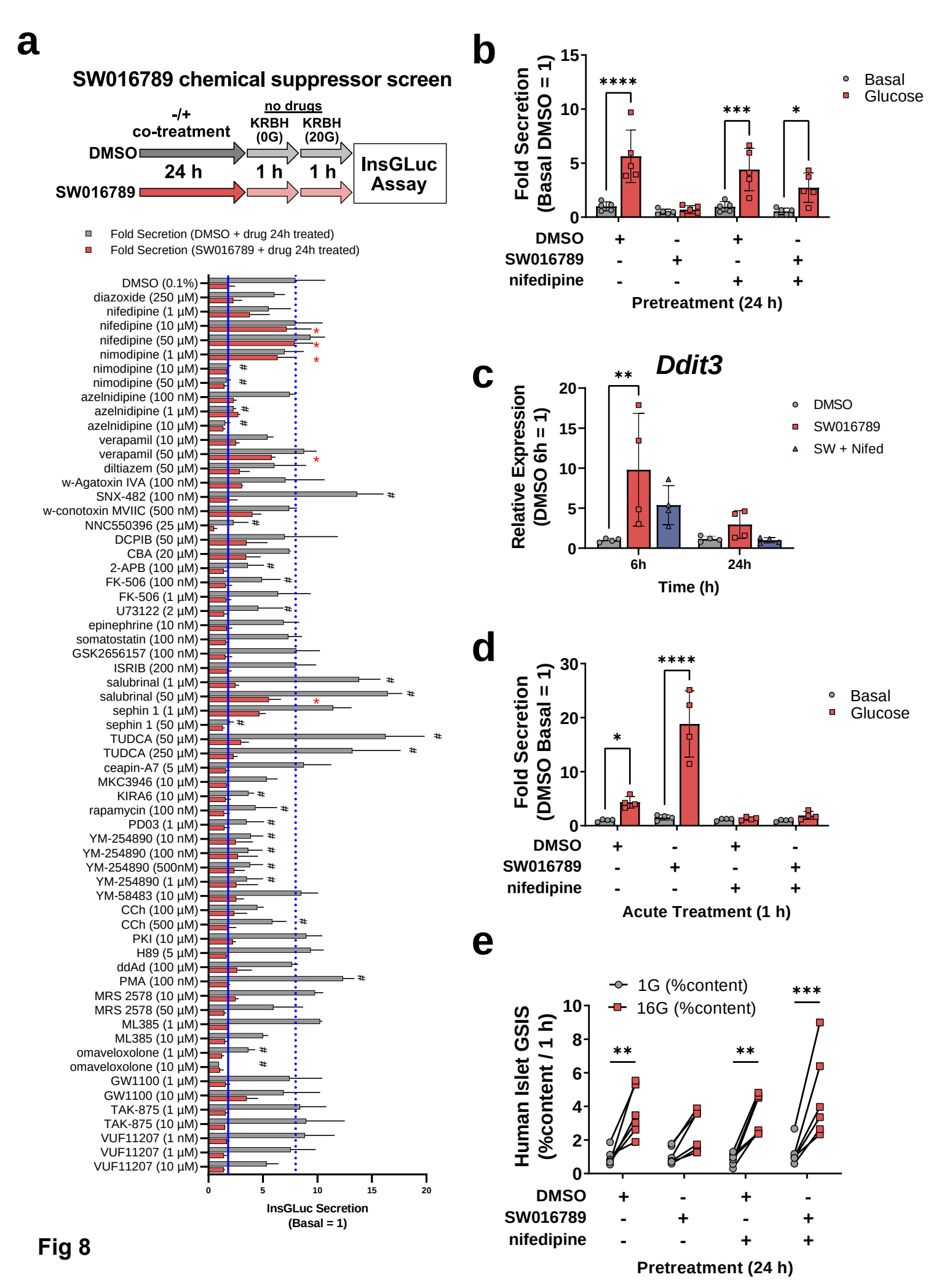
a
SW016789 chemical suppressor screen
-/+
co-treatment
no drugs
KRBH (0G)
KRBH (20G)
DMSO
SW016789
24 h
1 h
1 h
InsGLuc Assay
Fold Secretion (DMSO + drug 24h treated)
Fold Secretion (SW016789 + drug 24h treated)
DMSO (0.1%)
diazoxide (250 μM)
nifedipine (1 μM)
nifedipine (10 μM)
nifedipine (50 μM)
nimodipine (1 μM)
nimodipine (10 μM)
nimodipine (50 μM)
azelnidipine (100 nM)
azelnidipine (1 μM)
azelnidipine (10 μM)
verapamil (10 μM)
verapamil (50 μM)
diltiazem (50 μM)
w-Agatoxin IVA (100 nM)
SNX-482 (100 nM)
w-conotoxin MVIIC (500 nM)
NNC550396 (25 μM)
DCPIB (50 μM)
CBA (20 μM)
2-APB (100 μM)
FK-506 (100 nM)
FK-506 (1 μM)
U73122 (2 μM)
epinephrine (10 nM)
somatostatin (100 nM)
GSK2656157 (100 nM)
ISRIB (200 nM)
salubrinal (1 μM)
salubrinal (50 μM)
sephin 1 (1 μM)
sephin 1 (50 μM)
TUDCA (50 μM)
TUDCA (250 μM)
ceapin-A7 (5 μM)
MKC3946 (10 μM)
KIRA6 (10 μM)
rapamycin (100 nM)
PD03 (1 μM)
YM-254890 (10 nM)
YM-254890 (100 nM)
YM-254890 (500nM)
YM-254890 (1 μM)
YM-58483 (10 μM)
CCh (100 μM)
CCh (500 μM)
PKI (10 μM)
H89 (5 μM)
ddAd (100 μM)
PMA (100 nM)
MRS 2578 (10 μM)
MRS 2578 (50 μM)
ML385 (1 μM)
ML385 (10 μM)
omaveloxolone (1 μM)
omaveloxolone (10 μM)
GW1100 (1 μM)
GW1100 (10 μM)
TAK-875 (1 μM)
TAK-875 (10 μM)
VUF11207 (1 nM)
VUF11207 (1 μM)
VUF11207 (10 μM)
0
5
10
15
20
InsGLuc Secretion (Basal = 1)
b
Fold Secretion (Basal DMSO = 1)
****
***
*
Basal
Glucose
DMSO + - + -
SW016789 - + - +
nifedipine - - + +
Pretreatment (24 h)
c
Ddit3
Relative Expression (DMSO 6h = 1)
**
DMSO
SW016789
SW + Nifed
6h
24h
Time (h)
d
Fold Secretion (DMSO Basal = 1)
*
****
Basal
Glucose
DMSO + - + -
SW016789 - + - +
nifedipine - - + +
Acute Treatment (1 h)
e
1G (%content)
16G (%content)
Human Islet GSIS (%content / 1 h)
**
**
***
DMSO + - + -
SW016789 - + - +
nifedipine - - + +
Pretreatment (24 h)

Fig 8

Electronic Supplementary Material (ESM): Rodrigues-dos-Santos K, Roy G, Binns DD, et al.

ESM Methods

Ca^{2+} measurements in the diazoxide paradigm or for store-operated Ca^{2+} entry (SOCE) – For Ca^{2+} measurements in the presence of diazoxide, after loading with Ca^{2+} indicator dye, cells were incubated in KRBH containing 250 μM diazoxide for 5 min prior to the baseline read and subsequent stimulation with 35 mM KCl and/or 20 mM glucose with DMSO or SW016789 in the continued presence of diazoxide. For measurements of ER Ca^{2+} and SOCE, beta cells were incubated in normal glucose-free KRBH for 1 h, then loaded with Fura-2-LR-AM (5 μM) in Ca^{2+}-free KRBH (5 mM KCl, 120 mM NaCl, 15 mM HEPES, pH 7.4, 24 mM $NaHCO_3$, 3 mM $MgCl_2$, and 1 mg/ml radioimmunoassay-grade BSA) for 25 min and a 5 min washout in the same buffer. Cells were placed in the BioTek Synergy H1 for a baseline read (30 s), followed by injection of thapsigargin (10 μM) for a 5 min read, and CaCl2 (2.5 mM) for another 5 min read.

cAMP reporter assays - For relative cAMP measurements, the genetically-encoded Epac-based bioluminescence-resonance energy transfer (BRET) reporter for cAMP (CAMYEL) was used as previously described [1]. CAMYEL MIN6 cells were preincubated in glucose-free KRBH for 1.5 h. Cells were incubated for 15 min at room temperature with coelenterazine-h (20 μM). After a 3 min baseline recording, stimulations were added, and plate read for an additional 15 min. Using the BRET1 cube from BioTek, emission signals at 460/40 and 540/25 nm (center/bandpass) were measured every 0.8 s. Data were normalized by subtracting the mean of the respective baseline reads. Area under the curves (AUCs) were calculated in GraphPad Prism using a baseline of 0 ΔRFU and ignoring peaks that are <10% of the distance from minimum to maximum ΔRFU and those defined by fewer than 15 adjacent points. All peaks must go above the baseline.

Chiral separation and structure-activity analysis - Separated enantiomers of racemic SW016789 were obtained from Lotus Separations using supercritical fluid chromatography [2]. Purified enantiomers were resuspended in DMSO and subjected to acute and chronic InsGLuc-MIN6 experiments as described. For structure-activity analysis, structures of SW016789 analogs and their respective activity scores were analyzed in Datawarrior software [3]. Glucose-stimulated InsGLuc secretory activity normalized to unstimulated secretion was input along with structures and activity-cliff analysis was performed.

ESM References

1. Jiang LI, Collins J, Davis R, Lin KM, DeCamp D, Roach T, et al. Use of a cAMP BRET sensor to characterize a novel regulation of cAMP by the sphingosine 1-phosphate/G13 pathway. J Biol Chem. 2007;282(14):10576-84. doi: 10.1074/jbc.M609695200. PMID: 17283075. PMCID: PMC2526465.
2. Wilson LJ, Mi C, Kraml CM. A preparative chiral separation of hydroxychloroquine using supercritical fluid chromatography. J Chromatogr A. 2020;1634:461661. doi: 10.1016/j.chroma.2020.461661. PMID: 33166894. PMCID: PMC7598365.
3. Sander T, Freyss J, von Korff M, Rufener C. DataWarrior: an open-source program for chemistry aware data visualization and analysis. J Chem Inf Model. 2015;55(2):460-73. doi: 10.1021/ci500588j. PMID: 25558886.

ESM Results

ESM Figure 1. Acute dose-response testing of SW016789 in InsGLuc-MIN6 cells. Cells were treated with varying concentrations of SW016789 or vehicle (0.1% DMSO) in the **(a)** presence and **(b)** absence of glucose (20 mM) for 1 h. Data are the mean ± SD of three independent experiments. The EC_{50} of SW016789 calculated in the presence of glucose was 2.7E-6 M. **(c)** Chiral separation of racemic mixture of SW016789 into two distinct peaks. **(d)** Enantiomeric structures of SW016789. **(e,f)** Secreted Gaussia activity from InsGLuc-MIN6 cells treated either **(e)** only during glucose stimulation (1 h) or **(f)** chronically (24 h) prior to glucose stimulation. Cells were exposed to DMSO (0.1%), or purified enantiomers of SW016789 (peak 1, peak 2, 5 μM each), or the SW016789 racemate (5 μM). Data are the mean ± SD of three independent experiments. *, P<0.05 by two-way ANOVA. **(g)** Structure-activity relationship of structural analogs assayed in chronic (24 h) treatment of InsGLuc-MIN6 cells. Fold InsGLuc activity is normalized to secretion in unstimulated conditions. Increased fold activity indicates a loss in chronic inhibitory activity, as seen for the structure with disrupted chiral center. DataWarrior was used to generate a network display organized by structural similarity and colored by activity.

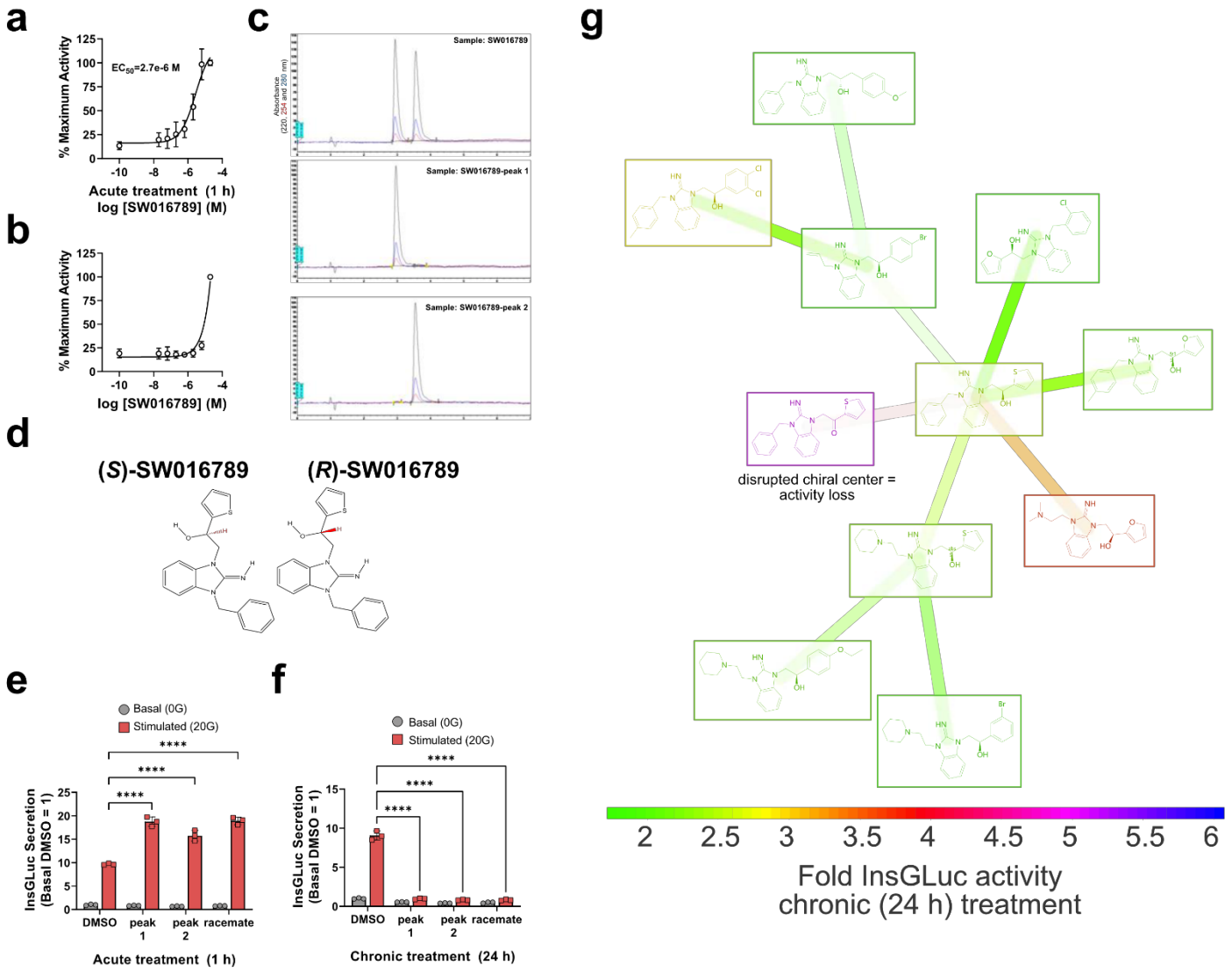

ESM Figure 2. Effects of SW016789 on Ca^{2+} influx under the diazoxide paradigm and during SOCE and ROCE. (a,b) InsGLuc-MIN6 cells were exposed to DMSO (0.1%) or SW016789 (5 μM) for **(a)** 24 h before Ca^{2+} influx assay or **(b)** were acutely co-stimulated with DMSO or SW016789, as indicated above each graph. Cells were incubated in the presence of diazoxide (Dz, 250 μM) and stimulated with either Dz + KCl 35 mM or Dz + KCl 35 mM + glucose 20 mM. Expectedly, the addition of glucose did not alter the amount of Ca^{2+} influx in the presence of diazoxide and KCl in either chronic or acute treatments. Associated AUC calculations are shown. Data are the mean ± SD of three independent experiments. *,P<0.05 by one-way ANOVA. **(c)** MIN6 cells were incubated in the presence or absence of diazoxide (250 μM) in the KRBH during Ca^{2+}-influx assays. Cells were then stimulated with glucose (20 mM), SW016789 (5 μM), or both at the time indicated by the arrow. Data are the mean ± SD of three independent experiments. **(d)** Endoplasmic reticulum (ER) Ca^{2+} stores and store-operated Ca^{2+} influx (SOCE) were assayed in MIN6 beta cells. Thapsigargin (Tg, 10 μM) elicited ER Ca^{2+} leakage into the cytosol and adding back $CaCl_2$ (2 mM) resulted in SOCE. AUCs were calculated separately for each peak. **(e)** MIN6 cells were stimulated with carbachol (CCh, 250 μM) to assess receptor-operated Ca^{2+} entry (ROCE) after a 10 min pretreatment with SW016789 or DMSO. Data are the mean ± SD of three independent experiments.

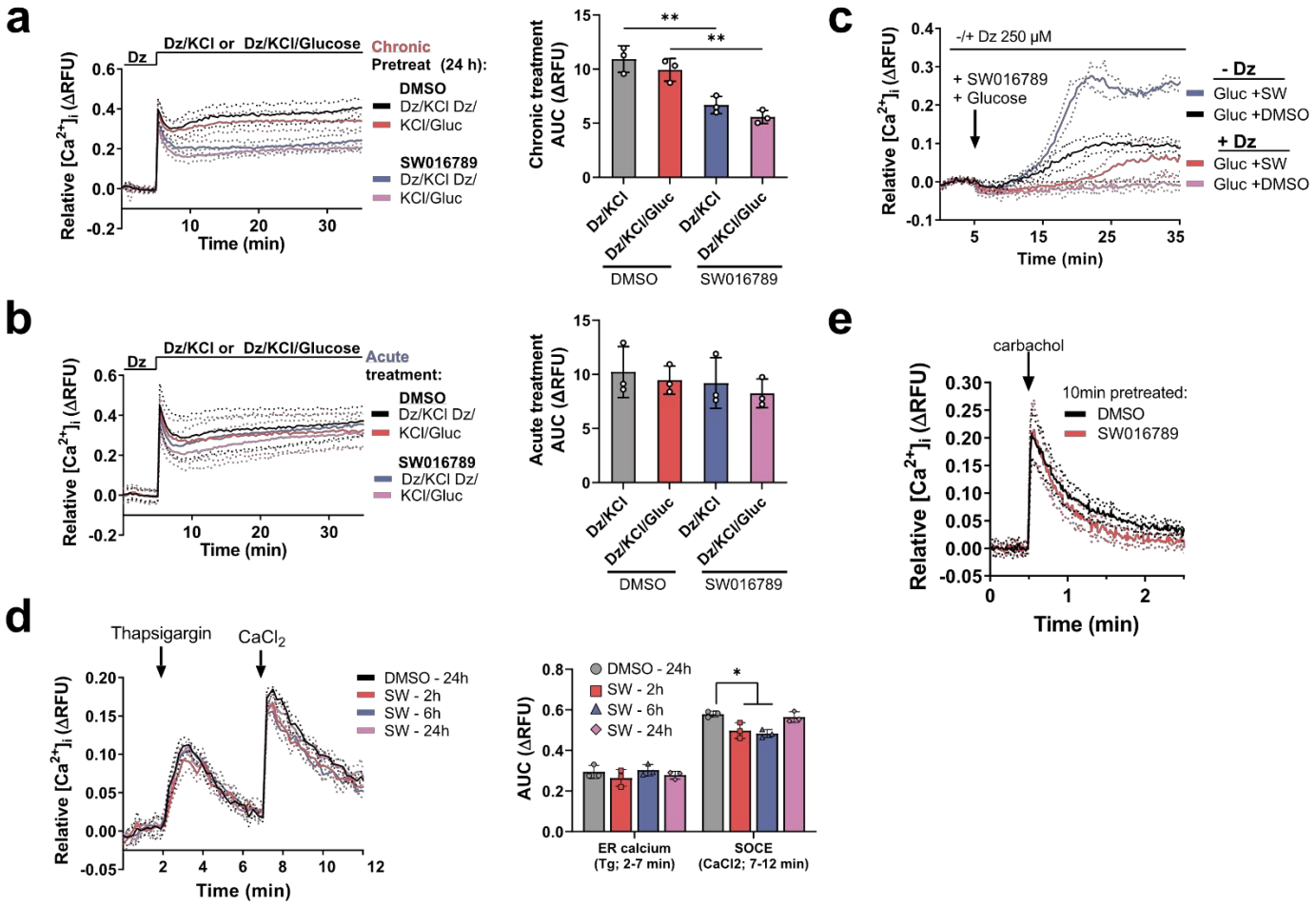

ESM Figure 3. GPCR screening of SW016789 in the PRESTO-TANGO assay. (a) MIN6 cells stably expressing the cAMP BRET sensor CAMYEL were preincubated in glucose-free KRBH for 1.5 h prior to treating with coelenterazine-400A for 15 min. Baseline BRET was read for 3 min prior to stimulation as indicated. Cells were stimulated with forskolin (Fsk, 10μM) and IBMX (1μM) as a positive control, SW016789 (10 μM) alone, glucose (20 mM) alone, SW016789 and glucose together, or DMSO (0.1%). **(b)** ΔBRET peak area defined using baseline of 0 and ignoring peaks under 0.5 units high and fewer than 10 adjacent points. Data are the mean ± SD of 3 independent experiments as indicated by individual data points on the AUC bar graph. *, P<0.05 by two-way ANOVA. **(c)** Results of PRESTO-TANGO assay using 10 μM SW016789 showed only one prominent hit, CXCR7. **(d)** Validation studies performed at the PDSP core show the EC50 of SW016789 on CXCR7 is ~26 μM.

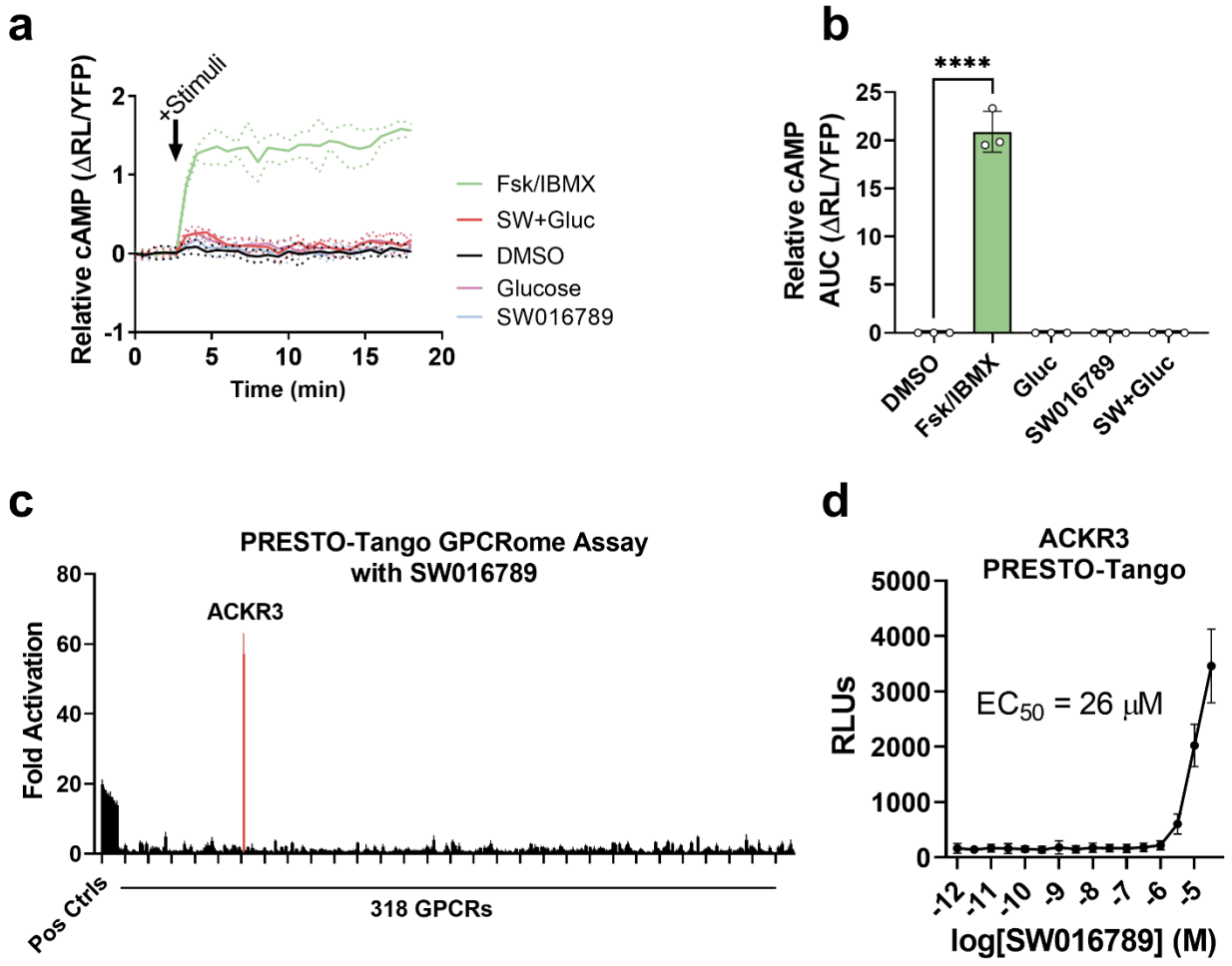

ESM Figure 4. SW016789 did not impact UPR^{ER} in other neuroendocrine cells nor cause maladaptive UPRER at high concentrations. (a) Relative UPR^{ER} gene expression in MIN6 cells treated for either 6 or 24 h with vehicle (0.1% DMSO) or increasing concentrations of SW016789 (1-20 μM). Thapsigargin (100 nM) was included as a positive control at each time point. Data are the mean ± SD of four independent experiments. *, P<0.05 by two-way ANOVA. **(b,c)** Relative gene expression in a mouse intestinal L-cell cell line (GLUTag) **(b)** and a human islet delta cell line (QGP1) **(c)** treated with DMSO (0.1%), SW016789 (5 μM), or thapsigargin (Tg, 100 nM) in complete medium for 6 or 24 h. Glucagon (*Gcg*) message was measured for L-cells as they produce GLP-1 encoded by *Gcg*. Somatostatin (*SST*) was measured as the major product of δ cells. All data are the mean ± SD of at least 3 independent experiments. *,P<0.05 by two-way ANOVA.

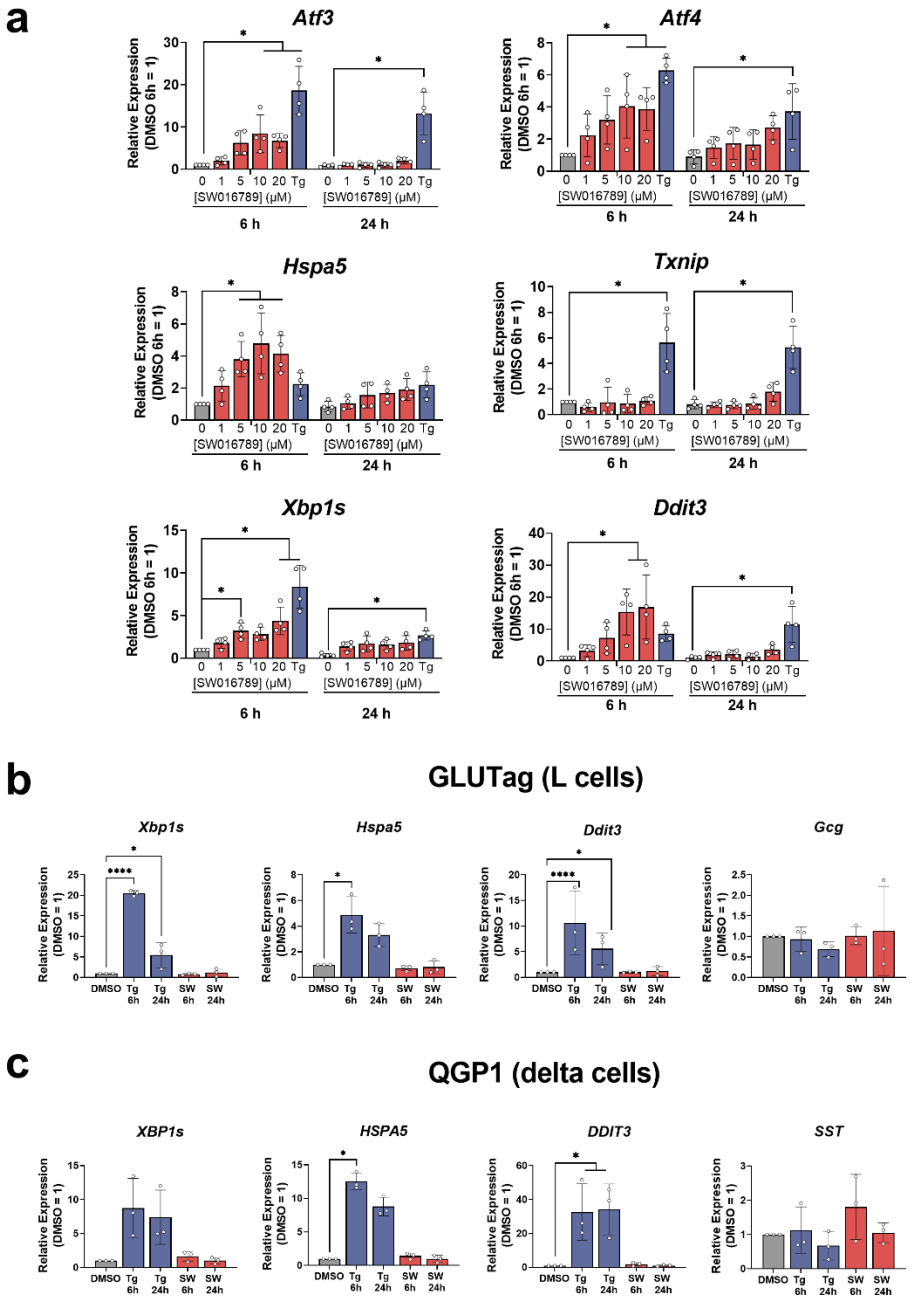

Table S1. GPCRome screen results with SW016789. Raw fold change data provided by the PDSP core for >300 GPCRs assayed using the Presto-Tango system.

		Replicates					
DNA	**ID#**	**I**	**II**	**III**	**IV**	**AVG**	**CV**
ACKR3	282	59.7	56.7	49.2	62.9	57.1	0.09
BB3	281	6.7	4.6	4.7	3.6	4.9	0.23
P2RY6	239	4.7	5.2	4.8	4.3	4.7	0.06
S1PR4	296	3.5	2.8	3.8	6.1	4.0	0.31
GPR34	188	3.2	3.5	3.6	5.7	4.0	0.25
FFA1	314	3.7	3.4	3.8	4.0	3.7	0.06
CHRM3	242	5.2	2.6	3.5	2.9	3.6	0.28
GPR52	316	3.2	3.2	3.4	4.1	3.5	0.11
OPRK1	207	2.9	3.4	3.9	3.6	3.5	0.10
NPY5R	199	3.4	3.2	3.4	3.5	3.4	0.04
GPR141	315	3.2	3.3	3.1	3.4	3.2	0.04
MRGPRE	230	3.3	3.2	3.1	3.0	3.2	0.04
ADRA2A	161	3.8	3.4	2.7	2.7	3.1	0.14
P2RY14	319	2.8	2.8	3.1	3.8	3.1	0.14
SSTR4	152	2.2	3.5	2.6	4.0	3.1	0.23
GAL1	226	3.2	3.3	3.0	2.5	3.0	0.10
GPR88	181	3.3	3.8	2.3	2.5	3.0	0.21
CCKBR	297	3.6	3.4	2.2	2.3	2.9	0.21
MTNR1A	167	2.1	3.0	2.8	3.6	2.9	0.18
MRGPRX1	142	3.4	2.7	2.9	2.4	2.8	0.13
OPRM1	127	2.5	3.0	3.3	2.4	2.8	0.13
VIPR1	240	3.2	1.8	1.8	4.3	2.8	0.37
ADRB1	169	3.7	2.7	2.5	2.2	2.8	0.20
HRH1	317	3.1	2.7	2.6	2.5	2.7	0.07
TACR3	320	1.9	2.8	2.4	3.8	2.7	0.25
MRGPRF	263	2.1	3.3	2.7	2.5	2.7	0.16
ADRA2B	113	3.4	2.8	1.8	2.1	2.5	0.25
ADORA1	241	2.9	2.2	2.7	2.1	2.5	
GPR55	245	2.7	2.4	2.0	2.7	2.4	0.12
CHRM1	98	3.2	1.8	2.8	1.8	2.4	0.25
P2RY1	223	2.2	2.9	2.1	2.3	2.4	0.12
CXCR2	258	2.3	2.4	2.6	2.1	2.4	0.06
CRHR1	114	2.8	2.2	2.2	2.3	2.4	0.11
GPR44	212	2.2	1.7	1.8	3.4	2.3	0.30
LTB4R	198	2.8	2.2	1.9	2.1	2.3	0.15
PTGER3	176	1.5	1.8	2.3	3.3	2.3	0.30
CHRM2	313	2.4	2.2	2.2	2.1	2.2	0.06
HTR2CVGV	102	2.6	2.4	1.8	1.7	2.1	0.18

FPR3	243	1.9	2.4	2.2	2.0	2.1	0.09
GPR6	261	3.5	2.0	1.2	1.8	2.1	0.41
SCTR	144	1.8	2.4	1.9	2.3	2.1	0.12
GHSR	251	2.3	1.9	2.4	1.7	2.1	0.14
GPR156	252	1.6	1.6	1.8	3.0	2.0	0.30
CCR3	305	2.8	1.8	1.8	1.7	2.0	0.22
CXCR3	162	2.1	2.0	2.5	1.3	2.0	0.21
GPR87	293	2.2	2.0	1.7	2.1	2.0	0.09
OPRD1	119	2.0	2.2	2.1	1.6	2.0	0.12
GPR150	116	2.5	1.5	2.1	1.7	1.9	0.19
GPR3	292	1.4	1.9	1.9	2.5	1.9	
CXCR5	274	1.9	2.0	1.7	2.0	1.9	0.06
PTAFR	272	1.8	1.8	1.8	2.2	1.9	
FPR1	50	2.0	1.8	2.0	1.7	1.9	0.07
TACR2	224	1.6	1.6	2.3	2.0	1.9	0.15
CD97	209	2.8	2.0	1.5	1.1	1.8	0.35
MAS1	247	1.7	2.2	1.7	1.7	1.8	0.12
HRH4	166	2.0	1.7	1.9	1.7	1.8	0.09
CYSLTR2	170	1.9	2.1	1.6	1.8	1.8	0.10
SSTR1	200	2.0	1.4	1.4	2.5	1.8	0.25
HTR1B	246	2.3	1.5	1.8	1.7	1.8	0.16
GPR84	165	2.5	1.8	1.5	1.3	1.8	0.25
MRGPRX4	150	1.6	2.5	1.7	1.3	1.8	0.25
ELTD1	290	1.8	1.7	1.7	1.8	1.8	0.01
AGTR2	257	2.1	1.8	1.6	1.5	1.7	0.13
GPR17	268	1.5	1.6	1.7	2.2	1.7	0.15
HTR1D	254	1.4	2.0	1.6	2.0	1.7	0.15
AVPR2	273	2.0	1.8	1.6	1.5	1.7	0.11
HRH3	61	1.7	1.2	3.0	1.0	1.7	0.44
TAAR5	48	1.3	2.1	1.2	2.3	1.7	0.26
TACR1	312	1.4	1.3	1.6	2.5	1.7	0.26
MTNR1B	175	1.8	1.6	1.6	1.7	1.7	0.06
CHRM4	217	2.0	0.9	1.4	2.3	1.7	0.33
MC5R	222	1.5	1.5	1.7	1.7	1.6	0.07
APJ	265	2.1	1.5	1.5	1.5	1.6	0.16
OPN5	295	1.5	2.0	1.4	1.5	1.6	0.15
GPR82	285	1.9	1.7	1.4	1.6	1.6	0.11
GPR12	299	1.5	1.5	1.8	1.4	1.6	0.10
HTR2C INI	157	1.8	1.3	1.6	1.6	1.6	0.12
NTSR1	287	1.5	1.5	1.5	1.6	1.5	0.02
MC4R	214	2.1	1.3	1.7	1.0	1.5	0.28
DRD2	154	0.9	1.1	3.5	0.7	1.5	0.74
S1PR1	192	1.1	1.5	1.4	2.1	1.5	0.24
GPR182	276	1.3	1.2	1.6	1.9	1.5	0.18

HCA2	309	1.5	1.6	1.3	1.5	1.5	0.06
MC1R	126	2.2	1.7	1.3	0.7	1.5	
HTR1F	270	1.3	1.4	1.3	1.9	1.5	0.16
PRRP	55	1.3	1.4	1.4	1.7	1.5	0.11
UTS2R	72	1.3	0.9	1.0	2.4	1.4	0.41
SSTR2	16	1.6	1.6	1.1	1.3	1.4	0.13
GPR32	52	1.1	1.0	1.2	2.4	1.4	0.41
QRFP	79	0.6	1.1	1.8	2.1	1.4	0.44
MC3Rb	22	1.1	1.3	1.4	1.7	1.4	0.15
HTR1E	262	1.1	1.5	1.3	1.7	1.4	0.16
GPR101	275	1.4	1.6	1.4	1.2	1.4	0.09
LPAR5	118	1.5	1.0	1.2	1.7	1.4	0.19
S1PR2	120	1.1	1.7	1.1	1.6	1.4	0.19
AGTR1	41	1.0	2.6	0.7	1.1	1.4	0.54
GPR146	51	3.3	0.7	0.8	0.6	1.4	0.83
MRGPRX2	271	1.2	1.4	1.4	1.4	1.3	0.07
0	256	1.4	2.1	0.8	1.1	1.3	0.38
GMR2	171	1.2	1.4	1.4	1.3	1.3	0.05
CRHR2	122	1.2	1.1	1.8	1.2	1.3	0.20
GPR85	173	1.7	1.5	1.0	1.1	1.3	0.22
NPBW2	279	1.4	1.5	1.4	1.0	1.3	0.12
HTR4	182	1.0	2.3	0.8	1.2	1.3	0.44
GPR18	227	1.3	1.1	1.3	1.5	1.3	0.10
GRM8	237	1.5	1.2	1.4	1.2	1.3	0.11
GAL3	115	1.3	1.5	1.1	1.4	1.3	0.10
CXCR4	266	1.6	1.5	1.0	1.0	1.3	0.22
GPR31	180	1.1	0.9	1.6	1.5	1.3	0.22
GPR27	44	1.3	1.2	1.1	1.5	1.3	0.13
CCR10	193	1.0	1.4	1.6	1.0	1.3	0.19
AVPR1A	49	1.9	1.3	0.9	0.8	1.2	0.35
GPR26	172	1.3	1.6	1.1	1.0	1.2	0.17
ADRB3	33	2.1	0.8	1.2	0.8	1.2	0.43
GPR173	156	1.0	1.1	1.3	1.5	1.2	0.16
GPR148	59	0.8	1.4	1.0	1.7	1.2	0.27
GPR45	60	0.7	1.2	1.0	1.9	1.2	0.34
S1PR5	136	1.5	0.8	1.3	1.2	1.2	0.23
GPRC5B	197	1.1	0.8	1.0	1.8	1.2	0.33
0	248	1.8	1.0	0.9	1.1	1.2	
VIPR2	80	1.1	1.4	1.0	1.3	1.2	0.14
HCTR2	53	0.8	1.7	1.1	1.2	1.2	0.29
GPR116	195	1.3	1.1	1.2	1.2	1.2	0.08
PTGDR	151	1.6	1.1	1.3	0.7	1.2	
GNRHR	66	1.1	1.1	1.5	1.0	1.2	0.17
GPR97	189	1.9	1.0	0.9	1.0	1.2	0.35

SSTR5	32	0.9	1.4	1.0	1.4	1.2	0.21
LPAR1	310	1.1	0.9	0.9	1.6	1.1	0.25
OXTR	23	1.8	1.0	0.9	0.8	1.1	0.32
GPR1	267	0.9	1.2	1.3	1.1	1.1	0.13
GPR56	253	1.4	0.9	1.0	1.2	1.1	0.15
HCA1	125	1.3	1.1	1.1	1.0	1.1	0.11
MRGPRD	255	1.0	1.2	1.1	1.1	1.1	0.07
HRH2	141	1.2	0.5	1.4	1.3	1.1	0.31
LHCGR	77	0.6	0.8	2.2	0.7	1.1	0.62
HTR2C VSV	94	1.0	1.2	1.2	1.0	1.1	0.09
GIPR	131	0.6	0.7	1.2	1.8	1.1	0.45
ADRA1A	89	1.3	1.0	1.0	0.8	1.1	0.17
GPR151	67	1.0	1.2	0.9	1.1	1.0	0.08
RXFP4	8	0.9	0.9	1.1	1.3	1.0	0.15
GPR110	283	1.0	1.1	1.0	1.0	1.0	0.04
GPBA	179	1.0	1.0	1.1	1.0	1.0	0.02
CCR2	2	1.0	0.7	1.0	1.4	1.0	0.23
CXCR1	138	1.2	0.5	1.5	0.9	1.0	0.35
OXGR1	303	0.7	1.1	1.1	1.1	1.0	0.16
HTR2B	278	1.1	1.0	1.0	0.9	1.0	0.07
GPR78	21	0.6	1.2	1.1	1.0	1.0	0.25
GPR22	28	0.8	1.0	1.0	1.1	1.0	0.11
GPR19	284	1.1	0.8	0.9	1.1	1.0	0.14
P2RY10	135	1.0	0.9	1.1	0.8	1.0	0.10
GPR77	277	0.8	1.2	0.7	1.2	1.0	0.22
GPR133	27	1.2	0.8	0.8	1.1	1.0	0.19
CCRL2	90	1.3	0.4	0.5	1.6	1.0	0.52
GPR114	147	0.9	1.0	1.0	0.9	1.0	0.03
EDNRB	42	1.1	0.9	1.0	0.9	1.0	0.09
PTGFR	96	0.8	1.3	0.6	1.1	1.0	0.27
HTR5	286	1.0	1.0	0.7	1.1	1.0	0.13
GPR171	4	0.9	0.8	0.9	1.2	1.0	0.15
GPR120	155	1.0	1.2	0.9	0.7	1.0	0.19
GPR135	35	1.0	1.4	0.6	0.7	0.9	0.33
GPR35	196	0.9	0.8	1.0	1.1	0.9	0.10
ADCYAP1R1	1	0.6	1.5	1.1	0.6	0.9	0.40
BDKBR2	177	1.4	0.8	0.7	0.8	0.9	0.28
MCHR1R	30	1.4	0.9	0.7	0.8	0.9	0.28
GPR176	12	0.9	0.9	1.1	0.8	0.9	0.11
F2RL2	306	1.0	1.0	0.8	0.9	0.9	0.06
GPR4	308	0.8	1.2	0.9	0.8	0.9	0.19
MLNR	38	1.1	0.8	1.0	0.8	0.9	0.16
ADORA2A	81	0.4	1.1	1.0	1.2	0.9	0.32
FPR2	99	1.2	0.9	0.7	0.8	0.9	0.22

FFA2	202	0.7	1.0	1.0	1.0	0.9	0.15
GPR20	20	0.8	0.8	1.3	0.8	0.9	0.23
DRD4	83	0.9	0.7	1.0	1.1	0.9	0.15
GPR21	164	0.8	0.8	1.0	1.1	0.9	0.15
DRD3	34	1.7	0.6	0.7	0.5	0.9	0.52
CXCR6	18	1.1	1.0	0.7	0.8	0.9	0.19
HTR7	294	1.0	1.0	0.7	0.9	0.9	0.12
CALCRb	65	0.9	0.9	1.0	0.8	0.9	0.07
GPR162	148	0.7	0.9	0.9	1.0	0.9	0.10
PTGER1	159	0.8	0.7	0.8	1.2	0.9	0.21
NPFF1	62	1.0	1.1	0.6	0.9	0.9	0.21
GPR126	19	0.8	1.0	0.9	0.8	0.9	0.07
OPRL1	15	0.7	0.8	1.0	1.0	0.9	0.14
CHRM5	250	0.9	0.9	0.8	0.9	0.9	0.06
NMBR	54	0.6	1.0	1.0	0.9	0.9	0.18
MCHR2R	134	1.1	1.1	0.7	0.5	0.9	0.28
P2RY13	311	0.6	0.6	0.9	1.4	0.9	0.37
CCR6	153	1.1	0.8	0.9	0.7	0.9	0.19
GPR113	187	1.0	0.8	0.7	0.9	0.9	0.13
CNR1	225	0.9	0.9	0.8	0.8	0.8	0.05
GPR61	220	0.7	0.9	1.0	0.7	0.8	0.13
GPR132	84	0.8	0.8	0.8	0.9	0.8	0.06
PK2	47	0.7	0.6	0.9	1.3	0.8	0.32
GPR183	235	0.7	0.9	0.8	1.0	0.8	0.16
GPR119	3	1.1	1.0	0.7	0.5	0.8	0.30
LPAR2	6	1.2	0.8	0.7	0.5	0.8	0.32
DRD1	146	0.8	0.9	0.7	0.8	0.8	0.06
NPY4R	78	0.9	0.7	0.9	0.8	0.8	0.12
F2R	298	0.8	0.8	0.9	0.8	0.8	0.05
GPR25	36	0.6	1.0	0.6	1.0	0.8	0.23
PTGIR	63	0.7	0.8	1.1	0.6	0.8	0.21
C5A	185	1.0	0.7	0.8	0.7	0.8	0.16
DRD5	91	0.7	0.7	1.0	0.8	0.8	0.18
GPR111	74	0.5	1.4	0.5	0.8	0.8	0.45
CYSLTR1	26	0.9	0.5	1.1	0.7	0.8	0.29
KISSPEPTIN	69	1.3	0.6	0.7	0.5	0.8	0.41
RXFP2	288	0.7	0.7	0.6	1.2	0.8	0.31
GPR65	269	0.7	0.9	0.7	0.8	0.8	0.07
CASR	137	0.9	0.7	0.5	1.0	0.8	0.26
NTSR2	111	0.7	1.2	0.8	0.4	0.8	0.35
HCTR1	45	0.8	0.9	0.5	0.9	0.8	0.20
CCR8	10	0.9	0.7	0.8	0.7	0.8	0.09
GRM5	221	0.7	0.6	0.7	1.1	0.8	0.26
GPRC5A	29	0.9	0.7	0.7	0.8	0.8	0.09

MAS1L	206	0.8	0.5	0.7	1.1	0.8	0.28
GPR15	108	0.7	0.8	0.7	0.8	0.8	0.09
EDNRA	178	0.8	0.7	0.8	0.8	0.8	0.08
NMUR1	158	0.9	0.7	0.7	0.8	0.8	0.11
SUCNR1	40	0.9	0.7	0.8	0.6	0.8	0.14
HTR6	110	0.7	0.5	0.8	1.1	0.8	0.29
MC2R	14	0.6	1.2	0.5	0.7	0.8	0.33
GPR149	100	0.6	0.8	0.9	0.7	0.8	0.11
CCKAR	289	0.9	0.8	0.7	0.7	0.7	0.13
LPAR6	190	0.9	0.6	0.7	0.8	0.7	0.12
GPR144	43	0.8	0.7	1.0	0.5	0.7	0.27
RXFP3	112	0.7	1.0	0.5	0.7	0.7	0.24
GPRC5D	205	1.1	0.7	0.6	0.6	0.7	0.30
TSHR	232	0.8	0.9	0.8	0.5	0.7	0.24
PTH1R	71	0.8	0.8	0.8	0.6	0.7	0.13
GPR115	291	0.7	0.7	0.7	0.8	0.7	0.06
NMUR2	87	0.7	0.7	0.7	0.8	0.7	0.06
PTH2R	184	1.1	0.7	0.6	0.5	0.7	0.35
TAAR6	304	0.6	0.6	0.7	0.9	0.7	0.16
ADRA1D	105	0.7	0.7	0.7	0.7	0.7	0.04
GPR123	307	0.9	0.4	0.8	0.8	0.7	0.27
GPR63	228	0.7	0.7	0.8	0.7	0.7	0.05
NPBW1	95	0.7	0.9	0.7	0.4	0.7	0.26
GPR160	75	0.7	0.7	0.7	0.8	0.7	0.09
GHRHR	234	0.5	0.8	0.4	1.0	0.7	0.34
LPA4	302	0.8	0.5	0.8	0.8	0.7	0.17
GPR174	219	1.1	0.5	0.5	0.6	0.7	0.38
GPR62	76	1.2	0.6	0.4	0.6	0.7	0.42
ADRA2C	17	0.5	0.5	0.9	0.8	0.7	0.29
BDKBR1	121	0.8	0.9	0.5	0.6	0.7	0.23
GABBR1	107	0.9	0.7	0.7	0.4	0.7	0.26
SSTR3	24	0.9	0.8	0.5	0.6	0.7	0.25
AVPR1B	57	0.9	0.7	0.6	0.6	0.7	0.19
GRM1	213	1.5	0.5	0.3	0.4	0.7	0.69
P2RY2	231	1.0	0.2	0.8	0.7	0.7	0.47
HTR2C VNV	86	0.9	0.7	0.5	0.6	0.7	0.28
GPR157	132	0.7	0.5	0.7	0.8	0.7	
OPN3	7	0.7	0.5	0.5	0.8	0.7	0.20
GPR153	244	0.5	0.6	0.7	0.7	0.7	0.12
GPR161	260	0.6	0.6	0.7	0.7	0.7	0.09
GPRC5C	37	0.8	0.7	0.5	0.6	0.7	0.15
GPR125	203	0.6	0.7	0.6	0.7	0.6	0.05
TA1	208	0.6	0.6	0.7	0.7	0.6	0.07
PTGER2	88	0.6	0.6	0.6	0.8	0.6	0.14

LTB4R2B	318	0.7	0.7	0.4	0.7	0.6	0.18
TBXA2R	64	0.5	0.8	0.5	0.7	0.6	0.22
GPER	139	0.6	0.6	0.6	0.7	0.6	0.11
GPRC6A	101	0.7	0.6	0.6	0.5	0.6	0.10
CALCRL	73	0.5	0.5	0.8	0.7	0.6	0.25
CX3CR1	130	0.5	0.7	1.0	0.3	0.6	0.41
GPR152	124	0.5	0.5	0.7	0.8	0.6	0.22
GLP1R	163	0.7	0.5	0.6	0.7	0.6	0.16
GPR64	5	0.7	0.5	0.7	0.5	0.6	0.15
GPR83	93	0.5	0.7	0.6	0.6	0.6	0.13
CMKLR1	106	0.7	0.6	0.6	0.6	0.6	0.09
F2R-L1	186	0.6	0.6	0.7	0.6	0.6	0.07
TAAR2	216	0.7	0.5	0.6	0.7	0.6	0.14
MRGPRX3	46	0.5	0.6	0.4	0.8	0.6	0.22
S1PR3	128	0.4	0.7	0.5	0.7	0.6	0.28
ADRA1B	97	0.6	0.7	0.6	0.5	0.6	0.12
PK1	39	0.5	0.7	0.6	0.5	0.6	0.15
CCR7	82	0.6	0.5	0.7	0.5	0.6	0.18
PTGER4	280	0.6	0.5	0.6	0.5	0.6	0.12
GPR68	236	0.5	0.6	0.5	0.6	0.6	0.10
P2RY4	264	0.4	0.6	0.3	0.8	0.6	0.37
HTR1A	149	0.4	0.6	0.5	0.7	0.6	0.18
HCA3	133	0.5	0.4	0.7	0.7	0.5	0.23
GCGR	123	0.5	0.5	0.3	0.7	0.5	0.26
HTR2A	174	0.6	0.6	0.6	0.4	0.5	0.15
FFA3	210	0.5	0.6	0.6	0.5	0.5	0.09
ADORA3	249	0.6	0.5	0.4	0.6	0.5	0.12
CCR4	201	0.5	0.4	0.7	0.6	0.5	0.20
NPY1R	183	0.4	0.5	0.6	0.6	0.5	0.13
GPR37L1	204	0.4	0.5	0.4	0.7	0.5	0.18
GPR142	92	0.5	0.8	0.5	0.2	0.5	0.38
GPR143	211	0.6	0.4	0.4	0.5	0.5	0.17
ADORA2B	9	0.6	0.4	0.6	0.3	0.5	0.28
GRM4	301	0.4	0.8	0.4	0.3	0.5	0.39
FSHR	218	0.4	0.5	0.6	0.5	0.5	0.12
GRM7	229	0.6	0.5	0.5	0.5	0.5	0.08
P2RY12	143	0.5	0.5	0.3	0.6	0.5	0.22
C3AR1	129	0.5	0.6	0.5	0.4	0.5	0.18
GPR124	11	0.6	0.3	0.6	0.5	0.5	0.20
NPS	103	0.6	0.6	0.3	0.4	0.5	0.27
CNR2	233	0.5	0.4	0.4	0.5	0.5	0.08
GRM6	109	0.5	0.4	0.5	0.4	0.5	0.07
GAL2	58	0.6	0.3	0.4	0.6	0.5	0.22
GRPR	117	0.5	0.5	0.4	0.4	0.5	0.08

NPFF2	70	0.4	0.4	0.4	0.5	0.4	0.05
ADRB2	25	0.4	0.4	0.3	0.5	0.4	0.14
NPY2R	191	0.4	0.4	0.4	0.4	0.4	0.07
P2RY8	168	0.4	0.4	0.5	0.3	0.4	0.23
P2RY11	31	0.4	0.4	0.3	0.5	0.4	0.16
GPR75	13	0.3	0.6	0.4	0.3	0.4	0.26
GLP2R	259	0.4	0.4	0.2	0.5	0.4	0.22
GPR50	68	0.3	0.5	0.4	0.4	0.4	0.18
GPR158	140	0.4	0.4	0.3	0.5	0.4	0.17
TAAR9	160	0.3	0.5	0.3	0.4	0.4	0.12
MRGPRG	238	0.5	0.4	0.4	0.3	0.4	0.15
OXER1	215	0.4	0.3	0.4	0.4	0.4	0.07
GPR39	85	0.4	0.4	0.4	0.3	0.4	0.19
GPR37	300	0.5	0.3	0.3	0.3	0.4	0.16
F2RL3	194	0.4	0.3	0.4	0.4	0.3	0.10
CCR5	145	0.4	0.3	0.3	0.3	0.3	0.12
TAAR8	56	0.3	0.3	0.3	0.3	0.3	0.10
RXFP1	104	0.2	0.3	0.2	0.2	0.2	0.05
Control	D2	21.2	18.6	20.7	18.8	19.8	0.06
Control	D2	17.4	19.0	18.2	18.3	18.2	0.03
Control	D2	18.4	16.6	17.3	16.5	17.2	0.04
Control	D2	17.6	15.5	16.3	16.6	16.5	0.05
Control	D2	17.5	15.1	14.8	17.6	16.3	0.08
Control	D2	15.4	16.5	14.7	14.5	15.3	0.05
Control	D2	14.0	14.8	15.0	13.2	14.2	0.05
Control	D2	14.9	14.3	12.2	14.3	13.9	0.07

Table S2. Chemical suppressor screen for mechanism of action studies on SW016789. Fold changes in glucose-stimulated InsGLuc release from MIN6 beta cells pre-exposed to either DMSO or SW016789 (5 μM) for 24 h in the presence or absence of candidate chemical suppressors.

Chemical	Target/MoA	Glucose/Basal (Chronic DMSO)			*2-way ANOVA vs. DMSO adj p-value*	Glucose/Basal (Chronic SW016789)			*2-way ANOVA vs. DMSO adj p-value5*
		mean	*SD*	*N*		*mean*	*SD*	*N*	
DMSO (0.1%)		7.97	2.76	39		1.81	0.62	39	
diazoxide (250 μM)	KATP opener	6.03	1.00	3	0.9703	2.27	0.81	3	0.9997
nifedipine (1 μM)	VDCC blocker	5.50	2.07	3	0.6284	3.79	1.84	3	0.9599
nifedipine (10 μM)		7.96	2.53	32	>0.9999	7.17	2.29	32	<0.0001
nifedipine (50 μM)		9.34	1.36	6	0.9801	7.90	1.72	6	<0.0001
nimodipine (1 μM)	VDCC blocker	6.98	1.77	6	0.9986	6.33	1.62	6	<0.0001
nimodipine (10 μM)		1.79	0.27	6	<0.0001	1.71	0.21	6	>0.9999
nimodipine (50 μM)		1.66	0.39	6	<0.0001	1.45	0.29	6	0.9996
azelnidipine (100 nM)	VDCC blocker	7.45	0.51	3	0.9996	2.30	0.28	3	0.9996
azelnidipine (1 μM)		2.29	0.25	3	<0.0001	2.72	0.19	3	0.9993
azelnidipine (10 μM)		1.53	0.48	3	<0.0001	1.35	0.22	3	0.9997
verapamil (10 μM)	VDCC blocker	5.40	0.57	2	0.8998	2.52	0.34	2	0.9996
verapamil (50 μM)		8.76	1.17	6	0.999	5.78	0.38	6	<0.0001
diltiazem (50 μM)	Ca2+ channel blocker	6.03	2.92	8	0.2066	2.88	0.90	8	0.998
w-Agatoxin IVA (100 nM)	P/Q-type calcium channel blocker	7.05	3.61	2	0.9994	3.07	0.12	2	0.9991
SNX-482 (100 nM)	R-type calcium channel blocker	13.63	2.43	2	0.0004	1.91	0.77	2	>0.9999
w-conotoxin MVIIC (500 nM)	N-type calcium channel blocker	7.40	0.73	2	0.9997	4.03	0.84	2	0.9822
NNC550396 (25 μM)	T-type (Cav3) calcium channel blocker	2.29	1.40	2	0.0004	0.51	0.29	2	0.999
DCPIB (50 μM)	VSAC blocker (SWELL1 inhibitor)	6.99	4.89	2	0.9994	3.49	1.93	2	0.9986
CBA (20 μM)	TRPM4 blocker	7.41	0.14	2	0.9997	3.45	1.34	2	0.9986
2-APB (100 μM)	IP3 receptor antagonist	3.61	1.48	5	<0.0001	1.40	0.35	5	0.9996
FK-506 (100 nM)	Calcineurin inhibitor	4.90	1.73	5	0.0122	1.58	0.60	5	0.9998
FK-506 (1 μM)		6.38	3.01	5	0.9523	1.64	0.45	5	0.9999
U73122 (2 μM)	PLCβ inhibitor	4.57	2.32	5	0.0024	1.43	0.47	5	0.9996
epinephrine (10 nM)	adrenergic receptor agonist	6.89	1.44	3	0.999	1.67	0.52	3	>0.9999
somatostatin (100 nM)	SST receptor agonist	7.32	1.28	3	0.9995	1.59	0.34	3	0.9999
GSK2656157 (100 nM)	PERK inhibitor	8.05	2.18	7	>0.9999	1.55	0.63	7	0.9997

ISRIB (200 nM)	eIF2B stabilizer	7.97	1.91	7	>0.9999	1.75	0.37	7	>0.9999
salubrinal (1 μM)	eIF2a phosphatase inhibitor	13.81	1.97	3	<0.0001	2.47	0.34	3	0.9995
salubrinal (50 μM)		16.43	1.35	3	<0.0001	5.54	1.11	3	0.0207
sephin 1 (1 μM)	eIF2a phosphatase inhibitor	11.43	1.70	3	0.0503	4.65	0.61	3	0.3033
sephin 1 (50 μM)		1.93	0.40	3	<0.0001	1.32	0.17	3	0.9996
TUDCA (50 μM)	bile acid / chemical chaperone	16.24	3.61	3	<0.0001	2.96	0.75	3	0.999
TUDCA (250 μM)		13.20	4.44	3	<0.0001	2.29	0.38	3	0.9997
ceapin-A7 (5 μM)	ATF6 inhibitor	8.74	2.53	4	0.9993	1.60	0.36	4	0.9998
MKC3946 (10 μM)	IRE1a inhibitor (RNAse)	5.33	1.02	4	0.1993	1.65	0.28	4	0.9999
KIRA6 (10 μM)	IRE1a inhibitor (kinase)	3.67	0.54	4	0.0002	1.57	0.49	4	0.9998
rapamycin (100 nM)	mTOR inhibitor	4.31	2.00	5	0.0006	1.44	0.50	5	0.9997
PD0325901 (1 μM)	MEK1/2 inhibitor	3.49	1.61	5	<0.0001	1.45	0.50	5	0.9997
YM-254890 (10 nM)	Gq (and G11/14) inhibitor	3.88	1.14	3	0.0053	2.49	1.59	3	0.9995
YM-254890 (100 nM)		3.63	1.34	3	0.002	2.70	1.85	3	0.9993
YM-254890 (500nM)		3.80	1.22	6	<0.0001	2.36	0.98	6	0.9994
YM-254890 (1 μM)		3.52	1.49	3	0.0012	2.56	2.00	3	0.9994
YM-58483 (10 μM)		8.50	1.56	2	0.9997	2.54	0.74	2	0.9996
CCh (100 μM)	muscarinic agonist	4.48	0.60	3	0.0459	2.35	1.20	3	0.9996
CCh (500 μM)		5.85	1.31	3	0.9015	1.83	0.72	3	>0.9999
PKI (10 μM)	Myristoylated PKA inhibitoir 14-22 amide	8.97	1.48	3	0.9991	2.23	0.30	3	0.9997
H89 (5 μM)	PKA inhibitor	9.38	1.20	3	0.9985	1.65	0.17	3	0.9999
ddAd (100 μM)	adenylyl cyclase inhibitor	7.65	0.57	3	0.9998	2.62	1.37	3	0.9994
PMA (100 nM)	PKC activator	12.34	1.06	3	0.0017	1.79	0.20	3	>0.9999
MRS 2578 (10 μM)	P2Y6 antagonist	9.77	0.76	3	0.9835	2.48	0.29	3	0.9995
MRS 2578 (50 μM)		5.96	2.73	3	0.9486	1.44	0.18	3	0.9997
ML385 (1 μM)	Nrf2 inhibitor	10.23	0.21	3	0.8061	1.82	0.08	3	>0.9999
ML385 (10 μM)		4.99	0.49	3	0.2171	1.51	0.31	3	0.9998
omaveloxolone (1 μM)	Nrf2 activator	3.64	0.66	3	0.0021	1.22	0.21	3	0.9996
omaveloxolone (10 μM)		0.95	0.03	3	<0.0001	1.04	0.36	3	0.9994
GW1100 (1 μM)	GPR40 antagonist	7.44	3.00	4	0.9996	1.57	0.42	4	0.9998
GW1100 (10 μM)		6.89	3.36	4	0.9988	3.51	1.04	4	0.9709
TAK-875 (1 μM)	GPR40 agonist	8.40	2.41	4	0.9996	1.57	0.34	4	0.9998
TAK-875 (10 μM)		8.96	3.55	4	0.999	1.50	0.04	4	0.9997
VUF11207 (1 nM)	CXCR7 agonist (CXCR4 antagonist)	8.83	2.74	4	0.9991	1.66	0.28	4	0.9999

VUF11207 (1 μM)	7.55	2.29	4	0.9997	1.42	0.36	4	0.9997
VUF11207 (10 μM)	5.34	1.09	4	0.201	1.40	0.14	4	0.9997

Table S3. Raw metabolomics data for SW016789-treated MIN6 cells. Raw total internal current (TIC) values for metabolomics screen.

					Samples											
HMDB	**PubChem**	**KEGG**	**Metabolite Name**	**MS Transition**	**DMSO_BAS_1**	**DMSO_BAS_2**	**DMSO_BAS_3**	**DMSO_G30_1**	**DMSO_G30_2**	**DMSO_G30_3**	**SW016789_BAS_1**	**SW016789_BAS_2**	**SW016789_BAS_3**	**SW016789_G30_1**	**SW016789_G30_2**	**SW016789_G30_3**
HMDB03331	27476	C02494	1-Methyladenosine	1-methyl-adenosine_pos-1	1.29E-03	1.16E-03	1.04E-03	1.20E-03	1.51E-03	1.55E-03	1.54E-03	2.14E-03	1.72E-03	2.13E-03	1.69E-03	1.54E-03
HMDB00699	457	C02918	1-Methylnicotinamide	1-methyl-nicotinamide_pos-3	1.58E-03	1.41E-03	2.38E-03	2.34E-03	2.26E-03	1.26E-03	1.63E-03	2.38E-03	1.14E-03	2.26E-03	1.48E-03	1.92E-03
HMDB00606	439391	C01087	2-Hydroxyglutaric acid	hydroxyglutaric acid_neg-44	1.61E-03	1.54E-03	1.24E-03	2.13E-03	2.54E-03	2.05E-03	1.64E-03	1.46E-03	1.14E-03	2.14E-03	2.67E-03	1.50E-03
HMDB00707	979	C01179	4-Hydroxyphenylpyruvic acid	hydroxyphenylpyruvate_pos-73	7.77E-04	7.28E-04	8.60E-04	7.92E-04	1.16E-03	8.42E-04	6.71E-04	8.08E-04	1.04E-03	9.90E-04	9.31E-04	7.84E-04
HMDB00725	5810	C01157	4-Hydroxyproline	hydroxy-proline_pos-74	3.48E-06	3.35E-04	4.01E-04	4.19E-06	3.64E-06	6.35E-04	3.37E-04	3.26E-06	3.93E-04	3.54E-06	3.48E-06	4.21E-04
HMDB00017	6723	C00847	4-Pyridoxic acid	4-pyridoxic acid_pos-7	1.22E-04	1.04E-04	2.03E-04	2.13E-04	1.70E-04	8.52E-05	1.94E-04	2.46E-04	2.07E-04	1.19E-04	1.38E-04	4.46E-06
HMDB01173	439176	C00170	5'-Methylthioadenosine	S-methyl-5-thioadenosine_pos-134	2.69E-02	3.47E-02	7.43E-02	5.00E-02	2.66E-02	4.75E-02	4.49E-02	4.72E-02	7.18E-02	3.89E-02	3.67E-02	5.76E-02
HMDB01107	445404	-	7-Methylguanosine	7-methylguanosine_pos-10	3.26E-04	5.50E-04	3.97E-04	3.02E-04	2.21E-04	2.70E-04	1.54E-03	1.83E-03	1.51E-03	1.62E-03	2.31E-03	1.13E-03
HMDB00895	187	C01996	Acetylcholine	acetyl-choline_pos-13	5.35E-03	4.71E-03	5.48E-03	4.72E-03	3.90E-03	4.09E-03	3.58E-03	4.76E-03	5.62E-03	6.64E-03	7.19E-03	3.91E-03
HMDB00034	190	C00147	Adenine	adenine_pos-15	1.12E-03	8.63E-04	8.89E-04	8.95E-04	1.05E-03	8.66E-04	1.01E-03	1.21E-03	1.17E-03	1.29E-03	1.06E-03	1.54E-03
HMDB00050	60961	C00212	Adenosine	adenosine_pos-16	1.53E-02	1.56E-02	1.87E-02	1.51E-02	1.97E-02	1.49E-02	1.15E-02	1.96E-02	2.40E-02	1.96E-02	2.60E-02	2.79E-02
HMDB00045	6083	C00020	Adenosine monophosphate	AMP_neg-16	3.47E-03	3.96E-03	3.44E-03	1.71E-03	1.99E-03	1.34E-03	2.81E-03	3.47E-03	4.50E-03	1.39E-03	1.54E-03	1.23E-03
HMDB00019	49	C00141	Alpha-ketoisovaleric acid	a-ketoisovaleric acid_neg-15	3.48E-06	3.35E-06	5.24E-06	1.32E-03	1.38E-03	1.11E-03	3.55E-06	3.26E-06	5.59E-06	1.82E-03	1.69E-03	1.22E-03
HMDB00510	469	C00956	Aminoadipic acid	aminoadipic acid_pos-21	2.56E-04	2.65E-04	4.21E-04	3.27E-04	2.89E-04	4.05E-04	2.16E-04	2.55E-04	4.72E-04	4.09E-04	2.78E-04	5.04E-04
HMDB01539	123831	C03626	Asymmetric dimethylarginine	Ng,Ng-dimethyl-arginine_pos-107	1.40E-04	3.34E-04	2.20E-04	6.98E-05	2.36E-04	9.49E-05	2.27E-04	2.01E-04	1.21E-04	1.82E-04	9.33E-05	1.07E-04
HMDB00043	247	C00719	Betaine	betaine_pos-26	1.79E-02	1.69E-02	2.69E-02	2.55E-02	2.62E-02	4.59E-02	2.11E-02	1.89E-02	3.09E-02	2.55E-02	2.66E-02	2.90E-02
HMDB02013	439829	C02862	Butyrylcarnitine	carnitine-C4_pos-37	1.33E-03	1.19E-03	2.47E-04	1.66E-03	3.18E-03	4.16E-04	1.09E-03	1.18E-03	2.22E-04	2.73E-03	2.08E-03	4.73E-04
HMDB0011671	NA	NA	cADP-ribose	cADP-ribose_neg-18	1.59E-03	1.60E-03	1.60E-03	1.85E-03	1.79E-03	2.32E-03	1.66E-03	1.12E-03	1.96E-03	1.76E-03	1.37E-03	1.47E-03
HMDB01096	278	C00169	Carbamoyl phosphate	carbamoylphosphate_neg-19	2.10E-04	2.64E-04	1.28E-04	2.52E-04	2.03E-04	9.13E-05	2.53E-04	2.85E-04	1.26E-04	2.51E-04	2.40E-04	5.62E-05
HMDB00062	10917	C00487	Carnitine	carnitine_pos-30	1.81E-02	2.15E-02	3.00E-02	3.15E-02	2.77E-02	2.80E-02	2.03E-02	1.67E-02	1.90E-02	3.05E-02	2.55E-02	1.94E-02
HMDB00097	305	C00114	Choline	choline_pos-41	1.43E-03	2.01E-03	1.26E-03	1.24E-03	1.43E-03	8.61E-04	1.91E-03	2.23E-03	2.97E-03	1.11E-03	1.64E-03	1.55E-03
HMDB00094	311	C00158	Citric acid	citrate-isocitrate_neg-22	3.60E-02	4.22E-02	3.85E-02	5.24E-02	6.90E-02	6.60E-02	3.47E-02	3.64E-02	2.88E-02	4.82E-02	5.80E-02	6.00E-02
HMDB00064	586	C00300	Creatine	creatine_pos-44	6.25E-03	9.22E-03	1.02E-02	4.52E-03	5.71E-03	5.63E-03	6.56E-03	6.38E-03	1.02E-02	4.13E-03	3.91E-03	4.18E-03
HMDB00562	588	C00791	Creatinine	creatinine_pos-45	1.09E-04	3.21E-04	2.99E-04	9.49E-04	5.86E-04	7.41E-04	1.17E-04	1.58E-04	1.81E-04	4.70E-04	2.96E-04	5.02E-04
HMDB00089	6175	C00475	Cytidine	cytidine_pos-49	9.49E-04	1.28E-03	1.98E-03	1.06E-03	6.18E-04	1.16E-03	1.60E-03	3.37E-03	1.04E-03	1.87E-03	1.64E-03	2.02E-03
HMDB00095	6131	C00055	Cytidine monophosphate	CMP_pos-43	1.92E-03	1.08E-03	9.29E-04	1.39E-03	1.61E-03	1.36E-03	1.26E-03	1.34E-03	6.96E-04	1.25E-03	9.23E-04	8.16E-04
HMDB00905	12599	C00360	Deoxyadenosine monophosphate	dAMP_pos-51	7.20E-04	1.24E-03	3.24E-03	1.04E-03	8.90E-04	2.41E-03	7.83E-04	9.28E-04	1.69E-03	2.10E-03	3.28E-03	1.51E-04

HMDB00014	13711	C00881	Deoxycytidine	2-deoxycytidine_pos-6	5.95E-05	7.59E-05	1.62E-04	1.14E-04	1.16E-04	1.48E-04	8.54E-05	1.27E-04	5.43E-05	9.66E-05	1.05E-04	1.20E-04
HMDB00071	65058	C05512	Deoxyinosine	deoxyinosine_pos-52	3.48E-06	9.76E-05	7.02E-05	6.10E-05	1.38E-04	5.26E-06	1.17E-04	1.29E-04	1.94E-04	2.67E-04	1.42E-04	1.96E-04
HMDB01351	439287	C00672	Deoxyribose 1-phosphate	deoxyribose-phosphate_neg-23	5.66E-04	5.12E-04	9.71E-04	6.06E-04	4.48E-04	9.17E-04	4.14E-04	5.29E-04	1.10E-03	3.72E-04	6.18E-04	8.30E-04
HMDB00122	5793	C00031	D-Glucose	glucose-fructose_neg-36	3.48E-06	2.79E-05	5.24E-06	4.22E-04	4.28E-04	2.60E-04	3.28E-05	2.71E-05	5.59E-06	3.72E-04	3.83E-04	3.59E-04
HMDB00127	444791	C00191	D-Glucuronic acid	glucuronate_neg-38	3.23E-04	2.68E-04	1.83E-04	4.38E-04	5.71E-04	5.13E-04	2.93E-04	2.95E-04	1.67E-04	4.55E-04	4.47E-04	5.34E-04
HMDB03339	23327	C00217	D-Glutamic acid	glutamate_neg-39	1.68E-02	1.58E-02	1.77E-02	1.73E-02	1.20E-02	1.60E-02	1.73E-02	1.50E-02	1.58E-02	1.25E-02	1.14E-02	1.34E-02
HMDB01473	668	C00111	Dihydroxyacetone phosphate	dihydroxyacetone-phosphate_neg-25	2.40E-04	3.19E-04	6.49E-04	4.57E-04	3.54E-04	7.18E-04	3.25E-04	2.58E-04	6.51E-04	4.04E-04	3.39E-04	5.25E-04
HMDB00092	673	C01026	Dimethylglycine	dimethylglycine_pos-54	2.85E-03	2.73E-03	2.44E-03	1.93E-03	1.97E-03	1.65E-03	2.97E-03	2.42E-03	3.24E-03	2.28E-03	2.22E-03	5.63E-03
HMDB01548	439167	C00117	D-Ribose 5-phosphate	ribose 5-phosphate_neg-66	1.11E-04	1.18E-04	2.25E-04	4.19E-06	3.64E-06	1.46E-04	1.14E-04	8.75E-05	2.40E-04	8.19E-05	3.48E-06	4.46E-06
HMDB01068	22833559	C00281	D-Sedoheptulose 7-phosphate	sedoheptulose-7-phosphate_neg-68	1.99E-04	2.80E-04	2.60E-04	2.50E-04	1.71E-04	2.91E-04	2.17E-04	2.11E-04	3.28E-04	1.84E-04	2.63E-04	2.85E-04
HMDB00121	6037	C00504	Folic acid	folic acid_pos-57	3.76E-04	3.94E-04	2.98E-04	3.04E-04	4.12E-04	2.38E-04	4.42E-04	3.68E-04	4.26E-04	2.96E-04	3.22E-04	2.85E-04
HMDB01058	172313	C00354	Fructose 1,6-bisphosphate	fructose-1,6-biphosphate_neg-27	3.48E-06	2.17E-05	4.12E-05	2.67E-04	3.33E-04	4.57E-04	3.55E-06	3.26E-06	6.72E-05	3.37E-04	3.80E-04	2.17E-04
HMDB00645	123912	C00446	Galactose 1-phosphate	galactose 1-phosphate_neg-30	1.24E-04	1.22E-04	6.78E-05	1.11E-04	1.75E-04	2.17E-04	1.18E-04	9.65E-05	1.68E-04	1.32E-04	1.40E-04	4.33E-05
HMDB00112	119	C00334	Gamma-Aminobutyric acid	y-aminobutyric acid_pos-155	5.12E-03	6.72E-03	5.94E-03	4.67E-03	6.56E-03	5.73E-03	5.61E-03	7.00E-03	1.16E-02	6.85E-03	7.08E-03	9.32E-03
HMDB00625	10690	C00257	Gluconic acid	gluconic acid_neg-34	1.24E-04	4.72E-05	1.67E-04	6.97E-05	3.64E-06	1.14E-04	9.85E-05	3.26E-06	1.60E-04	3.76E-05	3.48E-06	4.46E-06
HMDB01401	5958	C00092	Glucose 6-phosphate	G6P-F6P_neg-29	6.75E-05	5.11E-05	7.02E-05	5.70E-04	3.53E-04	6.55E-04	2.79E-05	6.33E-05	3.62E-05	4.13E-04	3.88E-04	4.09E-04
HMDB00125	124886	C00051	Glutathione	GSH_pos-64	3.12E-02	1.26E-02	2.02E-02	1.64E-02	1.51E-02	3.01E-02	1.67E-02	1.31E-02	2.71E-02	1.64E-02	1.69E-02	1.88E-02
HMDB00126	439162	C00093	Glycerol 3-phosphate	sn-glycero3-phosphate_neg-69	2.11E-04	2.23E-04	4.02E-04	1.90E-04	1.09E-04	1.48E-04	3.51E-04	2.35E-04	4.60E-04	1.47E-04	1.67E-04	1.39E-04
HMDB00086	71920	C00670	Glycerophosphocholine	glycerophosphorylcholine_pos-61	8.38E-02	7.55E-02	4.72E-02	5.81E-02	5.82E-02	4.07E-02	6.16E-02	6.49E-02	2.65E-02	6.85E-02	6.22E-02	3.76E-02
HMDB00123	750	C00037	Glycine	glycine_pos-62	1.82E-04	2.06E-04	2.94E-04	1.57E-04	1.55E-04	1.29E-04	1.58E-04	1.67E-04	1.47E-04	1.32E-04	1.01E-04	1.90E-04
HMDB00119	760	C00048	Glyoxylic acid	glyoxylate_neg-42	3.48E-06	3.35E-06	5.24E-06	2.46E-04	2.66E-04	1.80E-04	3.28E-05	3.26E-06	7.75E-05	3.34E-04	1.51E-04	3.47E-04
HMDB00128	763	C00581	Guanidoacetic acid	guanidoacetic acid_pos-66	1.98E-03	2.26E-03	1.10E-03	2.53E-03	2.66E-03	1.01E-03	2.48E-03	1.68E-03	1.53E-03	1.89E-03	2.37E-03	1.54E-03
HMDB00132	764	C00242	Guanine	guanine_pos-67	9.78E-04	1.16E-03	6.25E-04	6.40E-04	6.79E-04	2.26E-04	1.08E-03	9.94E-04	5.19E-04	6.16E-04	6.08E-04	2.29E-04
HMDB00133	6802	C00387	Guanosine	guanosine_pos-68	5.85E-03	9.17E-03	3.39E-03	1.06E-02	5.31E-03	6.52E-03	1.60E-02	1.69E-02	6.75E-03	2.11E-02	2.03E-02	1.45E-02
HMDB00157	790	C00262	Hypoxanthine	hypoxanthine_pos-75	2.26E-03	1.08E-03	2.47E-03	1.13E-03	1.43E-03	8.83E-04	2.06E-03	1.76E-03	3.27E-03	1.62E-03	2.14E-03	1.04E-03
HMDB00738	798	C00463	Indole	indole_pos-79	7.86E-04	8.57E-04	4.96E-04	8.10E-04	8.64E-04	4.82E-04	7.39E-04	7.31E-04	5.21E-04	7.99E-04	9.18E-04	5.93E-04
HMDB00195	6021	C00294	Inosine	inosine_pos-90	3.89E-03	2.62E-03	1.43E-03	4.59E-03	3.53E-03	9.84E-03	1.17E-02	8.08E-03	3.66E-03	7.77E-03	7.33E-03	7.64E-03
HMDB00175	8582	C00130	Inosinic acid	IMP_pos-78	1.19E-02	1.59E-02	1.43E-02	5.27E-03	6.57E-03	5.42E-03	1.03E-02	1.12E-02	9.58E-03	3.80E-03	4.45E-03	4.65E-03
HMDB00688	6426851	-	Isovalerylcarnitine	carnitine-C5_pos-38	7.73E-04	1.77E-03	3.56E-04	1.60E-03	2.93E-03	7.98E-04	1.09E-03	1.33E-03	4.24E-04	3.16E-03	2.08E-03	7.10E-04
HMDB00748	643327	C05607	L-3-Phenyllactic acid	phenyl-lactic acid_neg-58	1.04E-03	8.35E-04	1.50E-03	1.11E-03	1.31E-03	1.10E-03	1.22E-03	8.36E-04	2.02E-03	9.50E-04	1.23E-03	1.26E-03
HMDB00201	1	C02571	L-Acetylcarnitine	acetyl-carnitine_pos-12	1.71E-01	1.24E-01	1.52E-01	1.31E-01	9.27E-02	1.39E-01	1.83E-01	1.60E-01	1.38E-01	1.35E-01	1.05E-01	1.57E-01
HMDB00161	5950	C00041	L-Alanine	alanine_pos-19	7.81E-04	7.40E-04	1.38E-03	9.96E-04	8.70E-04	1.39E-03	7.05E-04	6.51E-04	1.25E-03	7.72E-04	7.99E-04	1.04E-03

HMDB00517	6322	C00062	L-Arginine	arginine_pos-22	3.46E-03	3.39E-03	2.56E-03	2.16E-03	2.21E-03	1.27E-03	2.08E-03	2.09E-03	1.89E-03	1.81E-03	1.50E-03	8.87E-04
HMDB00168	6267	C00152	L-Asparagine	asparagine_pos-23	1.01E-02	9.13E-03	5.46E-03	1.07E-02	9.93E-03	6.17E-03	8.87E-03	8.14E-03	6.31E-03	8.93E-03	1.02E-02	8.41E-03
HMDB00191	5960	C00049	L-Aspartic acid	aspartate_pos-24	2.09E-03	1.79E-03	2.84E-03	1.12E-03	9.93E-04	1.64E-03	1.17E-03	1.65E-03	2.65E-03	1.00E-03	6.72E-04	1.35E-03
HMDB00099	439258	C02291	L-Cystathionine	cystathionine _pos-46	1.24E-03	8.77E-04	1.51E-03	2.26E-03	1.56E-03	1.81E-03	1.75E-03	1.49E-03	1.28E-03	1.43E-03	1.15E-03	1.59E-03
HMDB00574	5862	C00097	L-Cysteine	cysteine_pos-47	6.43E-05	9.14E-05	8.72E-05	4.19E-06	3.64E-06	5.26E-06	6.40E-05	1.01E-04	8.53E-05	4.26E-05	3.48E-06	4.46E-06
HMDB00641	5961	C00064	L-Glutamine	glutamine_pos-60	1.42E-03	1.95E-03	7.78E-04	1.39E-03	2.82E-03	1.23E-03	1.11E-03	1.19E-03	9.24E-04	1.20E-03	2.39E-03	9.97E-04
HMDB00756	3246938	-	L-Hexanoylcarnitine	carnitine-C6_pos-39	3.40E-03	2.70E-03	2.70E-03	1.83E-03	1.37E-03	1.21E-03	3.94E-03	2.77E-03	3.38E-03	2.33E-03	1.98E-03	9.37E-04
HMDB00177	6274	C00135	L-Histidine	histidine_pos-69	1.44E-04	2.06E-04	5.24E-06	1.47E-04	1.63E-04	1.36E-04	1.24E-04	1.53E-04	1.49E-04	1.72E-04	1.77E-04	1.28E-04
HMDB00719	12647	C00263	L-Homoserine	homoserine_pos-72	9.73E-04	1.09E-03	7.48E-04	7.71E-04	8.08E-04	6.78E-04	9.36E-04	8.29E-04	5.12E-04	8.11E-04	7.80E-04	7.93E-04
HMDB00172	6306	C00407	L-Isoleucine	isoleucine_pos-91	8.79E-02	1.09E-01	5.70E-02	9.63E-02	1.04E-01	5.65E-02	9.13E-02	9.36E-02	6.73E-02	1.06E-01	9.98E-02	7.69E-02
HMDB00190	107689	C00186	L-Lactic acid	lactate_neg-48	3.08E-04	2.78E-04	7.05E-04	2.69E-03	2.52E-03	3.09E-03	2.24E-04	1.67E-04	8.35E-04	3.09E-03	2.41E-03	4.02E-03
HMDB00182	5962	C00047	L-Lysine	lysine_pos-96	3.45E-03	3.98E-03	2.43E-03	1.42E-03	1.36E-03	1.04E-03	2.22E-03	2.05E-03	1.48E-03	1.14E-03	1.88E-03	9.41E-04
HMDB00156	222656	C00149	L-Malic acid	malic acid_neg-49	3.48E-06	3.35E-06	5.24E-06	7.70E-04	8.63E-04	6.01E-04	3.55E-06	3.26E-06	5.59E-06	8.76E-04	8.73E-04	6.54E-04
HMDB00696	6137	C00073	L-Methionine	methionine_pos-98	2.45E-03	3.34E-03	1.60E-03	3.39E-03	4.07E-03	2.23E-03	3.61E-03	3.40E-03	1.62E-03	3.27E-03	3.35E-03	2.28E-03
HMDB00791	11953814	C02838	L-Octanoylcarnitine	carnitine-C8_pos-40	1.98E-03	2.37E-03	1.11E-03	2.29E-03	1.62E-03	6.47E-04	2.32E-03	2.16E-03	1.26E-03	1.41E-03	1.23E-03	1.09E-03
HMDB00159	6140	C00079	L-Phenylalanine	phenyl-alanine_pos-113	1.66E-02	1.87E-02	1.06E-02	2.51E-02	2.29E-02	9.32E-03	1.91E-02	1.44E-02	1.20E-02	2.44E-02	1.82E-02	1.49E-02
HMDB00162	145742	C00148	L-Proline	proline_pos-118	6.03E-02	7.42E-02	5.60E-02	5.31E-02	8.30E-02	5.27E-02	5.26E-02	6.46E-02	4.56E-02	5.04E-02	5.87E-02	3.92E-02
HMDB00187	5951	C00065	L-Serine	serine_pos-130	6.94E-04	5.16E-04	7.63E-04	1.25E-03	6.35E-04	6.45E-04	4.95E-04	7.68E-04	1.12E-03	6.07E-04	8.32E-04	5.80E-04
HMDB00158	6057	C00082	L-Tyrosine	tyrosine_pos-146	8.80E-03	8.59E-03	8.35E-03	1.17E-02	1.28E-02	6.85E-03	1.00E-02	1.13E-02	1.05E-02	8.35E-03	1.32E-02	1.05E-02
HMDB00883	6287	C00183	L-Valine	valine_pos-152	1.84E-03	1.90E-03	1.36E-03	1.74E-03	2.43E-03	1.28E-03	1.73E-03	1.99E-03	1.04E-03	1.95E-03	1.79E-03	1.51E-03
HMDB02005	847	-	Methionine sulfoxide	methionine sulfoxide_pos-97	2.96E-04	3.45E-04	3.85E-04	3.98E-04	4.11E-04	3.99E-04	3.14E-04	4.69E-04	3.49E-04	3.36E-04	3.35E-04	3.08E-04
HMDB00211	892	C00137	Myoinositol	myo-inositol_pos-99	2.12E-04	4.25E-04	4.53E-04	3.68E-04	4.63E-04	2.90E-04	3.38E-04	3.76E-04	3.41E-04	3.45E-04	3.55E-04	6.11E-04
HMDB01325	440120	C03793	N6,N6,N6-Trimethyl-L-lysine	trimethyllysine_pos-144	2.87E-03	3.44E-03	2.15E-03	3.70E-03	3.83E-03	1.68E-03	2.17E-03	2.51E-03	1.68E-03	2.74E-03	2.36E-03	1.47E-03
HMDB00215	439174	C00140	N-Acetyl-D-glucosamine	N-acetyl-D-glucosamine 1-phosphate _neg-54	1.42E-04	1.37E-04	2.03E-04	7.69E-05	8.10E-05	8.89E-05	2.55E-04	1.10E-04	2.44E-04	3.95E-05	6.86E-05	6.39E-05
HMDB00766	88064	C00624	N-Acetyl-L-alanine	N-acetyl-alanine_neg-53	5.41E-04	3.77E-04	5.84E-04	6.59E-04	5.15E-04	9.46E-04	2.69E-04	3.74E-04	4.53E-04	7.20E-04	3.34E-04	3.43E-04
HMDB00812	65065	C01042	N-Acetyl-L-aspartic acid	N-acetyl-aspartic acid_pos-101	7.25E-04	5.25E-04	2.82E-04	2.88E-04	6.03E-04	8.21E-04	5.29E-04	7.96E-04	1.11E-03	7.02E-04	6.50E-04	4.66E-04
HMDB00902	5893	C00003	NAD	NAD_pos-105	1.30E-01	1.43E-01	1.65E-01	1.57E-01	1.52E-01	1.83E-01	1.24E-01	1.27E-01	1.70E-01	1.33E-01	1.61E-01	1.49E-01
HMDB00446	192590	C12989	N-Alpha-acetyllysine	acetyllysine_pos-14	2.68E-03	2.57E-03	1.74E-03	2.13E-03	2.81E-03	1.48E-03	2.05E-03	2.06E-03	1.54E-03	1.63E-03	2.18E-03	1.05E-03
HMDB01406	936	C00153	Niacinamide	nicotinamide_pos-108	7.08E-04	1.05E-03	7.10E-04	1.35E-03	1.58E-03	2.21E-03	9.36E-04	1.00E-03	3.02E-04	1.25E-03	8.50E-04	7.52E-04
HMDB00214	6262	C00077	Ornithine	ornithine_pos-111	2.95E-04	2.53E-04	3.54E-04	1.82E-04	2.15E-04	1.37E-04	1.44E-04	1.98E-04	1.99E-04	1.39E-04	9.97E-05	1.35E-04
HMDB03337	975	C00127	Oxidized glutathione	GSSG_pos-65	1.30E-03	3.36E-03	1.99E-03	6.08E-04	1.37E-03	1.34E-03	1.32E-03	1.76E-03	3.00E-03	9.54E-04	5.73E-04	1.37E-03
HMDB00208	51	C00026	Oxoglutaric acid	a-keto-glutarate_neg-14	1.60E-04	2.11E-04	5.24E-06	5.20E-04	8.14E-04	5.54E-04	9.69E-05	1.50E-04	5.59E-06	5.41E-04	6.65E-04	3.54E-04

HMDB00210	988	C00864	Pantothenic acid	pantothenic acid_pos-112	2.79E-02	2.46E-02	2.39E-02	3.43E-02	3.08E-02	2.47E-02	2.21E-02	2.54E-02	2.00E-02	2.90E-02	2.55E-02	3.64E-02
HMDB01511	587	C02305	Phosphocreatine	phospho-creatine_neg-60	1.11E-04	1.24E-04	1.59E-04	4.31E-04	3.87E-04	4.40E-04	8.54E-05	1.55E-04	8.01E-05	3.00E-04	3.04E-04	3.81E-04
HMDB01565	1014	C00588	Phosphorylcholine	phosphorylcholine_pos-115	2.33E-02	2.01E-02	4.01E-02	1.73E-02	2.16E-02	3.22E-02	2.31E-02	1.73E-02	4.40E-02	2.38E-02	1.27E-02	4.70E-02
HMDB00070	849	C00408	Pipecolic acid	pipecolic acid_pos-116	7.90E-03	5.44E-03	5.08E-03	6.95E-03	8.67E-03	6.26E-03	6.46E-03	6.33E-03	4.31E-03	6.98E-03	5.91E-03	5.32E-03
HMDB00824	107738	C03017	Propionylcarnitine	carnitine-C3_pos-36	3.31E-02	2.93E-02	9.61E-03	9.61E-03	1.31E-02	3.39E-03	3.09E-02	4.00E-02	2.48E-02	1.62E-02	2.16E-02	4.66E-03
HMDB13305	75612	-	Propionylcholine	propionylcholine_pos-119	1.08E-02	1.14E-02	1.13E-02	1.27E-02	1.31E-02	1.32E-02	1.09E-02	1.20E-02	1.11E-02	1.10E-02	1.27E-02	1.04E-02
HMDB01414	1045	C00134	Putrescine	putrescine_pos-121	1.32E-04	1.73E-04	2.42E-04	1.69E-04	1.82E-04	1.70E-04	1.77E-04	1.69E-04	2.51E-04	1.08E-04	4.04E-04	1.03E-04
HMDB01431	1052	C00534	Pyridoxamine	pyridoxamine_pos-122	1.11E-04	1.78E-04	5.24E-06	2.65E-04	3.58E-04	2.94E-04	9.19E-05	1.06E-04	5.59E-06	2.37E-04	3.62E-04	1.97E-04
HMDB00232	1066	C03722	Quinolinic acid_pos-125	quinolinate_pos-125	4.40E-04	2.35E-04	6.94E-04	9.00E-04	7.32E-04	1.15E-03	4.10E-04	3.69E-04	4.70E-04	6.97E-04	5.15E-04	6.65E-04
HMDB00244	493570	C00255	Riboflavin	riboflavin_pos-127	2.85E-04	2.43E-04	3.08E-04	3.49E-04	3.62E-04	2.07E-04	8.84E-04	6.92E-04	5.45E-04	4.77E-04	8.98E-04	3.18E-04
HMDB00939	439155	C00021	S-Adenosylhomocysteine	S-adenosyl-homocysteine_neg-67	6.63E-04	7.63E-04	1.64E-03	6.92E-04	5.99E-04	1.04E-03	1.09E-03	9.23E-04	2.70E-03	5.65E-04	5.60E-04	1.11E-03
HMDB01185	16757548	C00019	S-Adenosylmethionine	S-adenosyl-methionine_pos-128	7.40E-03	1.21E-02	1.07E-02	8.25E-03	1.86E-02	1.81E-02	1.22E-02	8.92E-03	1.51E-02	8.63E-03	9.65E-03	1.86E-02
HMDB03070	8742	C00493	Shikimic acid	shikimic acid_pos-131	1.13E-02	8.70E-03	9.38E-03	6.23E-03	6.24E-03	4.53E-03	6.70E-03	8.18E-03	5.65E-03	5.03E-03	4.05E-03	3.11E-03
HMDB01066	440018	C03451	S-Lactoylglutathione	S-lactoylglutathione _pos-133	3.48E-06	3.35E-06	5.24E-06	1.84E-03	1.83E-03	3.00E-03	3.55E-06	3.26E-06	5.59E-06	2.01E-03	1.18E-03	2.20E-03
HMDB01257	1102	C00315	Spermidine	spermidine_pos-135	8.12E-03	1.34E-02	1.22E-02	8.27E-03	1.24E-02	1.42E-02	1.23E-02	1.40E-02	2.50E-02	1.51E-02	1.75E-02	1.44E-02
HMDB01256	1103	C00750	Spermine	spermine_pos-136	1.44E-03	1.78E-03	3.24E-03	5.26E-03	3.15E-03	3.81E-03	3.29E-03	4.43E-03	2.81E-03	2.25E-03	7.24E-03	1.71E-03
HMDB00848	6426855	-	Stearoylcarnitine	carnitine-C18_pos-34	9.05E-04	7.81E-04	4.19E-04	3.64E-04	1.89E-04	1.73E-04	9.93E-04	9.43E-04	4.96E-04	3.90E-04	1.22E-04	2.02E-04
HMDB00254	1110	C00042	Succinic acid	succinate_neg-70	2.54E-03	2.71E-03	2.16E-03	2.27E-03	3.48E-03	3.62E-03	2.82E-03	2.38E-03	2.26E-03	2.73E-03	4.66E-03	2.69E-03
HMDB00251	1123	C00245	Taurine	taurine_neg-71	2.67E-02	2.29E-02	3.47E-02	2.65E-02	2.33E-02	2.79E-02	2.73E-02	2.17E-02	3.17E-02	2.34E-02	2.11E-02	2.52E-02
HMDB05066	53477791	-	Tetradecanoylcarnitine	carnitine-C14_pos-32	7.75E-04	1.47E-03	5.06E-04	2.77E-04	3.20E-04	2.80E-04	6.72E-04	1.11E-03	4.65E-04	4.04E-04	1.33E-04	3.08E-04
HMDB00235	1130	C00378	Thiamine	thiamine_pos-139	5.75E-04	6.64E-04	4.65E-04	5.81E-04	5.41E-04	3.83E-04	3.66E-04	5.01E-04	3.67E-04	5.55E-04	6.79E-04	2.29E-04
HMDB00273	5789	C00214	Thymidine	thymidine_pos-142	6.75E-05	9.91E-05	5.24E-06	4.19E-06	7.24E-05	5.26E-06	7.64E-05	1.12E-04	6.46E-05	1.26E-04	1.20E-04	4.46E-06
HMDB00300	1174	C00106	Uracil	uracil_pos-147	1.83E-04	9.91E-05	8.72E-05	6.20E-05	3.64E-06	9.00E-05	1.13E-04	9.65E-05	1.65E-04	3.54E-06	6.92E-05	6.40E-05
HMDB00296	6029	C00299	Uridine	uridine_neg-77	3.48E-06	3.25E-05	5.24E-06	2.71E-05	2.19E-05	5.11E-05	6.40E-05	3.77E-05	2.07E-05	3.77E-05	4.02E-05	4.33E-05
HMDB00295	6031	C00015	Uridine 5'-diphosphate	UDP_neg-72	8.68E-05	8.98E-05	7.26E-05	1.09E-04	9.93E-05	8.52E-05	8.37E-05	5.73E-05	1.45E-04	1.24E-04	3.59E-04	7.43E-05
HMDB00292	1188	C00385	Xanthine	xanthine_neg-78	2.80E-04	3.55E-04	1.69E-04	2.50E-04	2.71E-04	1.07E-04	3.25E-04	3.20E-04	2.92E-04	2.42E-04	2.61E-04	1.44E-04
HMDB00299	64959	C01762	Xanthosine	xanthosine_pos-154	4.16E-04	4.56E-04	1.79E-04	6.49E-04	5.54E-04	7.28E-04	3.28E-04	4.41E-04	3.62E-05	4.42E-04	1.07E-03	5.18E-04

Table S4. Research material sources. All information pertaining to chemical reagents, antibodies, qPCR primers, and donor human islets.

Reagents

Name	Company	Catalog#
2-APB	Sigma	100065
Antimycin A	Sigma	A8674
azelnidipine	Fisher	AC465060010
carbachol	Sigma	C-4382
CBA	Tocris	6724
ceapin-A7	Sigma	SML2330-5MG
coelenterazine	Nanolight	3035MG
coelenterazine-h	Promega	S2011
DCPIB	Tocris	1540/10
diazoxide	Sigma	D9035
dideoxyadenosine	Santa Cruz Biotechnology	c-201562
diltiazem	Fisher	AC329080010
epinephrine	Sigma	E4375
FCCP	Fisher	NC0904863
FK-506	LC Labs	F-4900
forskolin	Sigma	F3917-10MG
FPL64176	Cayman	20122
fura-2-LR-AM	Fisher	34-491-11SET
GSK2656157	Sigma	5046510001
GW1100	Fisher	50-190-5117
H89	Sigma	B1427
IBMX	Sigma	I5879
ISRIB	Sigma	SML0843
KIRA6	Sigma	5322810001
MKC3946	Sigma	5327580001
ML385	Medchem Express	HY1005235MG
MRS 2578	Selleck	S285510MG
nifedipine	Sigma	N7634-1G

nimodipine	Acros	329280010
NNC550396	Santa Cruz Biotechnology	sc-203647A
oligomycin	Sigma	O4876
omaveloxolone	Apexbio	B3576
PD0325901	LC Labs	P-9688
PKI (myr-PKA inhibitor 14-22 amide)	Fisher	47-648-5500UG
PMA (phorbol 12-myristate)	Sigma	P1585
rapamycin	LC Labs	R-5000
salubrinal	Fisher	50-101-1234
sephin 1	Sigma	SML1356
SNX-482	Tocris	2945
somatostatin	Fisher	11-571-R
SW016789	Chembridge	CB 5785370
TAK-875	Fisher	NC1376701
thapsigargin	Fisher	50-464-293
TUDCA	Fisher	NC1266953
U73122	Sigma	U6881
verapamil	Sigma	V4629
VUF11207	Sigma	SML0669
YM-254890	Fisher	50-149-0016
ω-Agatoxin IVA	Tocris	2799
ω-conotoxin MVIIC	Fisher	50-168-6383
Cell Titer Glo	Fisher	PR-G7572
Multitox Fluor	Promega	G9200
2X Sybr qPCR master mix	Bio-Rad\	1725125

Antibodies

Protein	Host Species	kDa	Company	Cat#	RRID	Dilution
CHOP	mouse	27	Cell Signaling Technology	2895	AB_2089254	1:1000
PARP (cleaved) mouse	mouse	89	Cell Signaling Technology	9548	AB_2160592	1:1000
BclXL (54H6)	rabbit	30	Cell Signaling Technology	2764	AB_2228008	1:1000
PERK (pThr980)	rabbit	170	Cell Signaling Technology	3179	AB_2095853	1:1000

anti-total PERK	rabbit	170	Cell Signaling Technology	3192	AB_2095847	1:1000
GRP78 / BiP	rabbit	78	Cell Signaling Technology	3177	AB_2119845	1:1000
ATF3	rabbit	23.24	Cell Signaling Technology	33593	AB_2799039	1:2000
ATF4	rabbit	49	Cell Signaling Technology	11815	AB_2616025	1:2000
Actin	mouse	42	Sigma	A2228	AB_476697	1:2000
MafA	goat	36-47	Santa Cruz	sc-27140	AB_2133149	1:250
Pdx1	goat	46	Santa Cruz	sc-14662	AB_653988	1:1000
eIF2a-pS51	rabbit	38	Cell Signaling Technology	3398	AB_2096481	1:1000
GAPDH	mouse	37	Cell Signaling Technology	97166	AB_2756824	1:1000

qPCR Primer Sequences

Gene name	Species	Fwd and Rev 5'->3'	Amplicon	Source
Atf3	Mouse	TGGAGATGTCAGTCACCAAGTCT	88	Primerblast: NM_007498.3
		GCAGCAGCAATTTTATTTCTTTCT		
Atf4	Mouse	ACTCTAATCCCTCCATGTGTAAAGG	84	Primerblast:NM_001287180.1
		CAGGTAGGACTCTGGGCTCAT		
Xbp1s	Mouse	CTGAGTCCGCAGCAGGT	66	PMID: 17890727
		TGTCAGAGTCCATGGGAAGA		
Fos	Mouse	CGGGTTTCAACGCCGACTA	166	Primerbank: 6753894a1
		TTGGCACTAGAGACGGACAGA		
Dusp1	Mouse	GTTGTTGGATTGTCGCTCCTT	129	Primerbank: 7305423a1
		TTGGGCACGATATGCTCCAG		
Npas4	Mouse	CTCTGGATGCTGATCGCCTT	117	Primerblast:NM_153553.5
		CAGGTGGGTGAGCATGGAAT		
Nr4a1	Mouse	CTGCGAAAGTTGGGGGAGT	126	Primerblast:NM_010444.2
		CTTGAATACAGGGCATCTCCAG		
Nr4a3	Mouse	GCTGTGACTCTCCCCCAATC	88	Primerblast:NM_015743.3
		AGTGGGCTTTGGGTGCTG		
Npas4	Mouse	CTCTGGATGCTGATCGCCTT	117	Primerblast:NM_153553.5
		CAGGTGGGTGAGCATGGAAT		
Ddit3	Mouse	CACCACACCTGAAAGCAGAAC	65	PMCID: PMC2582538
		GGTGAAAGGCAGGGACTCA		

Hspa5	Mouse	TGGAGTTCCCCAGATTGAAG	728	PMCID: PMC2798684
		CCTGACCCACCTTTTTCTCA		
Txnip	Mouse	TCTTTTGAGGTGGTCTTCAACG	104	Primerbank: 13994378a1
		GCTTTGACTCGGGTAACTTCACA		
Mct1	Mouse	ACGCCGGAGTCTTTGGATTT	162	Primerblast:NM_009196.4
		TGAGGCGGCCTAAAAGTGG		
XBP1S	Human	GCTGAGTCCGCAGCAGGT	130	PMCID: PMC6645673
		CTGGGTCCAAGTTGTCCAGAAT		
SST	Human	ACCCAACCAGACGGAGAATGA	108	Primerbank: 71979669c1
		GCCGGGTTTGAGTTAGCAGA		
DDIT3	Human	GGAAACAGAGTGGTCATTCCC	116	Primerbank: 304282228c1
		CTGCTTGAGCCGTTCATTCTC		
HSPA5	Human	ATCAACGAGCCTACGGCAG	197	Primerblast:NM_005347.5
		TCCATGACACGCTGGTCAAA		

Checklist for reporting human islet preparations used in research

Adapted from Hart NJ, Powers AC (2018) Progress, challenges, and suggestions for using human islets to understand islet biology and human diabetes. Diabetologia https://doi.org/10.1007/s00125-018-4772-2

Islet preparation	**1**	**2**	**3**	**4**	**5**	**6**	**7**	**8**	**9**
MANDATORY INFORMATION									
Unique identifier	SAMN09091256	SAMN09228907	SAMN09370567	SAMN10784981	SAMN10977276	SAMN15770453	SAMN15851500	SAMN15877725	SAMN15894111
Donor age (years)	45	62	32	45	52	48	33	31	58
Donor sex (M/F)	Male	Male	Male	Female	Male	Female	Female	Male	Female
Donor BMI (kg/m^2)	29.3	36.1	28.5	35.7	27.2	30.9	44.2	27.4	26.8
Donor HbA_{1c} or other measure of blood glucose control	5.0%	5.8%	5.2%	5.7%	5.7%	5.8%	5.3%	5.6%	5.5%
Origin/source of islets[b]	IIDP	IIDP	IIDP	IIDP	IIDP	IIDP	IIDP	IIDP	IIDP
Islet isolation centre	Scharp-Lacy	Scharp-Lacy	University of Wisconsin	Scharp-Lacy	Southern California Islet Cell Resource Center	University of Wisconsin	University of Wisconsin	University of Wisconsin	Scharp-Lacy
Donor history of diabetes? Please select yes/no from drop down list	No	No	No	No	No	No	No	No	No
If Yes, complete the next two lines if this information is available									
Diabetes duration (years)									
Glucose-lowering therapy at time of death[c]									

RECOMMENDED INFORMATION									
Donor cause of death	cerebrovascular/ stroke	anoxia	head trauma	cerebrovascular/ stroke	cerebrovascular/ stroke	cerebrovascular/ stroke	anoxia	head trauma	cerebrovascular/ stroke
Warm ischaemia time (min)	No	No	5	No	No	yes, unknown	15	No	No
Cold ischaemia time (min)	655	643	690	672	486	328	353	465	552
Estimated purity (%)	90	90	95	90	85	90	85	95	90
Estimated viability (%)	95	95	91	95	96	99	98	98	95
Total culture time prior to shipment (d,h)[d]	2d	2d 17h	20 h	3d 7h	21h	1d 9h	1d 18h	2d 16h	2d 23h
Glucose-stimulated insulin secretion from IIDP	1.8	3.9	1.8	7.2	2.8	5.4	1.8	2.2	5.9
Handpicked to purity? Please select yes/no from drop down list	Yes	Yes	Yes	Yes	Yes	Yes	Yes	Yes	Yes
Additional notes: Associated Figure:	Fig 1D	Fig 1D	Fig 1D	Fig 8E	Fig 8E	Fig 8E	Fig 8E	Fig 8E	Fig 8E

[a]If you have used more than eight islet preparations, please complete additional forms as necessary
[b]For example, IIDP, ECIT, Alberta IsletCore
[c]Please specify the therapy/therapies
[d]Time of islet culture at the isolation centre, during shipment and at the receiving laboratory
[e]Please specify the test and the results